FEDERAL UNIVERSITY OF SÃO CARLOS

CENTER OF EXACT SCIENCES AND TECHNOLOGY

PHYSICS GRADUATE PROGRAM

Bruno Augusto Veloso Nunes Silva

Quantum transistor using superconducting qubits

São Carlos

2022

UNIVERSIDADE FEDERAL DE SÃO CARLOS

CENTRO DE CIÊNCIAS EXATAS E DE TECNOLOGIA

PROGRAMA DE PÓS-GRADUAÇÃO EM FÍSICA

Bruno Augusto Veloso Nunes Silva

Transistor quântico em qubits supercondutores

São Carlos

2022

FEDERAL UNIVERSITY OF SÃO CARLOS

CENTER OF EXACT SCIENCES AND TECHNOLOGY

PHYSICS GRADUATE PROGRAM

Bruno Augusto Veloso Nunes Silva

Quantum transistor using superconducting qubits

Master thesis presented to the Physics Graduate Program (PPGF) of the Federal University of São Carlos (UFSCar) as a requirement to obtain the title of MASTER IN PHYSICS.

Advisor: Prof. Dr. Celso Jorge Villas-Bôas

Co-advisor: Dr. Alan Costa dos Santos

São Carlos

2022

UNIVERSIDADE FEDERAL DE SÃO CARLOS
CENTRO DE CIÊNCIAS EXATAS E DE TECNOLOGIA
PROGRAMA DE PÓS-GRADUAÇÃO EM FÍSICA

Bruno Augusto Veloso Nunes Silva

Transistor quântico em qubits supercondutores

Dissertação de Mestrado apresentada ao Programa de Pós-Graduação em Física da Universidade Federal de São Carlos como requerimento fundamental para a obtenção do título de MESTRE EM FÍSICA.

Orientador: Prof. Dr. Celso Jorge Villas-Bôas
Coorientador: Dr. Alan Costa dos Santos

São Carlos
2022

Bruno Augusto Veloso Nunes Silva

Quantum transistor using superconducting qubits

Dissertação de Mestrado apresentada ao Programa de Pós-Graduação em Física da Universidade Federal de São Carlos como requerimento fundamental para a obtenção do título de MESTRE EM FÍSICA.

Prof. Dr. Celso Jorge Villas-Bôas
Orientador

Dr. Alan Costa dos Santos
Coorientador

Prof. Dr. Maycon Motta
Convidado 1

Prof. Dr. Roberto Silva Sarthour Junior
Convidado 2

São Carlos
2022

Acknowledgements

Firstly, I would like to acknowledge my advisor, Prof. Dr. Celso Jorge Villas-Bôas for his guidance, teachings and great companionship. The lessons I learned from you were fundamental both for my academic career and personal life.

I also thank my co-advisor, Dr. Alan Costa dos Santos, for having guided me throughout this journey, your guidance was a fundamental part of this process and without your help, this work would not be possible.

I thank my mother, Silvana Veloso Nunes for raising me, always with love and friendship. Any form of thanks would be little compared to the much I owe you. Everything I am today I owe to you and I couldn't be more grateful to have you in my life.

To my family members, especially to my grandmother Mariluza and my grandfather Itamar for the love and affection they gave me throughout my life.

To my colleagues in the quantum optimization group for the good discussions we had during my master's degree and which certainly helped a lot in my growth as a researcher.

To all the professors I had during my academic life for paving the way I walk today.

Finally, I would like to thank my girlfriend and friend Isabela Dias, for her companionship, encouragement and conversations during the writing of this work. May we, together, celebrate many achievements.

Agradecimentos

Primeiramente gostaria de agradecer meu orientador, Prof. Dr. Celso Jorge Villas-Bôas pela orientação, ensinamentos e pelo grande companheirismo. As lições que aprendi com o senhor foram inestimáveis tanto para minha carreira acadêmica, como pessoal.

Também agradeço ao meu coorientador, o Dr. Alan Costa dos Santos, por ter me guiado durante todo este percurso, sua orientação foi parte fundamental deste processo e sem sua ajuda, este trabalho não seria nada do que foi.

Agradeço à minha mãe, Silvana Veloso Nunes por ter me criado, sempre com carinho e amizade. Qualquer forma de agradecimento seria pouco perto do muito que lhe devo. Tudo o que sou hoje, devo à você e não poderia ser mais grato por ter você em minha vida.

Aos meus familiares, em especial à minha avó Mariluza e meu avô Itamar pelo amor e carinho que me deram durante toda a minha vida.

Aos meus colegas do grupo de otimização quântica pelas boas discussões que tivemos durante o mestrado e que certamente ajudaram muito no meu crescimento como pesquisador.

À todos os professores que tive durante minha vida acadêmica por terem pavimentado o caminho que hoje posso trilhar.

Por fim, agradeço à minha namorada e amiga Isabela Dias, pelo companheirismo, incentivo e conversas durante a escrita deste trabalho. Que possamos, juntos, comemorar muitas conquistas.

Do not go gentle into that good night,
Old age should burn and rave at close of day;
Rage, rage against the dying of the light.

Dylan Thomas

Abstract

In recent times, quantum computation has become a flourishing field of research with increasing investment due to its promise to revolutionize computing, increasing the speed of information processing to levels far beyond the supercomputers available today. However, implementing these machines is not a simple task and several physical systems are proposed for developing quantum processors. One of the most promising plataforms and focus of this work are the artificial atoms built in superconducting circuits, also known as superconducting qubits (two-level quantum systems). In this master dissertation, we will describe how these superconducting circuits can be used as qubits. We will also apply Hamiltonian engineering techniques to study a system of two superconducting qubits coupled through a superconducting loop. The analysis of this system will allow us to demonstrate that it behaves as a quantum transistor, allowing to coherently transfer quantum information. To optimize the interactions in this system, we use the methods of effective dynamics, which will allow us to find the optimal parameters of the system and will allow us to understand in more detail its physics. Although it is standard to treat artificial atoms as simple qubits, we will show that such a simplification does not completely describe the dynamics of our transistor. It will be necessary to take in consideration the existence of the third energy level, so that the dynamics of the system can be adequately described. Our results reveal the fundamental importance that the most excited levels of superconducting qubits play in its dynamics, even if such states are never populated.

Keywords: Quantum Computation. Superconducting Qubits. Quantum Transistor. Effective Dynamics.

Resumo

Recentemente a computação quântica vem se tornando um campo de pesquisa extremamente fértil e com crescentes investimentos devido à sua promessa de revolucionar a computação, aumentando a velocidade de processamento de informação para níveis muito além dos supercomputadores atuais. No entanto, a implementação destas maquinas não é uma tarefa simples, com diversos sistemas físicos sendo candidatos à plataforma padrão dos computadores quânticos. Um dos sistemas que ganha cada dia mais notoriedade e é foco deste trabalho, são os átomos artificiais construídos em circuitos supercondutores, também conhecidos como qubits (sistemas quânticos de dois níveis) supercondutores. Nesta dissertação, faremos uma descrição sobre como estes circuitos supercondutores podem desempenhar o papel de qubits. Também aplicaremos técnicas de engenharia de Hamiltonianos para estudar um sistema de dois qubits acoplados por meio de um loop supercondutor. As análises do sistema nos permitirão demonstrar que este circuito se comporta como um transistor quântico, conseguindo transferir informação quântica de forma coerente. Para optimizar as interações neste sistema utilizamos métodos de dinâmicas efetivas, que nos permitirão entender os parâmetros ótimos do sistema e nos permitirão entender em mais detalhes a física do mesmo. Embora seja padrão tratar átomos artificiais como qubits simples, mostraremos que tal simplificação não descreve adequadamente a dinâmica de nosso transistor. Será necessário considerar a existência do terceiro nível de energia, para que a dinâmica do sistema seja descrita adequadamente. Nossos resultados revelam a importância fundamental que os níveis mais excitados do sistema desempenham em sua dinâmica, mesmo que tais estados nunca sejam populados.

Palavras-chave: Computação Quântica. Qubits Supercondutores. Transistor Quântico. Dinâmicas Efetivas.

List of Figures

Contents

Chapter 1

Introduction

Computation is one of the most disruptive technologies we have been able to develop. The ability to store, process and share information as never before, is one of the bases of our society, with computers being fundamental in all aspects of our lives. Since its initial developments, with Alan Turing's theoretical propositions on computing machines [1] until recent times, computers have completely changed our world. One of the most impressive signs of progress in the field is the dramatic shrinkage, both in size and cost of computers.

Such enhancement was primarily allowed due to a simple yet powerful component, the transistor. Composed of semiconductors doped with impurities [2], the transistors enabled the miniaturization of processors, once they replaced the fragile and big electric valves, by tiny and reliable electronic components. The continuous improvements in the manufacture of those transistors in circuit boards, allowed to the so called Moore law, that predicted the exponential reduction in the size of computer processors over time [3].

Allied with this technological leap, another revolution that began in the early XX century and dramatically changed our understanding of the world was the Quantum Mechanics. Starting with Max Plank's demonstration that energy could be quantized [4] and leading to Schrödinger's description of particles through his wave equation [5]. The verification that matter could have a dual aspect, behaving both as a particle and a wave, was a fundamental turning point in our interpretation and description of the physical phenomena.

On their own, both those revolutions changed the world in unprecedented ways. Therefore, the idea of joining those fields was naturally a promise of great progress. This mixture is the field of quantum computing.

The field gained much relevance when Richard Feynman proposed that quantum computers would be more efficient in solving some computational problems than the traditional ones [6]. This prediction fomented an expanding interest in the field, with notable

progress in the past three decades. In this time we have faced the development of a huge number of algorithms [7] [1] and quantum computers being capable to overcome traditional ones in some tasks [8–10].

In the same manner, as in traditional computation where the fundamental concept is the unity of information (bit), in quantum computation, we resort to an analogous concept, the quantum bit or qubit, for short [11]. Just as bits can be either in 0 or 1 states, also qubits can be in the states $|0\rangle$ and $|1\rangle$. Where $|\ \rangle$ is the Dirac notation for representing quantum states of a system. The fundamental difference relies on the fact that quantum bits can also be in a linear combination of those states, i.e., the famous superposition quantum states, with no counterpart in the classical world [11].

To the present date, one of the leading physical systems for developing quantum logic elements is using anharmonic oscillators built in superconducting circuits, devices known as superconducting qubits [12]. Those qubits are built using lithographic techniques on superconducting materials so that it is possible to joint several qubits in a circuit to perform logical operations [13].

Notwithstanding the techniques to realize those systems have been improved [14], implementing quantum processors with more than a dozen of qubits is not yet a simple task. Therefore, developing systems that can perform logical operations with the highest fidelity and in a faster way, even with a few numbers of qubits, is a fundamental concern if we want to improve the viability of using quantum computers in the near-future noisy intermediate-scale quantum (NISQ) era [15].

Given that scenario, in this work, we will use a system of two superconducting qubits coupled by a superconducting quantum device, to perform logic operations with the highest possible fidelity and in a faster way. Specifically, we implement a quantum transistor, the analogous of a classical transistor, which can handle quantum states. By properly manipulating the Hamiltonian of the system, by choosing the best set of qubit frequencies and couplings we were able to find the conditions needed to implement a conditional transference of quantum information.

With this application, we were able to verify the existence of a correction term in the effective coupling of the system. Such correction has significant consequences on the theory of how the dynamics of superconducting qubits occur. Using the methods of effective Hamiltonians, we theoretically demonstrated that the third level of superconducting quantum anharmonic oscillators has a significant influence on the system's effective dynamics. This influence will be used to tune the system parameters to achieve the behavior of the quantum transistor.

Both results described here were experimentally verified by a Chinese experimental

[1] In the website https://quantumalgorithmzoo.org/ one can find a few hundred articles on quantum algorithms.

group, with which we have a collaboration that started more than two years ago. And the experimental results demonstrate good agreement with the theory.

In this master dissertation, we will discuss the theory necessary to obtain and interpret our results. In the second chapter, we present the theoretical framework needed to understand the theory of quantum computation. Then we describe the theory of effective dynamics and how to obtain effective Hamiltonians, the main technique we will use to analyze our system. Chapter 4 is dedicated to understanding the physics and the functioning of superconducting qubits, where we will introduce the physics of the Josephson junction and deduce the Hamiltonian of a superconducting anharmonic oscillator. Chapter 5 will be dedicated to show a deduction of the Hamiltonian for the specific superconducting circuit we used to implement the quantum transistor. In chapter 6 we will introduce the dynamics of the system and demonstrate that using the traditional two-level approximation for the circuit can not describe the system behavior. In chapter 7, we will demonstrate that the effective dynamics can precisely describe the system dynamics only when taking into account the third level of energy, with total agreement with the experimental results. In chapter 8 we will simulate the system in the dissipative regime, to demonstrate the quantum signature of the system. The work will be finished in chapter 9, with some conclusions about the results achieved and prospects.

Chapter 2

Theoretical Framework

In this chapter, we present the basic concepts necessary for this work. First, we do a basic introduction to the concepts of quantum mechanics and the linear algebra used in this work. Then we describe some basic principles of the theory of quantum computation and define what is a quantum gate.

2.1 Basic concepts of quantum mechanics

To initiate our work, it is useful to introduce some of the basic principles of quantum mechanics, so we can understand how those concepts will be applied to quantum computation. Therefore, this section will be dedicated to introducing the basics of the "Bracket" notation and some concepts of linear algebra important to our work. However, our approach will be synthetic and any reader seeking more detailed explanations should resort to the references [16–19] in which this section is based.

In classical mechanics, the description of a system is carried out using its position and momentum, with its time evolution being described using Newton's second law or, equivalently, using Langrange equations. In quantum mechanics, on the other hand, the description of a quantum system is carried out using the quantum wave equation. The wave function $\Psi(x,t)$ may be a complex-valued function of position x and time t, that completely describes the quantum system. In the quantum mechanical world, the analogous to Newton's second law is the Schrödinger wave equation, a linear differential equation that describes how a quantum state will evolve in time

$$i\hbar\frac{\partial}{\partial t}\Psi(x,t) = \left[\frac{-\hbar^2}{2m}\frac{\partial^2}{\partial x^2} + V(x,t)\right]\Psi(x,t), \tag{2.1}$$

where "i" is the imaginary unity, m the mass of the system, $V(x,t)$ the potential applied to the system, and $\hbar = h/2\pi$ is the normalized Planck constant, with h the Planck constant. Most quantum mechanical problems will be concerned with solving Eq. (2.1) a task that, in general, is not trivial. However, some techniques can be applied to facilitate this task.

Assuming that the potential in Eq. (2.1) is time independent, we can do a separation of variables, which will lead to two ordinary differential equations

$$\frac{d\phi(t)}{dt} = -\frac{iE}{\hbar}\phi(t), \tag{2.2}$$

$$-\frac{\hbar^2}{2m}\frac{d^2\psi(x)}{dx^2} = E\psi(x) - V(x)\psi(x), \tag{2.3}$$

where E stands for the separation constant and represents the energy of the system, $\phi(t)$ the time dependent part of the wave function, and $\psi(x)$ the spatial part. It is simple to integrate Eq. (2.2) and verify that it has a simple solution $\phi(t) = e^{-iEt/\hbar}$, independently of the potential. Eq. (2.3), by the other hand, is called time independent Schrödinger Equation, and its solution depends on the form of $V(x)$, naturally. Therefore, obtaining an exact solution for this equation is a fundamental task when dealing with quantum systems.

Just as in classical mechanics, in quantum mechanics the Hamiltonian of the system plays a central role. Thus, we can define the Hamiltonian operator as

$$\hat{H} = -\frac{\hbar^2}{2m}\frac{d^2}{dx^2} + \hat{V}(x), \tag{2.4}$$

where the hat (ˆ) indicates that we are dealing with an operator and not a c-number. With that, we can rewrite Schrödinger time independent equation as

$$\hat{H}\psi = E\psi. \tag{2.5}$$

Despite describing the state of a quantum system, the wave equation does not have a physical meaning, since it is a complex-valued function. To acquire a physical interpretation of it, we need to take the square of the absolute value of the wave equation, $|\Psi(x,t)|^2$, which defines the probability density of a measurement finding the particle in a defined position x at a given time t. This description of the measurements in terms of probabilities leads directly to the probabilistic interpretation of quantum mechanics.

As we mentioned, the Schrödinger equation is a linear differential equation, which means that the phenomena that it describes will also be linear. Therefore, to deal with the quantum world, we need to take into account the tools of linear algebra. In this framework, the state of a system will be denoted by a vector in the Hilbert space $\mathscr{H}$. A vectorial space of infinite dimensions defined over the complex numbers.

A vector in this space can be represented in the Dirac notation as a *ket* denoted by $|\Psi\rangle$ and can be interpreted as a column vector

$$|\Psi\rangle = \begin{pmatrix} a_1 \\ a_2 \\ \vdots \end{pmatrix}, \tag{2.6}$$

with $a_i \in \mathbb{C}$ the components of this vector. For every element in this Hilbert space, it is possible associate one single element belonging to a dual space. The dual of a ket $|\Psi\rangle$ is called in Dirac notation *bra* and denoted as $\langle\Psi|$. The components of such element can be represented in a line vector as

$$\langle\Psi| = \begin{pmatrix} a_1^* & a_2^* & \cdots \end{pmatrix}, \tag{2.7}$$

where the asterisk denotes the complex conjugate of each component.

This dual elements allow us to calculate the scalar product of a ket $|\Psi\rangle$ with a bra $\langle\Phi|$, that will return a number $a \in \mathbb{C}$

$$\langle\Phi|\Psi\rangle = a = \langle\Psi|\Phi\rangle^*, \tag{2.8}$$

with the third equality demonstrating that the order we calculate the scalar product does matter in this situation. Given the scalar product, we can calculate the norm of a quantum state simply making

$$||\Psi||^2 = \langle\Psi|\Psi\rangle = a_1 a_1^* + a_2 a_2^* + \cdots = 1, \tag{2.9}$$

where the last equality stands for the fact that states must be normalized.

Just as we can define bras, which acts over kets to return a complex number, we can also define linear operators, that will act over a ket to return another ket, or its adjoint operator (defined below) will act over a bra, to return another bra. In matricial notation, they can be represented as square matrices and their action can be read as

$$\hat{R}\,|\Psi\rangle = |\Phi\rangle\,, \qquad\qquad \langle\Psi|\,\hat{R}^{\dagger} = \langle\Phi|\,. \tag{2.10}$$

Just as the order matter when calculating the scalar products, also it matter when applying an operator. We can define the adjoint of an operator $\hat{R}$ as

$$\langle\Psi|\,\hat{R}^{\dagger}\,|\Phi\rangle = \langle\Phi|\,\hat{R}\,|\Psi\rangle^{*}\,, \tag{2.11}$$

in matricial notation, one could obtain the adjoint of an operator simply transposing the matrix, and taking the complex conjugate of its elements.

A class of operators with special relevance for quantum mechanics are the Hermitian or self-adjoint operators. They are defined as the operators that are equal to their own adjoint $\hat{R}^{\dagger} = \hat{R}$. Such operators are especially relevant since they can be used to represent measurable properties. It is worth to notice that there is also a quantum mechanical theory that does not use Hermitian operators, the so called "non-Hermitian quantum mechanics" [20]. However, it will not be the focus of our work.

We can also define the inverse of an operator $\hat{R}$ as the operator $\hat{R}^{-1}$ that respects the relation

$$\hat{R}\hat{R}^{-1} = \hat{R}^{-1}\hat{R} = \mathbb{1}, \tag{2.12}$$

with $\mathbb{1}$ the identity matrix. If the inverse of an operator $\hat{U}$ is equal to its adjoint, then $\hat{U}$ is said to be unitary and we can write,

$$\hat{U}\hat{U}^{\dagger} = \hat{U}^{\dagger}\hat{U} = \mathbb{1}. \tag{2.13}$$

One last class of operators that will be useful in our work is the one composed by projection operators. They are defined as the Hermitian operators that are equal to their own square

$$\hat{P}^{2} = \hat{P}, \tag{2.14}$$

for instance the operator $|\Psi\rangle\langle\Psi|$. Once acting over another state $|\Phi\rangle$ this operator leads to the projection of $|\Phi\rangle$ over $|\Psi\rangle$,

$$(|\Psi\rangle\langle\Psi|)\,|\Phi\rangle = \langle\Psi|\Phi\rangle\,|\Psi\rangle = \alpha\,|\Psi\rangle\,, \tag{2.15}$$

with $\alpha \in \mathbb{C}$ the component of $|\Phi\rangle$ on $|\Psi\rangle$.

The definition of operators allow us to define the eigenvectors (or eigenstates) of an operator as the vectors that obeys the eigenvector equation,

$$\hat{R}\,|\Psi\rangle = \lambda\,|\Psi\rangle\,, \tag{2.16}$$

where $\lambda \in \mathbb{C}$ are the eigenvalues associated to the eigenvectors $|\Psi\rangle$ of the operator $\hat{R}$. The importance of this equation for quantum mechanics relies on the fact that Schrödinger time independent equation (Eq. 2.5) is an eigenvector equation.

2.1.1 Composite systems

So far we assumed the system in analysis is composed of a single particle in a Hilbert space $\mathscr{H}$. However, if a system is composed of n quantum entities, each one will lie in its own Hilbert space $\mathscr{H}_i$. Therefore, the system as a whole lives in a composite Hilbert space $\mathscr{H}_{total} = \mathscr{H}_1 \otimes \mathscr{H}_2 \otimes ... \otimes \mathscr{H}_n$, where $\otimes$ denotes the tensor product. Then, we can write the state of the composite system

$$|\Psi\rangle = |\psi\rangle_1 \otimes |\psi\rangle_2 \otimes ... \otimes |\psi\rangle_n\,. \tag{2.17}$$

In such case, also the operators acting over this system must be written in a composite form as

$$\hat{R} = \hat{r}_1 \otimes \hat{r}_2 \otimes ... \otimes \hat{r}_n. \tag{2.18}$$

This tensorial notation for composite systems has the great advantage of allowing us to operate separately on each particle of this system. For example, if we have a bipartite system and want to operate $\hat{r}_1$ over the state $|\psi\rangle_1$ maintaining the estate $|\psi\rangle_2$ unchanged, we could write

$$\hat{R}\,|\Psi\rangle = (\hat{r}_1 \otimes \mathbb{1})(|\psi\rangle_1 \otimes |\psi\rangle_2) = \hat{r}_1\,|\psi\rangle_1 \otimes |\psi\rangle_2\,, \tag{2.19}$$

where $\mathbb{1}$ is the identity matrix and we used the property $\mathbb{1}\,|\psi\rangle = |\psi\rangle$.

To simplify the notation it is also common to omit the $\otimes$ signal and write $|\psi\rangle_1\,|\psi\rangle_2 ... |\psi\rangle_n$ or, alternatively, $|\psi_1, \psi_2, ..., \psi_n\rangle$.

2.1.2 Density matrix

In some situations, the state of a quantum system is not completely known. In these cases, the system could be in a given state $|\psi_i\rangle$ with a probability p_i, with $i = 1, 2, ..., n$. As an example, we could mention a source that emits a particle in a state $|\psi_i\rangle$ with probability p_i. This situation adds a randomness to the description of the system, which should not be confused with the probabilistic nature of quantum mechanics [21].

Those systems are in what is called mixture states, and are described using the density matrix formalism. The density matrix of a given system is the generalization of a quantum pure state and is defined as

$$\hat{\rho} = \sum_{i}^{N} p_i \left|\psi_i\right\rangle \left\langle\psi_i\right|, \tag{2.20}$$

with pure states being the special case when $N = 1$ and $p_1 = 1$.

In those mixture states, an observable $\hat{A}$ will have an expectation value $\langle\psi_i|\hat{A}|\psi_i\rangle$ for each state and then, the mean value of this observable will be

$$\langle\hat{A}\rangle = \sum_{i}^{N} p_i \left\langle\psi_i\right|\hat{A}\left|\psi_i\right\rangle, \tag{2.21}$$

then, applying Eq. (2.20) we find

$$\langle\hat{A}\rangle = tr\left(\hat{\rho}\hat{A}\right), \tag{2.22}$$

with $tr()$ being the trace of the matrix $\hat{\rho}\hat{A}$.

The evolution of the density matrix will be given in terms of the von-Neumann equation,

$$\frac{d\hat{\rho}}{dt} = \frac{1}{i\hbar}\left[\hat{H}, \hat{\rho}\right], \tag{2.23}$$

with $\hat{H}$ the system Hamiltonian. This equation can be understood as a generalization of Schrödinger equation for mixed states [22].

2.1.3 The Bloch Sphere

It may be useful to have a graphical way to represent the state of a given qubit. This is achieved, representing the qubit in a sphere called Bloch Sphere like that one shown in Figure 1. In this sphere, the top of the z-axis (also called longitudinal axis) represent the $|1\rangle$ state and the bottom the $|0\rangle$. In this representation, we can parameterize the state of the qubit as

$$|\psi\rangle = \cos\left(\frac{\theta}{2}\right)|0\rangle + e^{i\varphi}\sin\left(\frac{\theta}{2}\right)|1\rangle, \tag{2.24}$$

with $0 \leq \theta \leq \pi$ and $0 \leq \varphi < 2\pi$.

Alternatively, we could also represent a mixed state $\hat{\rho}$ using the unitary matrix $\mathbb{1}$, the three Pauli matrices $\hat{\sigma}_x$, $\hat{\sigma}_y$ and $\hat{\sigma}_z$ and a vector $\vec{a}$ called Bloch vector (or coherence vector) as

$$\hat{\rho} = \frac{1}{2}\left(\mathbb{1} + \vec{a}\cdot\vec{\sigma}\right) = \frac{1}{2}\begin{pmatrix} 1+a_z & a_x - ia_y \\ a_x + ia_y & 1-a_z \end{pmatrix}, \tag{2.25}$$

with $\vec{\sigma} = (\hat{\sigma}_x, \hat{\sigma}_y, \hat{\sigma}_z)$. In this representation the mixture states are represented inside the Bloch sphere, while pure states are represented over the surface. To demonstrate that, first we use Eq.(2.25) to find the eigenvalues of $\hat{\rho}$

$$\det(\hat{\rho} - \lambda \mathbb{1}) = \lambda^2 - \lambda + \frac{1}{4}(1 - a_x^2 - a_y^2 - a_z^2) = 0, \tag{2.26}$$

since density matrices must be positive semi-definite (must have non-negative eigenvalues), the eigenvalues λ must satisfy $\lambda \geq 0$. Defining the magnitude of the Bloch vector $|\vec{a}| = \sqrt{a_x^2 + a_y^2 + a_z^2}$ we can find the condition,

$$\lambda = \frac{1}{2} \pm \frac{|\vec{a}|}{2} \geq 0 \implies |\vec{a}| \leq 1, \tag{2.27}$$

we can notice that, when $|\vec{a}| = 1$ there is only one non-zero eigenvalue corresponding to a pure state. On the other hand, when $|\vec{a}| < 1$ there are two different eigenvalues, implying we have a mixture state and the Bloch vector will lie inside the Bloch sphere.

Figure 1 – An arbitrary vector $|\psi\rangle$ in the Bloch sphere. In such representation, the north pole represents the $|1\rangle$ state and the south, the $|0\rangle$ state. Once we are representing quantum normalized states, the sphere have unitary radius.

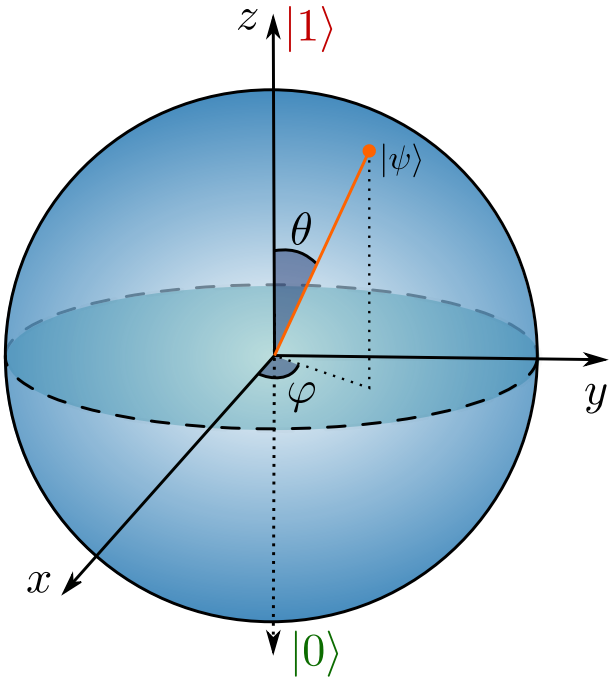

Source: The author.

2.2 Quantum computation

In view of the basic concepts of quantum mechanics introduced previously, we can focus on analyzing how those concepts can be applied to store and process information, which is the main focus of quantum computation [11].

In classical computation, information is represented using bits, which are systems with two distinguishable states, which are commonly called 0 and 1. In the same sense, quantum computation represents information in qubits (abbreviation for quantum bits), which are two states $|0\rangle$ and $|1\rangle$ of a quantum system [23], forming the so called computational basis $\{|0\rangle, |1\rangle\}$.

The major difference of a qubit over its classical counterpart is the fact that, while traditional bits can only be in states 0 or 1, the quantum bits can be in a state $|\psi\rangle$ which is a linear combination of those two states, forming the superposition states of $|0\rangle$ and $|1\rangle$. In addition, considering two or more subsystems, the whole system can exist in collective superposition states that cannot be factorized as a product of individual states of each subsystem. In this case we say the system is in an entangled state. It is precisely these two kinds of states: superposition of a single qubit or entangled state of two (or more) qubits, that enable quantum computers to have advantages over the classical ones. Mathematically a superposition state is written as a linear combination of the states in the computational basis

$$|\psi\rangle = a\,|0\rangle + b\,|1\rangle\,, \tag{2.28}$$

with a and b complex numbers satisfying the normalization condition $|a|^2 + |b|^2 = 1$ [23].

To understand how to use superposition to speed up calculations, we first analyze how a quantum computer works. As an example we can consider the Deutsch algorithm, which is used to know if a function is constant or balanced. Assuming we want to implement a function $f(x) : (0,1) \mapsto (0,1)$, a quantum computer will take a two qubit initial state $|x, y\rangle$ and apply a transformation $\hat{U}_f$ in order to find

$$\hat{U}_f\,|x, y\rangle \mapsto |x, y \oplus f(x)\rangle\,, \tag{2.29}$$

where $\oplus$ is the addition modulo 2 operation. However, if the input state $|x\rangle$ is a superposition of n states, then the linear operator $\hat{U}_f$ would act in all states simultaneously

$$\hat{U}_f \sum_x |x, y\rangle \mapsto \sum_x a_x\,|x, y \oplus f(x)\rangle\,, \tag{2.30}$$

which means that, in practical terms, all possible inputs of a given function would be evaluated at the same time. This concept of using superposition to do calculations simultaneously is called quantum parallelism and is the heart of quantum algorithms advantages.

Although this capability of being in superposition, quantum parallelism on its own, is not able to generate useful outputs, since, to acquire information from a quantum state (e.g. state in Eq. (2.28)), it is necessary to measure it. However, in this process, one will find either the qubit in state $|0\rangle$ with probability $|a|^2$ or in state $|1\rangle$ with probability $|b|^2$. In this scenario, to fully determine the coefficients of this superposition state, it would be needed to do a high number of measurements, diminishing the advantage of these quantum computers in some cases [23].

To have a significant gain, a quantum algorithm should be able to maximize one of those values $|a|^2$ or $|b|^2$, to maximize the probability of measuring the state of interest [21].

2.2.1 Quantum Gates

As mentioned above, to do a calculation, a quantum computer must be able to apply transformations $\hat{U}_f$ to quantum states such as in Eq. (2.29). Those transformations are the central part of the manipulation of quantum information and can be achieved using quantum logic gates. They are deeply related to the classical logic gates in which bits are manipulated in a circuit to return the desired output.

In quantum computation, a quantum gate is a unitary matrix $\hat{U}$ which acts on a initial state $|\psi_{\text{in}}\rangle$ in order to return a final state $|\psi_{\text{out}}\rangle = \hat{U}\,|\psi_{\text{in}}\rangle$ [11]. It is interesting to notice that, since any unitary operator can be understood as a quantum gate, there are many possible gates to be used in quantum computation. Here, we mention some of the more relevant:

- **Single qubit gates**

The more basic quantum gates are those acting upon a single qubit. While in classical computation there are only one of those gates (the NOT gate) in quantum computing, there are infinite of them (since every unitary matrix is a valid gate), however the most relevant are the $\hat{X}$, $\hat{Y}$ and $\hat{Z}$ gates, defined as

$$\hat{X} = |1\rangle\langle 0| + |0\rangle\langle 1| = \begin{pmatrix} 0 & 1 \\ 1 & 0 \end{pmatrix}, \tag{2.31a}$$

$$\hat{Y} = \mathrm{i}\,|0\rangle\langle 1| - \mathrm{i}\,|1\rangle\langle 0| = \begin{pmatrix} 0 & -\mathrm{i} \\ \mathrm{i} & 0 \end{pmatrix}, \tag{2.31b}$$

$$\hat{Z} = |0\rangle\langle 0| - |1\rangle\langle 1| = \begin{pmatrix} 1 & 0 \\ 0 & -1 \end{pmatrix}, \tag{2.31c}$$

such gates are also called Pauli gates, once they are the Pauli matrices $\hat{\sigma}_x$, $\hat{\sigma}_y$, $\hat{\sigma}_z$ respectively [23]. It is interesting to notice that, while the $\hat{X}$ gate acts in the same manner as the NOT classical gate, swapping states $|0\rangle$ and $|1\rangle$, the $\hat{Z}$ gate inverts the signal of the state $|1\rangle$, leaving state $|0\rangle$ unchanged.

Another relevant single qubit gate is Hadamard,

$$\hat{H} \equiv \frac{1}{\sqrt{2}}\begin{pmatrix} 1 & 1 \\ 1 & -1 \end{pmatrix}, \tag{2.32}$$

which is a genuine quantum gate, once it have no classical counterpart. It can be used to generate a superposition between $|0\rangle$ and $|1\rangle$. Once acted on a $|0\rangle$ state, Hadamard returns $(|0\rangle + |1\rangle)/\sqrt{2}$ and in state $|1\rangle$ it produces $(|0\rangle - |1\rangle)/\sqrt{2}$.

- **Multiqubit Gates**

Gates that act on multiple qubits at once are called multiqubit gates. They are fundamental to do more complex manipulation of information. Some of those gates are specifically meant to be used in specific algorithms, others can be demonstrated to be useful in many different algorithms. Also, as discussed in detail in [11], it is possible to decompose any complex logic gates in a small set of single- and two-qubit gates. For instance, arbitrary single qubit rotations, as described previously, and the C-NOT gate (described below) are called universal gates since any computation can be done using those gates. Among most relevant multiqubit gates we could mention the CNOT, the Fredkin and the Toffoli gates.

The **C-NOT gate** is a two-qubit gate, with a control qubit and a target one. This gate implement the $\hat{X}$ gate on the target, only when the control qubit is in the state $|1\rangle$. Its action can be written as

$$U_{CNOT} = |0\rangle\langle 0| \otimes \mathbb{1} + |1\rangle\langle 1| \otimes \hat{X}, \tag{2.33}$$

and its representation along with the possible outputs of it action can be seen in Figure 2.

Figure 2 – Representation of the circuit of a C-NOT gate. This gate is composed of a control bit and a target one. As we see in the table, when the control qubit is in the state $|0\rangle$ the outputs are equal to the inputs. However, when the control is in state $|1\rangle$, the target qubit is flipped.

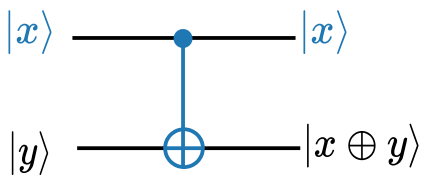

Control	Input	Output
$\|0\rangle$	$\|0\rangle$	$\|0\rangle$
	$\|1\rangle$	$\|1\rangle$
$\|1\rangle$	$\|0\rangle$	$\|1\rangle$
	$\|1\rangle$	$\|0\rangle$

Source: The author.

Originally proposed by Fredkin and Toffoli in 1982 [24], the Controlled-SWAP (c-SWAP) or **Fredkin gate**, is a 3 bit logic gate that can perform a conditional transference of states as depicted in Figure 3.

The implementation of such gate to deal with quantum information is of special importance due to its wide usability in quantum computation, for instance to implement quantum algorithms such as Shor's algorithm [25], to perform codes for quantum error correction [26], and to implement quantum cryptography protocols [27].

Figure 3 – Schematic representation of the functioning of a Fredkin Gate. When the control bit (the bit on the top) is in the state $|0\rangle$, the states $|a\rangle$ and $|b\rangle$ remain the same. However, when the controller is in the state $|1\rangle$ the states $|a\rangle$ and $|b\rangle$ are flipped.

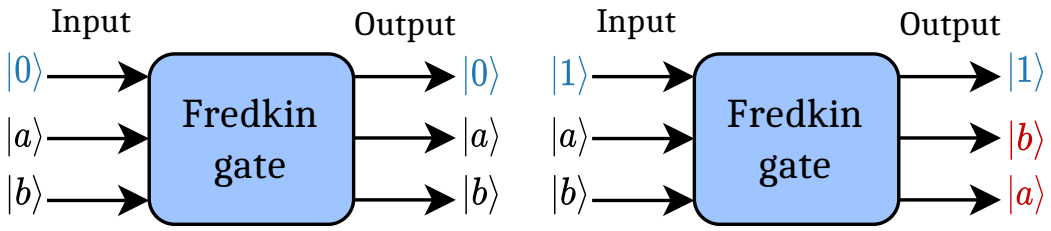

Source: The author.

The third multiqubit gate we emphasize here is **Toffoli** gate or controlled-controlled-not [24]. It is composed of three qubits, and acts implementing an $\hat{X}$ gate in one of the states, only if the two control qubits are on state $|1\rangle$. Its representation can be seen in Figure 4.

Figure 4 – Circuit representation of a Toffoli gate along with the possible output for each input. As we can see the Toffoli acts as a controlled-controlled-not gate, that switches the state of a target qubit only when both control qubits are in state $|1\rangle$.

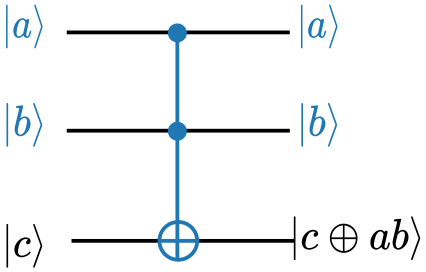

Input	Output
$\|0\rangle\|0\rangle\|0\rangle$	$\|0\rangle\|0\rangle\|0\rangle$
$\|0\rangle\|0\rangle\|1\rangle$	$\|0\rangle\|0\rangle\|1\rangle$
$\|0\rangle\|1\rangle\|0\rangle$	$\|0\rangle\|1\rangle\|0\rangle$
$\|0\rangle\|1\rangle\|1\rangle$	$\|0\rangle\|1\rangle\|1\rangle$
$\|1\rangle\|0\rangle\|0\rangle$	$\|1\rangle\|0\rangle\|0\rangle$
$\|1\rangle\|0\rangle\|1\rangle$	$\|1\rangle\|0\rangle\|1\rangle$
$\|1\rangle\|1\rangle\|0\rangle$	$\|1\rangle\|1\rangle\|1\rangle$
$\|1\rangle\|1\rangle\|1\rangle$	$\|1\rangle\|1\rangle\|0\rangle$

Source: The author.

Chapter 3

Effective dynamics

In this chapter, we will discuss the methods of effective dynamics. Those methods consists of a wide class of mathematical tools applied to simplify Hamiltonians, to allow analytical insights into the dynamics of the system. This method will be a fundamental part of the analysis of our system, and allied with numerical methods implemented to solve Schrödinger equation, will constitute the core of the analysis in this work. In the first section, we present the three most important representations of quantum dynamics, namely Shrödinger, Heisenberg, and interaction pictures. Then, the second section is focused on developing and describing the method we will use to obtain the effective Hamiltonians in this work.

3.1 The different representations of quantum mechanics

There are three most common ways to describe the time evolution of a quantum system, named Schrödinger, Heisenberg and interaction pictures. The fundamental difference between them relies on which mathematical entity will carry the time dependency [18]. Through this section, we will add an index 'S', 'H', and 'I' to denote kets and operators in Schrödinger, Heisenberg, and Interaction pictures, respectively. It is important to highlight that such different descriptions does not implies in a different physics or in different behaviours of the systems. Those pictures are simply, different forms to represent the same phenomena.

The first and more commonly used in simple systems is the *Schrödinger picture*, where it is assumed that the observable are constant in time, and the quantum state $|\psi(t)\rangle_S$ will evolve according the equation

$$i\hbar\frac{d}{dt}|\psi(t)\rangle_S = \hat{H}_S|\psi(t)\rangle_S, \tag{3.1}$$

which is the usual Schrödinger equation. Integrating it, we can find that the evolution of a state will be given using a unitary operator, that acts on an initial state $|\psi(t_0)\rangle_S$ to return a new state

$$|\psi(t)\rangle_S = \hat{U}(t,t_0)|\psi(t_0)\rangle_S = e^{-i(t-t_0)\hat{H}_s/\hbar}|\psi(t_0)\rangle_S, \tag{3.2}$$

this operator $\hat{U}(t,t_0)$ is called the evolution operator [19].

While Schrödinger picture assumes that the operators are constant in time and the vector states are the ones responsible for carrying the information about the dynamics, *Heisenberg picture* assumes the exact opposite. In this representation, the state is constant in time and the observable have a time dependency. The operator $\hat{A}_H(t)$ can be written in terms of its Schrödinger representation as

$$\hat{A}_H(t) = e^{it\hat{H}_s/\hbar}\hat{A}_S e^{-it\hat{H}_s/\hbar}. \tag{3.3}$$

The evolution of this operator is given by Heisenberg equation of motion

$$\frac{d\hat{A}_H(t)}{dt} = \frac{1}{i\hbar}\left[\hat{A}_H(t),\hat{H}_S\right], \tag{3.4}$$

which is analogous to Schrödinger equation in this representation. It is important to notice that, despite the different descriptions, scalar quantities (mean values and probabilities) will be equal in every representation, meaning that the phenomena studied should be independent on the picture used to describe it.

The third representation, that will play a major role in our analysis is the *Interaction picture* (or Dirac picture), which is an intermediate between the former representations. Here, both operators and states evolve in time. This description is commonly used when the

Hamiltonian in Schrödinger picture can be split into two parts, one constant and the other time-dependent

$$\hat{H} = \hat{H}_0 + \hat{V}(t). \tag{3.5}$$

In this representation, the vector state $|\psi(t)\rangle_I$ is defined in terms of its form in Schrödinger picture as,

$$|\psi(t)\rangle_I = \hat{U}_0(t)\,|\psi(t)\rangle_S\,, \tag{3.6}$$

where, for simplicity we call $t_0 = 0$, and defined the evolution operator $\hat{U}_0(t) = e^{\mathrm{i}t\hat{H}_0/\hbar}$ in terms only of the constant Hamiltonian. With Eq.(3.6) we can calculate the dynamics of a system in the Interaction picture as

$$\mathrm{i}\hbar\frac{d}{dt}|\psi\rangle_I = -\hat{H}_0\hat{U}_0(t)\,|\psi\rangle_S + \hat{U}_0(t)\hat{H}\,|\psi\rangle_S\,, \tag{3.7}$$

then defining the interaction Hamiltonian in the interaction picture,

$$\hat{V}_I(t) = \hat{U}_0\hat{V}(t)\hat{U}_0^\dagger, \tag{3.8}$$

we can write the Schrödinger equation in the interaction picture

$$\mathrm{i}\hbar\frac{d}{dt}|\psi\rangle_I = \hat{V}_I(t)\,|\psi(t)\rangle_I\,. \tag{3.9}$$

In a similar way, observable will be defined in terms of the same unitary operators,

$$\hat{A}_I(t) = e^{\mathrm{i}t\hat{H}_0/\hbar}\,\hat{A}_S e^{-\mathrm{i}t\hat{H}_0/\hbar}, \tag{3.10}$$

and the time evolution of the observable will be described with Heisenberg equation in the interaction picture

$$\frac{d\hat{A}_I(t)}{dt} = \frac{1}{\mathrm{i}\hbar}\left[\hat{A}_I(t), \hat{H}_0\right]. \tag{3.11}$$

When we analyze Eq.(3.6) and Eq.(3.10) we can notice the intermediate character of Interaction picture. In this frame of reference, both states and observable are evolving in time, however, the states evolve only with the interaction part of the Hamiltonian. While the observable evolve with the time-independent part of the Hamiltonian, H_0 [16].

3.2 Time dependent perturbation theory

In quantum mechanics, one can entirely describe the time evolution of a state $|\Psi(t)\rangle$ using the Schrödinger equation. This means that knowing the Hamiltonian of a given system and its initial state $|\Psi(0)\rangle$, we could deterministically describe the evolution of any system by

just solving the Schrödinger equation [18]. However, for most systems of practical interest, the form of the Hamiltonian is so complex that analytical approaches are unfeasible. Then, a wide variety of methods have been developed to approximate the solution for different problems. These techniques are called approximation methods. A class with especial relevance to our work are the time dependent perturbation methods.

A perturbation method assumes that the Hamiltonian of a given system can be split in two terms,

$$\hat{H} = \hat{H}_0 + \hat{H}_1(t), \tag{3.12}$$

with H_0 the "unperturbed Hamiltonian" describing the simple part of the system, which is assumed to have known eigenvalues and eigenvectors. In the time dependent methods, we aim to find the solution for the Schrödinger equation. For that, first we write the system dynamics in the Interaction picture,

$$\mathrm{i}\hbar\frac{d}{dt}\left|\psi(t)\right\rangle_I = \hat{V}_I\left|\psi(t)\right\rangle_I, \tag{3.13}$$

with,

$$\hat{V}_I = \hat{U}\hat{H}_1(t)\hat{U}^\dagger, \tag{3.14}$$

where $\hat{U} = e^{-\mathrm{i}\hat{H}_0(t-t_0)/\hbar}$ is the time evolution operator as defined in the previous section. Here, however, we do not assume $t_0 = 0$. Then, the time evolution of the state vector in the Interaction picture will be

$$\left|\psi(t)\right\rangle_I = \hat{U}(t,t_0)\left|\psi(t_0)\right\rangle_I. \tag{3.15}$$

Then, applying Eq.(3.15) in Eq.(3.13) we find the equation for the motion of the time propagator,

$$\mathrm{i}\hbar\frac{d}{dt}\hat{U}_I(t) = \hat{H}_I(t)\hat{U}(t), \tag{3.16}$$

where we applied the initial condition,

$$\hat{U}(t_0,t_0) = \mathbb{1}. \tag{3.17}$$

Eq.(3.16) can be integrated over time, to find the following integral equation,

$$\hat{U}(t,t_0) = \mathbb{1} + \frac{1}{\mathrm{i}\hbar}\int_{t_0}^{t}\hat{H}_I(t_1)\hat{U}(t_1,t_0)dt_1, \tag{3.18}$$

this equation can be integrated recursively to give,

$$\begin{aligned}\hat{U}(t,t_0) &= \mathbb{1} + \frac{1}{\mathrm{i}\hbar}\int_{t_0}^{t}\hat{H}_I(t_1)\left(\mathbb{1} + \frac{1}{\mathrm{i}\hbar}\int_{t_0}^{t_1}\hat{H}_I(t_2)\hat{U}(t_2,t_0)dt_2\right)dt_1 \\ &= \mathbb{1} + \frac{1}{\mathrm{i}\hbar}\int_{t_0}^{t}\hat{H}_I(t_1)dt_1 + \left(\frac{1}{\mathrm{i}\hbar}\right)^2\int_{t_0}^{t}dt_1\int_{t_0}^{t_1}dt_2\hat{H}_I(t_1)\hat{H}_I(t_2) \\ &+ \cdots + \left(\frac{1}{\mathrm{i}\hbar}\right)^n\int_{t0}^{t}dt_1\int_{t0}^{t1}dt_2\ldots\int_{t0}^{t_{n-1}}dt_n\hat{H}_I(t_1)\hat{H}_I(t_2)\ldots\hat{H}_I(t_n)+\ldots,\end{aligned} \tag{3.19}$$

which is the Dyson series [16]. If the energies in the perturbative terms are small compared to the energies in the unperturbed Hamiltonian H_0, Eq.(3.19) will converge after a few terms and we could truncate the series, in order to find an approximation for $\hat{U}(t, t_0)$ [28], which is the core concept on the perturbation methods we implement.

3.3 Effective Hamiltonians

Due to its usability, a wide range of techniques to obtain effective Hamiltonians have been developed [28, 29], each one with particular purposes. In this work we will implement the method described in Ref. [30]. This approach uses Schrödinger equation in the interaction picture as in Eq.(3.9). Integrating over time, we verify that a solution for such a equation have the form

$$|\psi(t)\rangle_I = |\psi(0)\rangle_I + \frac{1}{i\hbar}\int_0^t \hat{V}_I(t')\,|\psi(t')\rangle_I\,dt'. \tag{3.20}$$

Then, applying Equation (3.20) in Equation (3.9) we find

$$i\hbar\frac{d}{dt}|\psi(t)\rangle_I = \hat{V}_I(t)\,|\psi(0)\rangle_I + \frac{1}{i\hbar}\hat{V}_I(t)\int_0^t \hat{V}_I(t')\,|\psi(t')\rangle_I\,dt'. \tag{3.21}$$

To simplify this dynamics, we can assume that $\hat{V}_I(t)$ has highly oscillatory terms in comparison with the terms in the time-independent Hamiltonian H_0. In this situation we can neglect the first term in the right-hand side of Eq.(3.21), since its contribution will be negligible, on average. The second term, by the other hand, will be simplified considering that the state $|\psi(t)\rangle_I$ will oscillate very slowly in comparison to the Hamiltonian $\hat{V}_I(t)$, since, in the Interaction picture, observable evolves according to $\hat{H}_0$ and states according to $\hat{V}_I(t)$. Therefore, the wave function can be assumed constant in time and removed from the integral. Then, we find the approximate dynamics

$$i\hbar\frac{d}{dt}|\psi(t)\rangle_I \approx \hat{H}_{eff}(t)\,|\Psi(t)\rangle_I\,, \tag{3.22}$$

where we define the effective Hamiltonian

$$\hat{H}_{eff} \approx \frac{1}{i\hbar}\hat{V}(t)\int_0^t \hat{V}(t')dt'\Big|_{RWA}\,, \tag{3.23}$$

where the *RWA* stands for *Rotating Wave Approximation*. This simplified Hamiltonian will also have some terms that oscillate fast, and those will also be removed using the same arguments. This simplification is analogous to doing a rotating wave approximation.

This simplified Hamiltonian will be fundamental to analyzing the qubit circuit in our work, because the system will operate in this regime where the interactions are weaker than the relevant frequencies. Then, simplifications will be possible, to achieve better insights into the system dynamics.

Chapter 4

Physical qubits

This chapter is focused on describing how to physically implement a qubit using superconducting circuits. First, we describe the simple form of this problem, the harmonic oscillator, in terms of a superconducting LC-circuit. Then we describe how this same circuit can be treated quantum-mechanically to find the Hamiltonian of the circuit. Then we apply the same methods to a circuit containing a nonlinear inductor, called Josephson junction [31,32] which allows us to create an atom-like structure in the energy levels of the system. At the end, we describe the transmon qubit [33,34], which is the type of qubit used in our system.

4.1 The artificial atom

In the path to developing quantum computers, it is crucial to understand how physical systems can be used as qubits. In this sense, many natural quantum systems have been used to implement quantum computers, like the spins of electrons in semiconductors [35,36], trapped ions [37, 38], cavity quantum electrodynamics (cQED) systems [39] and others [40–42]. One of the most promising techniques now available and the focus of our work is the use of "artificial atoms" built in superconducting circuits, which are called superconducting qubits.

Those type of qubits have a fundamental difference in comparison to the other platforms for quantum technologies, since they are built using lithographic techniques in macroscopic circuits [13]. Therefore, in superconducting qubits it is possible to use the macroscopic parameters of the circuit, to control the microscopic quantum behavior of the system [43]. This possibility to control the parameters, and the scalability of this model of qubits is what has drawn great attention to this framework in the past years, with some of the state-of-the-art quantum processors being built with those components [8, 44–47].

The name "artificial atom" is due to the fact that those circuits use quantum anharmonic oscillators to simulate the different energy states of a real atom. To understand what are those anharmonic oscillators, first we resort to the simple and classical counterpart, the harmonic oscillator.

4.2 Harmonic oscillator - The LC circuit

To introduce the problem of the harmonic oscillator, both quantum and classical, we begin by describing a simple LC circuit such as the one depicted in Figure 5. This system is composed of a linear capacitor with capacitante C and a linear inductor of inductance L. In this analysis, we assume the wires connecting the components to be perfect conductors and then no resistance exists in the circuit. An assumption that is valid, since we deal with superconducting circuits.

To describe our system, we define the total charge in the circuit and the magnetic flux through the circuit as

$$Q(t) = \int_{-\infty}^{t} I(t')dt', \tag{4.1a}$$

$$\Phi(t) = \int_{-\infty}^{t} V(t')dt', \tag{4.1b}$$

where the first equation uses the definition of a current $I(t)$ through a circuit and the second is Faraday's induction law, for an electric potential $V(t)$ [48] assuming both potential and currents are zero at time $t \to -\infty$.

Figure 5 – Simple LC circuit, composed of a capacitor of capacitance C, and an inductor of inductance L. This circuit behaves in the same manner as a classical harmonic oscillator.

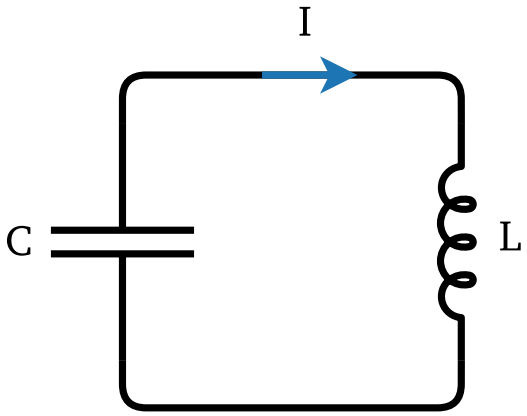

Source: The author.

In the linear capacitor, the difference of potential is linearly dependent on the instantaneous charge $q(t)$ stored in its plates

$$V(t) = \dot{\Phi}(t) = \frac{q(t)}{C}, \tag{4.2}$$

where the dot denotes the time derivative. Then we can describe the energy stored in the capacitor as

$$E_{\text{cap}} = \int_{-\infty}^{t} I(t')V(t')dt' = \int_{-\infty}^{t} \dot{\Phi}(t')\left[\frac{dq}{dt'}\right]dt' = \int_{0}^{\Phi} \dot{\Phi}(t)C\, d\dot{\Phi} = \frac{1}{2}C\dot{\Phi}^2(t) \tag{4.3}$$

In the inductor, by the other hand, we can describe the current in it as linearly proportional to the magnetic flux,

$$I(t) = \dot{q}(t) = \frac{1}{L}\Phi(t). \tag{4.4}$$

Then, we can calculate the energy in this component integrating over time as in Eq. (4.3) to find

$$E_{\text{ind}} = \frac{\Phi^2(t)}{2L}. \tag{4.5}$$

With the energies in both elements, we can now write the Lagrangian of this circuit as

$$\mathscr{L} = T - V = \frac{1}{2}C\dot{\Phi}^2(t) - \frac{1}{2L}\Phi^2(t), \tag{4.6}$$

where we can notice that, the capacitive term is the kinetic part of the Lagrangian and the inductive term, the potential. Then, choosing the generalized coordinates as

$$q = \Phi(t), \qquad p = \frac{\partial \mathscr{L}}{\partial \dot{q}} = C\dot{\Phi}(t) = q(t), \tag{4.7}$$

we can write the Euler-Lagrange equation

$$\frac{d}{dt}\frac{\partial \mathscr{L}}{\partial \dot{q}} = \frac{\partial \mathscr{L}}{\partial q}, \tag{4.8}$$

to find the equation of motion of the circut,

$$\ddot{\Phi} + \frac{1}{LC}\Phi = 0, \tag{4.9}$$

which is the equation of a simple classic harmonic oscillator with angular frequency $\omega = 1/\sqrt{LC}$. Then, we verify the analogous behavior of an LC circuit, with the mechanical oscillator. Here, with the magnetic flux oscillating in time.

To obtain the system's Hamiltonian we use the method of Legendre transformation to obtain the expression [49]

$$H(p,q,t) = \dot{q}p - \mathscr{L}(q,\dot{q},t), \tag{4.10}$$

and apply Eq.(4.6) and (4.7) to find,

$$H = \frac{1}{2}C\dot{\Phi}^2 + \frac{1}{2L}\Phi^2 = \frac{p^2}{2C} + \frac{q^2}{2L} = \frac{1}{2C}q^2 + \frac{1}{2L}\Phi^2, \tag{4.11}$$

where the third equality was obtained by applying Eq. (4.3).

4.2.1 Quantization of the LC circuit

The Hamiltonian in Eq.(4.11) describes the classical electric oscillator. The quantum description of this system can be obtained from promoting the canonical coordinates and the Hamiltonian, to quantum operators,

$$\begin{aligned} q &\to \hat{q}, \\ p &\to \hat{p}, \\ H &\to \hat{H}, \end{aligned} \tag{4.12}$$

where the position and momentum operators respects the commutation relation $[\hat{q},\hat{p}] = i\hbar\mathbb{1}$, where $\mathbb{1}$ is the identity matrix.

It should not be surprising the possibility to quantize the electric charge $q(t)$, since it is given by the electrons dislocated in the capacitor plates. The quantization of the magnetic flux $\Phi(t)$, by the other hand is less obvious, but it is possible in integrated superconducting circuits.

When cooled to very low temperatures, some metals can conduct electricity without resistance and for that reason are called superconductors. In this situation, two electrons of the metal can become bounded in a state called Cooper pair [50] which behaves as a bosonic particle [51]. These pairs are the quasiparticles responsible for conducting the currents in

superconductors, therefore, when describing the charges in a superconductor, it is convenient to write the charge as $\hat{q} = 2e\hat{c}$, with e the electronic charge and $\hat{c}$ the number of Cooper pairs. This behaviour of electrons gives rise to a wide variety of interesting phenomena. Among them there is the fact that all external magnetic fields are expelled from the metal what is called Meissner effect [51]. However, in a cylindrical superconductor, it is possible "trap" a small magnetic flux, which will be quantized [52]. This is called the magnetic flux quantum $\Phi_0 = h/2e$ [53], and can be used to write a quantum operator called the reduced magnetic flux $\hat{\phi} = 2\pi\Phi/\Phi_0$.

We can apply the quantization to find the Hamiltonian of the quantum LC circuit,

$$\hat{H} = \frac{\hat{\boldsymbol{p}}^2}{2C} + \frac{\hat{\boldsymbol{q}}^2}{2L} = 4E_C\hat{c}^2 + \frac{1}{2}E_L\hat{\phi}^2, \tag{4.13}$$

where we defined $E_C = e^2/2C$, that represents the energy required to add a Cooper pair in the capacitor and $E_L = \Phi_0^2/(2\pi)^2 h$ the inductive energy. In general, however, it is more convenient to write the Hamiltonian $\hat{H}$ in terms of the creation and annihilation operators $\hat{a}$ and $\hat{a}^\dagger$. For that, we do the transformation

$$\hat{\boldsymbol{p}} = \mathrm{i}\sqrt{\frac{\hbar\omega C}{2}}\left(\hat{a} - \hat{a}^\dagger\right), \tag{4.14}$$

$$\hat{\boldsymbol{q}} = \sqrt{\frac{\hbar\omega L}{2}}\left(\hat{a} + \hat{a}^\dagger\right), \tag{4.15}$$

which will allow us to write the Hamiltonian in the form

$$\hat{H} = \frac{\hbar\omega}{2}\left(\hat{a}\hat{a}^\dagger + \hat{a}^\dagger\hat{a}\right). \tag{4.16}$$

Applying the commutation relation $[\hat{a}, \hat{a}^\dagger] = \mathbb{1}$, we obtain the Hamiltonian of the quantum harmonic oscillator

$$\hat{H} = \hbar\omega\left(\hat{a}^\dagger\hat{a} + \frac{\mathbb{1}}{2}\right). \tag{4.17}$$

This simple Hamiltonian is one of the most basic systems in quantum mechanics, and a very powerful tool to describe the behavior of quantum systems, since it is possible to solve it analytically. In this system, we define the states $|n\rangle$, called Fock or number states [54], to be the eigenstates of the number operator $\hat{n} = \hat{a}^\dagger\hat{a}$ with correspondent eigenenergies $n\hbar\omega$. This means that all states in the quantum harmonic oscillator will be equally spaced as represented in Figure 6, where we plot the energy states of the quantum harmonic oscillator as a function of ϕ.

Such a property of having equally spaced states is a problem if we seek to use this quantum system as a qubit, since the same energy $\hbar\omega$ can induce any transition in the system, not just the ones in the computational basis ($|0\rangle \longleftrightarrow |1\rangle$). To mitigate this problem, it is necessary to introduce some anharmonicity in the system.

Figure 6 – Illustration of the energy levels of a quantum harmonic oscillator, as a function of the reduced magnetic flux. Every transition in this system is equally spaced, as denoted by the red arrows.

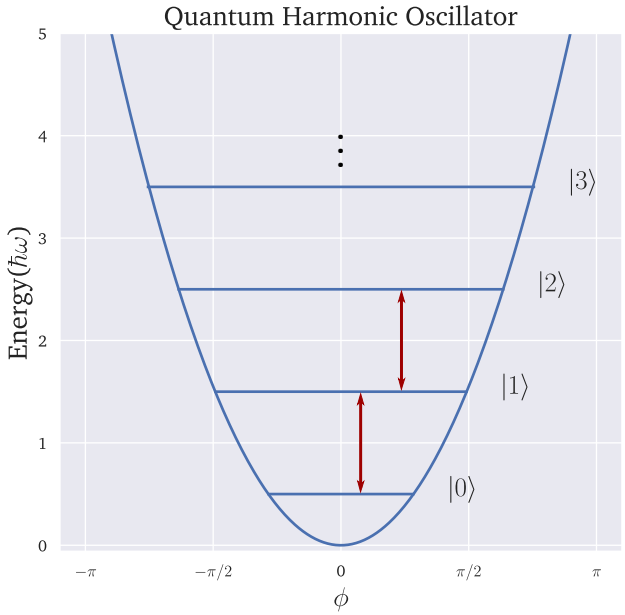

Source: The author.

4.3 Anharmonic oscillator - The artificial atom

In order to use a superconducting circuit as a qubit, it is necessary to introduce an anharmonicity to the harmonic behavior of the LC circuit. This anharmonic term can be achieved once we change the inductor in Figure 5 by a superconducting device called Josephson junction [31, 32], which is composed of two superconductors separated by a thin potential barrier, which can be a layer of insulator or a non-superconducting material [55]. This setup, creates a potential barrier that could prevent the flow of Cooper pairs. However, if the barrier is sufficiently thin, the wave functions of the pairs can extend through the insulator, and the charge can tunnel from one side of the junction to the other one. This will lead to a nonlinear dependency of the change with the magnetic flux, what means that the system will act as a nonlinear inductor [56].

Figure 7 is a sketch of a Josephson junction with ψ_1 and ψ_2 representing the collective wave functions of Cooper pairs in each side. These wave functions describe the charge densities $\rho_1(x)$ and $\rho_2(x)$ of all Cooper pairs at a point x of the junction, with θ_1 and θ_2 the phases of these wave functions. Once applying a difference of potential to this system, the Cooper pairs in the superconductors can tunnel from one side of the barrier to the other. This

Figure 7 – Schematic representation of a Josephson junction, composed of two superconductors separated by an insulator. The charge densities ρ_1 and ρ_2 are separated by a potential barrier, however, if the barrier is sufficiently narrow, the wave functions of the Cooper pairs (ψ_1, ψ_2) can tunnel and a highly nonlinear current can flow through the superconductor.

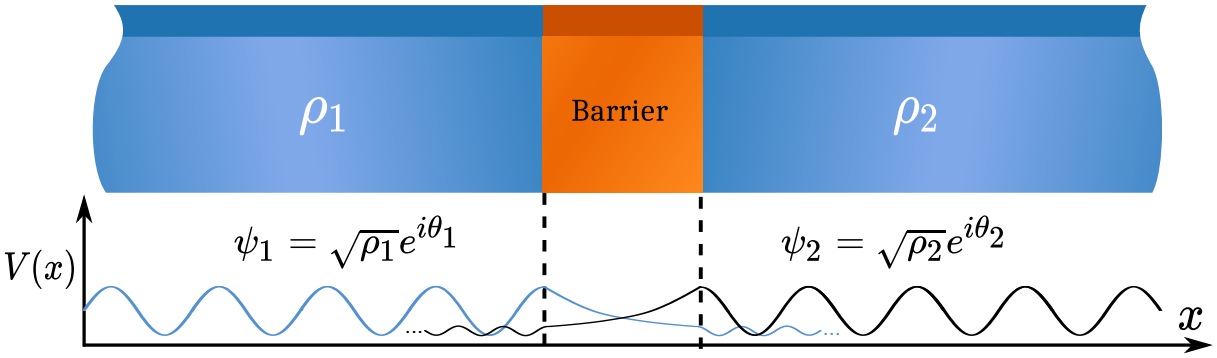

Source: The author.

effect, will create a current that will depend on the phase difference ϕ between ψ_1 and ψ_2

$$I(t) = I_c \sin(\phi(t)), \tag{4.18}$$

with I_c the critical current, a parameter that depends on the geometry of the junction, and $\phi(t) = \theta_1(t) - \theta_2(t)$ [57]. The difference of potential in this device will be given by

$$V(t) = \frac{\hbar}{2e}\dot{\phi}. \tag{4.19}$$

Using Eq.(4.18) we can write an equation that relates the charge q and the magnetic flux Φ

$$\dot{q}(t) = I_c \sin\left(2\pi\frac{\Phi(t)}{\Phi_0}\right), \tag{4.20}$$

what can be used to find the energy in the Josephson junction in the same manner as done with the inductor and the capacitor

$$E_{jj} = E_J\left[1 - \cos\left(\frac{2\pi\Phi}{\Phi_0}\right)\right], \tag{4.21}$$

where we defined the Josephson energy $E_J = I_c\Phi_0/2\pi$ the parameter that characterizes the junction. It is important to notice that, when dealing with the Lagrangian or Hamiltonian of this system, we can omit the constant term, since it does not contributes to the dynamics.

We can now, substitute the linear inductor of the LC circuit, by a Josephson junction, which is represented by a boxed "X" as seen in Figure 8. This new circuit will then be described by the Hamiltonian

$$\hat{H} = 4E_C\hat{c} - E_J\cos\left(\hat{\phi}\right). \tag{4.22}$$

Figure 8 – Representation of the circuit of a superconducting circuit. This system is composed of a linear capacitor of capacitance C and a Josephson junction characterized by the Josephson energy E_J

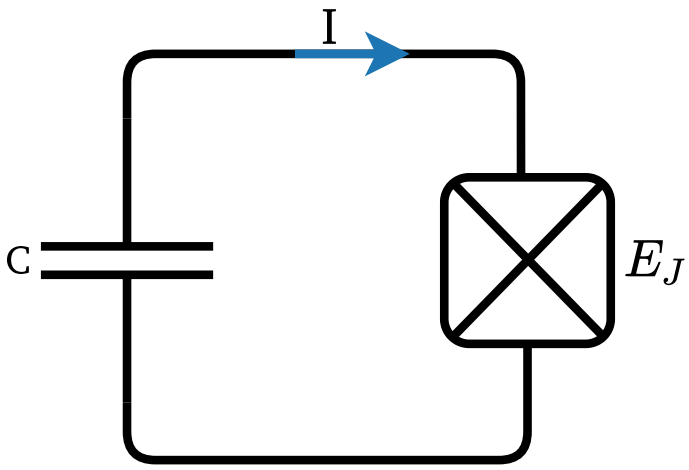

Source: The author.

To better understand how this change in the Hamiltonian affects the system behavior, it is interesting to study the transmon regime, where we assume $E_J \gg E_C$ [34, 56]. In this situation, the qubit will be much less sensitive for charge fluctuations and the cossine term will lead the dynamics. Thus, it allows us to expand the cossine in a Taylor series,

$$E_J \cos\hat{\phi} = E_J - \frac{1}{2}E_J\hat{\phi}^2 + \frac{1}{24}E_J\hat{\phi}^4 + O(\hat{\phi}^6), \tag{4.23}$$

and discard the terms of order higher than the fourth along with the irrelevant constant term. Applying this expansion in the Hamiltonian, we notice that the second order term and the capacitive one, form again the Hamiltonian of the quantum harmonic oscillator and one more can be written using the annihilation and creation operators,

$$\hat{c} = \mathrm{i}\sqrt{\frac{1}{2\zeta}}\left(\hat{a} - \hat{a}^\dagger\right), \tag{4.24}$$

$$\hat{\phi} = \sqrt{\frac{\zeta}{2}}\left(\hat{a} + \hat{a}^\dagger\right), \tag{4.25}$$

where we call $\zeta = \sqrt{8E_C/E_J}$. Applying the same transformation to the quartic term, we find the Hamiltonian written in terms of the ladder operators

$$\hat{H} = \omega_0\,\hat{a}^\dagger\hat{a} + \frac{\alpha}{12}\left(\hat{a} + \hat{a}^\dagger\right)^4, \tag{4.26}$$

where we defined $\omega_0 = \sqrt{8E_CE_J}$ the qubit frequency and $\alpha = -E_J\zeta^2/8 = -E_C$ the anharmonicity.

The quartic term, describing the anharmonicity can be better understood, if we apply a simplification that remove terms that do not conserves the total number of excitations in

the system and that will oscillate rapidly in the rotating frame. The details of this calculations can be seen in the Appendix A. This process yields the Hamiltonian

$$\hat{H} = \omega\,\hat{a}^{\dagger}\hat{a} + \frac{\alpha}{2}\left(\hat{a}^{\dagger}\hat{a}^{\dagger}\hat{a}\hat{a}\right), \tag{4.27}$$

where $\omega = \omega_o + \alpha$. Therefore, we can verify that when the system is excited to states higher than the first excited state, the energy levels will be shifted by a quantity proportional to α. This change in the energy levels can be seen in Figure 9 and is the key feature that allows us to use superconducting circuits as qubits. The unequal energy difference between the states allows us to excite only a specific transition and leave the other states unpopulated. This preserves the computational basis needed to perform quantum computing. However, as it will be discussed later, despite being unpopulated, the higher levels still play a fundamental role in the effective dynamics of the system and their effects can not be completely neglected.

Figure 9 – Schematic illustration the potential energy in a quantum harmonic oscillator –QHO– (left) and a superconducting qubit (right), as a function of the superconducting phase ϕ. In the QHO, the energy states (horizontal lines) are equally spaced, while in the qubit, the anharmonicity leads to unequal energy separations.

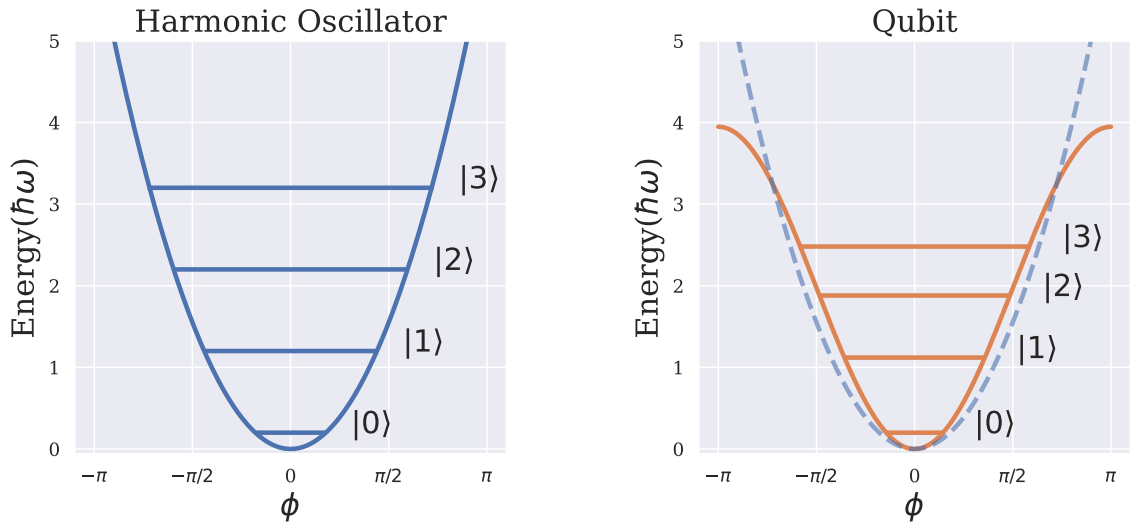

Source: The author.

4.4 The tunable frequency qubit

In the previous section, the qubit Hamiltonian was characterized with two parameters, namely, the frequency ω and the anharmonicity α. Since those two quantities have been defined using the capacitance and the Josephson energy, the only way to choose a specific value to the parameters of the circuit is during the qubit lithography. However it is possible to build a qubit in which an external parameter (an external magnetic flux) can control the qubit frequency. These are called transmon qubits [34].

Figure 10 – **a)** Schematic representation of a SQUID, composed of a superconducting ring with two Josephson junctions in parallel (in orange). To tune the frequency of this qubit, we apply an external flux $\tilde{\Phi}$ through the ring. **b)** Circuit representation of a tunable frequency qubit.

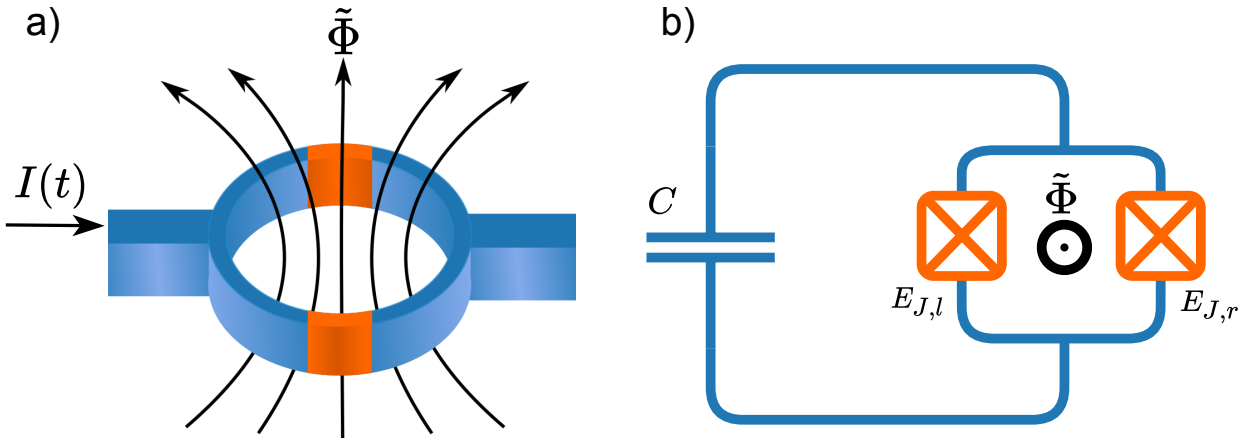

Source: The author.

This tunable qubit is made changing the single Josephson junction of a traditional qubit by a superconducting quantum interference device (SQUID): a superconducting ring with two Josephson junctions in parallel [58]. In this geometry, it is possible to introduce an external magnetic flux $\tilde{\Phi}$ through the ring that will allow us to externally control the frequency of the qubit. In Figure 10, we show the sketch of a SQUID and the circuit representation of the transmon qubit.

To understand how this parameter will allow to build a frequency tunable qubit, we first write the energy of the SQUID. Given by the sum of two Josephson energies of independent junctions

$$\hat{E}_{SQUID} = -E_{J,l}\cos(\hat{\phi}_l) - E_{J,r}\cos(\hat{\phi}_r), \tag{4.28}$$

where the indices stands for the left and right junctions. The relation between superconducting phases $\hat{\phi}_l$ and $\hat{\phi}_r$ will have a constraint, due to the physics of superconductors. Since the wave functions that describe the collective Cooper pairs must be single valued, at a given point, to have physical meaning, the total phase difference around the loop must be an integer multiple of 2π, which is called the fluxoid quantization condition [59]. Since the magnetic external flux will also affect the phase in the loop, we will have the condition,

$$\hat{\phi}_l - \hat{\phi}_r = 2\pi\hat{c} + 2\pi\frac{\tilde{\Phi}}{\Phi_0}. \tag{4.29}$$

Then, we can write

$$\hat{\phi}_l = \frac{\hat{\phi}_l - \hat{\phi}_r}{2} - \frac{\hat{\phi}_l + \hat{\phi}_r}{2}, \quad \text{and} \quad \hat{\phi}_r = \frac{\hat{\phi}_l - \hat{\phi}_r}{2} + \frac{\hat{\phi}_l + \hat{\phi}_r}{2}, \tag{4.30}$$

to apply the trigonometric identity $\cos(\alpha \pm \beta) = \cos(\alpha)\cos(\beta) \mp \sin(\alpha)\sin(\beta)$ to rewrite Eq.(4.28)

$$E_{SQUID} = -E_{J\Sigma}\left[\cos(\hat{\alpha})\cos(\hat{\beta}) - d\sin(\hat{\alpha})\sin(\hat{\beta})\right], \tag{4.31}$$

where $E_{J\Sigma} = E_{J,l} + E_{J,r}$, $\hat{\alpha} = (\hat{\phi}_1 - \hat{\phi}_2)/2$, $\hat{\beta} = (\hat{\phi}_1 + \hat{\phi}_2)/2$ and we defined the asymmetry between the two junctions $d = (E_{J,l} - E_{J,r})/E_{J\Sigma}$. Experimentally the asymmetry is due to imperfections during the qubit manufacture and usual values of the parameter d are close to 0.1 [34]. However, it is possible to assume that both junctions are identical, since this assumption does not change the overall behaviour of the system.

Assuming junctions perfectly symmetrical ($E_J = E_{J,l} = E_{J,r}$) and using Eq.(4.29) we can write the energy on the SQUID as a function of $\tilde{\Phi}/\Phi_0$ as

$$E_{SQUID} = -2E_J \cos\left(\pi\frac{\tilde{\Phi}}{\Phi_0}\right)\cos\hat{\varphi}, \tag{4.32}$$

where one defines the new superconducting average phase $\hat{\varphi} = (\hat{\phi}_1 + \hat{\phi}_2)/2$ and a new Josephson energy $E_J'(\tilde{\Phi}) = 2E_J\cos\left(\pi\tilde{\Phi}/\Phi_0\right)$ that is function of the external flux. Applying Eq.(4.32) to derive the Hamiltonian of the transmon qubit, it leads to a similar result as made in the previous section for the fixed frequency qubit, with the final Hamiltonian

$$\hat{H}_{transmon} = 4E_C\hat{c} - E_J'(\tilde{\Phi})\cos(\hat{\varphi}). \tag{4.33}$$

By applying the second quantization to write the Hamiltonian in terms of $\hat{a}$ and $\hat{a}^\dagger$ we will have a qubit frequency that varies with the external flux as $\omega(\tilde{\Phi}) = \sqrt{8E_CE_J'(\tilde{\Phi})} - E_C$. This dependence on the external flux will allow us to control the interaction between the elements of the circuit during the experiments. It allows, for example, for the possibility to set multiple qubits in resonance for a desired period of time, a fundamental request for interaction engineering between different qubits.

Chapter 5

The circuit of the quantum transistor

After understanding all the concepts regarding our work, we are able to build and analyze the circuit of the quantum transistor. In this chapter, first we describe all the components present in the real circuit that was used to obtain the experimental data. With this information the circuit is modeled and the Hamiltonian is derived. For that, we will start with the classical Lagrangian of the system and do a similar approach as described in [43].

5.1 The experimental circuit

The circuit considered in our work is composed of two superconducting artificial atoms (Q_1 and Q_2) coupled via a superconducting loop (called coupler C) which can be used to create a tunable coupling between the atoms Q_1 and Q_2 [60]. Our system is composed of three Xmon qubits [61].

A photo of the real circuit can be seen in Figure 11, where we can understand better the different components of the studied circuit. The ressonators $R1$ and $R2$ that connects the qubits Q_1 and Q_2 to the transmission line are the components that allow the reading of the population in those qubits during the experiment. The XY lines are controls that implement the pulses used to implement single qubit gates. Finally, the Z line, is used to control the external flux through the superconducting loops in order to allow the frequency tuning of each element. This means that, only the populations in Q_1 and Q_2 can be measured during the experiment. Also, the population in the coupler can only be set before the beginning of the experiment. Those two characteristics of the coupler are the fundamental differences on the motivation for treating qubits and coupler in a different manner, despite the fact that all elements are composed of the same types of superconducting loops. Another important point to notice is that only the frequencies of Q_1 and C can be tuned, with Q_2 being a fixed frequency qubit, since there is no Z line to control its external flux.

As we mentioned, the artificial atoms used in the circuit are Xmon qubits, however, apart from some differences in the way the circuit is grounded, Xmon and transmon qubits are equivalent. Both Xmons and transmons are built with a SQUID in parallel with a capacitor and operate in the same regime $E_J \gg E_C$ [61]. Therefore, Xmon qubits will be described by the same Hamiltonian as the transmon. Therefore, for simplicity, in our work we will refer to all qubits as transmons.

5.2 Obtaining the system Hamiltonian

To analyze the system dynamics, it is fundamental to derive its Hamiltonian. To do that, we will use the method described in [43], where we begin by describing the classical Lagrangian of the circuit and proceed to derive its quantum Hamiltonian. Here we only describe the results of implementing this method, but the details can be seen in the Appendix B. For instance, let the circuit in analysis be described as seen in the scheme in Figure 12. Each of the superconducting qubits is assumed as a transmon tunable frequency qubit. Since our main focus in this work is the description of the circuit dynamics, here we omit the resonators from this scheme, assuming they will have no effect on the dynamics. Each of the j qubits is directly coupled to the coupler, here depicted as a capacitor of capacitance C_{jc}. There is also a capacitive coupling C_{12} that connects both qubits. This coupling is much weaker than the direct couplings and exists, for instance, due to the proximity of the qubits

Figure 11 – Photography of the real circuit used in the experiments with the qubits highlighted. Both Q_1 (green) and Q_2 (blue) are connected to the transmission line via the resonators $R1$ and $R2$, allowing the population reading. The XY lines are used to control the qubit initial state and the Control Z line is used to control the frequencies on both Q_1 and C.

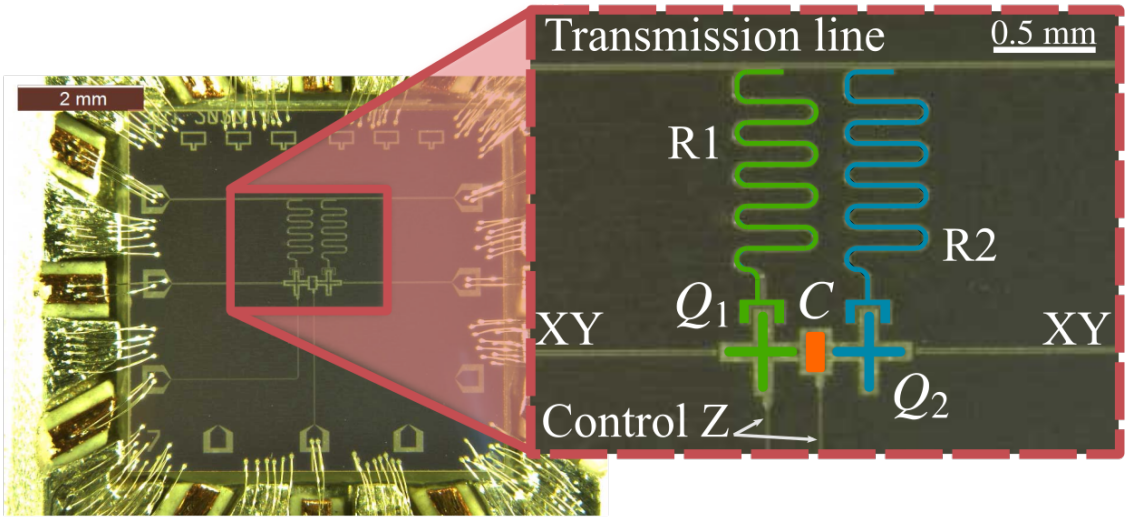

Source: Adapted from original photo published in [62].

Q_1 and Q_2 in the circuit. In the circuit geometry, the arms of the qubits will act as parallel plates of a capacitor, generating a capacitance that will affect the system behaviour.

The approach we used is similar to the implemented in Section 4.2 to derive the Hamiltonian of the qubit. Here, however, to simplify the calculations, we define the relevant quantities in terms of a capacitance matrix $\boldsymbol{C}$ and the conjugated coordinates of the circuit are written as vectors $\vec{\phi}$ and $\vec{q}$. This approach allow us to write the Lagrangian in Eq. (4.6) in the matricial form

$$\mathscr{L} = \frac{1}{2}\dot{\vec{\phi}}^T \mathbf{C} \dot{\vec{\phi}} - \sum_{i=1,C,2} E_{J_i} \cos\phi_i, \tag{5.1}$$

with the second term the Josephson energy for each transmon qubit. Using this matricial notation, the work of finding the corresponding Hamiltonian for given a Lagrangian is a simple task, that involves only inverting the capacitance matrix and calculating,

$$H = \frac{1}{2}\vec{q}^T \mathbf{C}^{-1} \vec{q} + U_J. \tag{5.2}$$

Computing the inverse of $\boldsymbol{C}$ for our system results in an matrix with a large number of terms. However, assuming that the capacitance from each transmon (C_1, C_C and C_2) is much greater than the capacitances that couples the qubits (C_{1C}, C_{2C} and C_{12}), it is possible to simplify the matrix, to just a few terms. Such assumption is based on the fact that, experimental capacitances for the qubit modes are of the order of 100fF, while the

Figure 12 – Diagram of the circuit in analysis. Each one of the three qubits are composed of two Josephson junctions (E_{J_i}) in parallel with a capacitor of capacitance C_i. The direct couplings between the qubits and the coupler are modeled with capacitors of capacitance C_{jC}. The capacitive coupling is modeled with a capacitor C_{12} that has a capacitance that respects $C_{jC} \gg C_{12}$. The frequencies of Q_1 and C can be tuned using the external fluxes Φ_1 and Φ_C. Experimentally, Q_2 is not connected to a line that enables frequency tuning, therefore, no external flux for the second qubit is considered in this diagram.

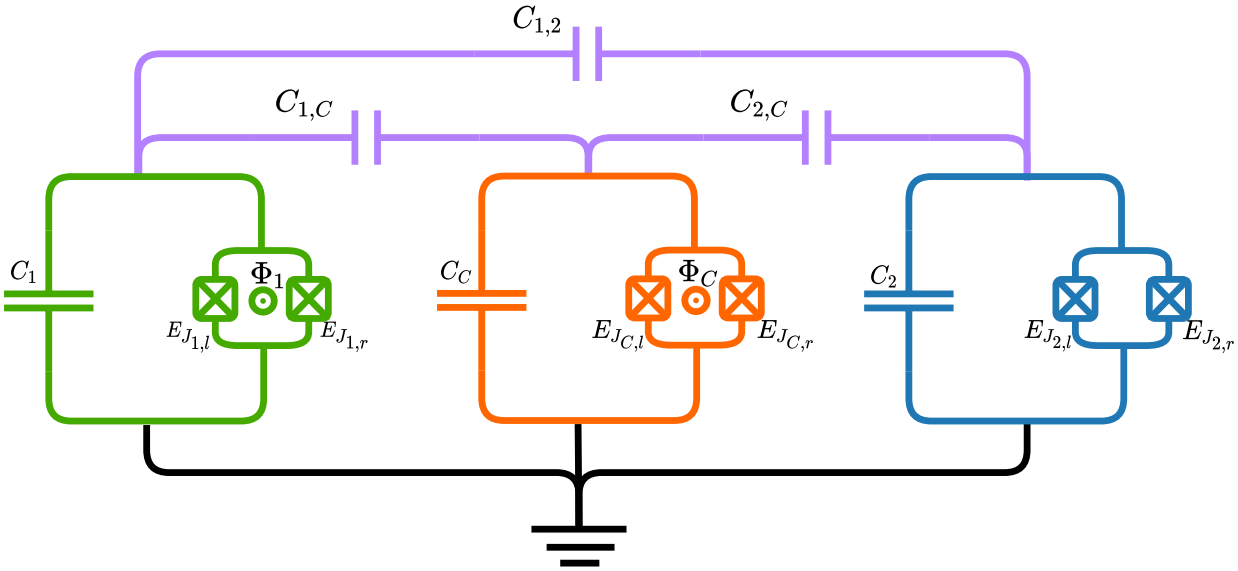

Source: The author.

qubit-coupler coupling is 1fF and the qubit-qubit capacitive coupling is closer to 0.01fF [62]. Applying the second quantization to this simplified Hamiltonian we can write it in terms of the creation and annihilation operators as done for the case of a single artificial atom. This process leads to the Hamiltonian,

$$H = \sum_{i=1,2,c} \left(\omega_i a_i^\dagger a_i + \frac{\alpha_i}{2} a_i^\dagger a_i^\dagger a_i a_i \right) + \sum_{j=1,2} g_j \left(a_j^\dagger a_c + a_j a_c^\dagger \right) + g_{12} \left(a_1^\dagger a_2 + a_1 a_2^\dagger \right), \tag{5.3}$$

with ω_i the qubit frequency and α_i the anharmonicity. g_i denotes the coupling frequency between the coupler and the i-th qubit and g_{12} the capacitive coupling between qubits 1 and 2. To simplify the notation, the hats ($\hat{}$) in the operators will be omitted from now on, and we assume $\hbar = 1$.

The first term in Eq.(5.3) represents the energy spectrum of the i-th qubit, with ω_i the energy difference between the states $|0\rangle_i$ and $|1\rangle_i$. The α_i parameter is the anharmonicity of each qubit. The second and third terms describe the interaction between the qubits, where the operators $a_j a_k^\dagger$ models the excitation of one mode of the j-th atom, with the consequent annihilation of one excitation in the k-th atom. This kind of term will conserve the total number of excitations on the circuit. The rates g_i and g_{12} will define how fast those

Figure 13 – Schematic representation of the circuit studied. The qubits Q_1 and Q_2 are coupled to a central superconducting loop C via the coupling frequencies g_1 and g_2. There is also a capacitive coupling (g_{12}) between Q_1 and Q_2.

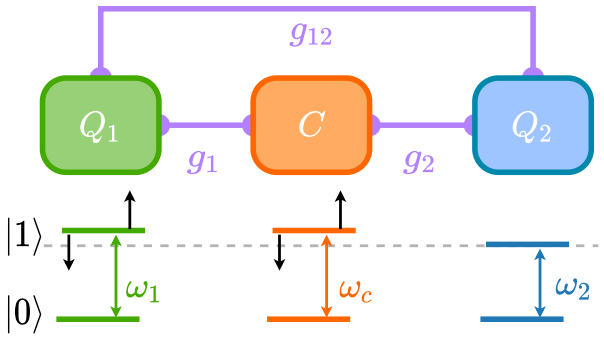

Source: The author.

interactions occur. It is important to notice that, $g_i \gg g_{12}$, since the capacitances C_{iC} are also much greater than C_{12} .

In Figure 13 we can see the schematic representation of the interactions that occur in our system and the representation of the energy levels of each qubit. As we can see, only ω_1 and ω_C can be changed, due to the absence of an external flux to control ω_2. Since frequency ω_2 is fixed, a fundamental part of the analysis of our circuit will be finding ways to tune Q_1 and C in order to control the interactions of the circuit to engineer the desired dynamics.

Chapter 6

Transistor dynamics

Once described the essential components of the circuit and defined its Hamiltonian, we can proceed to simulate its dynamics and analyze the system behavior. In this chapter, we demonstrate why the circuit is analogous to a classical transistor and demonstrate how it could be used to control the information flux. Also, we present the techniques used to simulate it.

6.1 Simulations and numerical methods

As discussed in Section 3.3, the dynamics of a quantum closed system is ruled by Schrödinger Equation (2.1), and by solving it we can completely describe the system dynamics. In theory, this equation could be solved simply by diagonalizing the Hamiltonian matrix, however, the level structure of our system is so complex, that analytical diagonalization is unfeasible. This difficulty forces us to resort to numerical methods when studying our system.

In our work, the numerical solution of the Schrödinger equation is calculated using the Quantum Toolbox in Python (QuTiP) [63, 64], a Python library specifically meant for numerical simulations of quantum optics and quantum information systems. To represent a quantum system, QuTiP describes both, quantum operators and states, as quantum objects (`Qobj`) which are sparse matrices in a Hilbert space of finite dimension [63]. This representation allows doing a wide range of operations needed to represent/manipulate quantum systems, such as matrix multiplication, tensorial products, conjugation, etc.

Once the Hamiltonian is written, QuTiP offers a number of routines to numerically solve the Schrödinger equation. These routines are accessed through the function `sesolve` which solves the quantum dynamics and returns the occupation probabilities for a desired state. There are also routines for solving the dynamics considering the system interaction with the environment, i.e., to solve the master equation, which is achieved, e.g., by using the function `mesolve`. The reader interested in further details on the effects of energy loss in quantum systems and how they will affect our system, can see the Appendix C where we treat the dissipative dynamics.

As mentioned above, QuTiP quantum objects are sparse matrices of finite dimension, however, the quantum operators a and $a^\dagger$ used in Equation (5.3) to describe the system Hamiltonian are infinite-dimensional. Once it is not possible to handle numerical calculations on infinite-dimensional matrices, we need to truncate the computational space of our problem to solve the dynamics with QuTiP. Since our system does not consider external sources, the initial number of excitation will be conserved. Then, we can truncate the system dimension with no loss of information.

It is important to highlight that the states and operators of our simulations will be defined using tensorial products. In the simulations, the total Hilbert space will be composed by the tensorial product of the spaces for each component, respecting the order $\mathcal{H} = \mathcal{H}_{Q_1} \otimes \mathcal{H}_C \otimes \mathcal{H}_{Q_2}$. Therefore, throughout the text, this same order will be implicit for all operators and states.

Figure 14 – Schematic representation of a bipolar-junction-transistor (BJT). In this type of transistor, two semiconductors of one type are separated by a thin layer of a different semiconductor. The three regions are called collector, base and emitter, with the base being the central part. In this schematic, the emitter is the part where the currents will be flowing *out* and collector the region where the charges flow *in*.

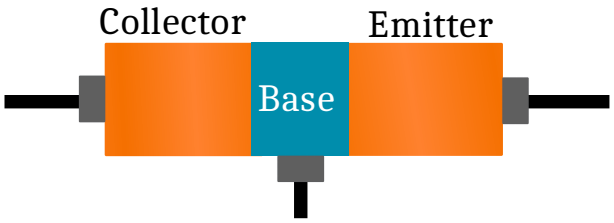

Source: The author.

6.2 A brief review on the classical transistor

In this work, we are interested in describing a quantum device that has the same properties as a classical transistor. However, classical transistors form a wide range of electrical components, with several different applications and constructions [65]. Then, it is fundamental to define which kind of transistor we aim to simulate and which applications it could have.

The class of transistors here analyzed is called a bipolar-junction-transistor (BJT), and their schematic representation can be seen in Figure 14 where two semiconductors of one type (P or N) are separated by a thin layer of another semiconductor of the opposite type [65]. In these transistors, the central region is called base and the other two are called collector and emitter. One should notice that the roles of emitter and base may vary depending on the type of semiconductor used. However, for our study, it is sufficient to assume the emitter as the region where the charges flow *out*, and the collector as the region where the charges flow *in*.

Although being used in several applications as an amplifier of signal [66], the application we discussed here, is the effect of an electrical switch. Any switch can be understood as a device that has two well-defined different states. Once in the off state, the switch acts as a cut in the electrical circuit, preventing the current to flow in the circuit. On the other hand, when in the on state, the switch acts as a shorted circuit and the current can pass with little resistance [66]. In the transistor, the switching between the on and off states can be done by applying a current to the base. If no current is applied in the base, it acts as a barrier and no current can flow through the circuit (off state). Once applying sufficient current, the base can become saturated and allow the passage of current from the emitter to the collector (on state).

This switching behavior of classical transistors has been one of the main reasons why

such devices were fundamental to build modern computers. The capability of efficiently controlling electricity with electricity unveiled a vast world of interactions that could be engineered to develop the classical gates fundamental to do computation. It is precisely this ability to control the passage of information conditioned to the state of a system, that we seek to emulate with our quantum transistor.

6.3 Effective dynamics for a two level system

The effective dynamics is a good approach to describe how the system evolves in time. By using this strategy we can find out a simplified version of driving Hamiltonian, what allow us to find the optimal parameters for implementing a given quantum task. The first approach we will use is considering the physical qubits of our circuit as perfect two-level systems. Such assumption was already considered in previous works for similar circuits [62, 67–74]. Once the qubits are anharmonic systems, the energy difference between the transitions should be high enough to prevent the qubit from populating the higher levels. Therefore, the effects of these higher levels could be neglected. It is indeed truth that no excitation to the higher levels will occur. However, as we shall see, despite not being populated, the third level of energy does play a fundamental role in the effective dynamics of the system.

To describe the system as a two level perfect system, first we replace the infinite-dimensional operators a and $a^\dagger$ by the two level raising/lowering operators $\sigma^\pm$ in Eq. (5.3)

$$H = \sum_{i=1,2} \omega\sigma_i^1 + \omega_c\sigma_c^1 + g_i(\sigma_i^+\sigma_c^- + h.c.) + g_{12}(\sigma_1^+\sigma_2^- + h.c.), \tag{6.1}$$

where $\sigma_i^+ = |1\rangle_i \langle 0|$ and $\sigma_i^- = |0\rangle_i \langle 1|$, such that in this notation we define the projectors $\sigma_i^0 = |0\rangle_i \langle 0|$ and $\sigma_i^1 = |1\rangle_i \langle 1|$. To simplify the calculations, we assumed $\omega_1 = \omega_2 = \omega$, an experimentally feasible frequency configuration for the qubits.

To calculate the effective Hamiltonian, first we have to write Eq. (5.3) in interaction picture. To do that, let $H_0 = \omega(\sigma_1^1 + \sigma_2^1) + \omega_c\sigma_c^1$ be the unperturbed Hamiltonian. The interaction picture for H can be found, using the unitary transformation

$$H_I = UHU^\dagger - H_0 = e^{-iH_0t}He^{iH_0t} - H_0, \tag{6.2}$$

to find the resulting Hamiltonian

$$H_I = g\left(\sigma_1^+ + \sigma_2^{(+)}\right)\sigma_c^- e^{i\Delta t} + g\left(\sigma_1^- + \sigma_2^-\right)\sigma_c^+ e^{-i\Delta t} + g_{12}\left(\sigma_1^+\sigma_2^- + h.c.\right), \tag{6.3}$$

where $\Delta = \omega - \omega_c$ and where are adopting, $g = g_1 = g_2$. Now, we can use Eq.(3.23) to derive the effective Hamiltonian. The details of this deduction can be seen in Appendix D, for now, it is worth to mention that the effective Hamiltonian is

$$H_{eff} \approx -iH_I(t)\int_0^t H_I(t')dt', \tag{6.4}$$

in which the product of $H_I(t)$ with its integral will result in a large amount of terms, some of them proportional to $\exp(\pm 2i\Delta t)$, some to $\exp(\pm i\Delta t)$ and some time independent. To simplify the Hamiltonian, we remember that $|\Delta| \gg g$, this means that terms with any dependency on time will be highly oscillatory and on average will not contribute to the dynamics. Then, we can remove them from the Hamiltonian to find

$$\begin{aligned} H_{eff} \approx & \frac{g^2}{\Delta}\left[(\sigma_1^1+\sigma_2^1)\sigma_c^0-(\sigma_1^0+\sigma_2^0)\sigma_c^1+(\sigma_1^-\sigma_2^++\sigma_1^+\sigma_2^-)(\sigma_c^0-\sigma_c^1)\right] \\ & +g_{12}(\sigma_1^-\sigma_2^++\sigma_2^-\sigma_1^+). \end{aligned} \tag{6.5}$$

In Eq. (6.5), it is possible to separate the obtained terms in two classes concerning qubit operators. The first are the phase terms, that do not promote changes in the population of the qubits but apply a phase to a defined state. Here, such terms are the ones proportional to the population operators $\sigma_{1,2}^j$. The second class are the hopping terms, they will describe the exchange of excitation between Q_1 and Q_2. For this reason they have the form $\sigma_{1,2}^{\pm}\sigma_{2,1}^{\mp}$. These interaction terms are the fundamental ones in the transistor description and therefore are the main elements we will focus on.

This simple effective Hamiltonian already has a useful property that can be used to deepen our understanding of the circuit and improve the information control. Since Δ is a tunable parameter, we can make $\Delta = -g^2/g_{12}$ to find a condition that completely blocks the transference of information between the qubits. By applying this condition, we find

$$H_{eff} \approx g_{12}(\sigma_1^0+\sigma_2^0)\sigma_c^1-g_{12}(\sigma_1^1+\sigma_2^1)\sigma_c^0+g_{12}(\sigma_1^+\sigma_2^-+\sigma_1^-\sigma_2^+)(\mathbb{1}_c+\sigma_c^1-\sigma_c^0), \tag{6.6}$$

with $\mathbb{1}_c$ the identity matrix for the coupler. Analyzing the third term of Eq.(6.6) one realizes that, when the coupler is initialized in the state $|0\rangle$, the term σ_c^0 will cancel out with the identity matrix. Then, all hopping terms will be removed, and only phase terms will be present. If on the other hand, we have $|1\rangle_c$, the population term σ_c^1 will add with $\mathbb{1}_c$ and the exchange of populations will appear. This behavior gives rise to a state-dependent on/off dynamics of the system, a characteristic of classical transistor.

This effective Hamiltonian approach is convenient to find the solution of the Schrödinger equation for the system, where the evolution operator reads $U = e^{-itH_{eff}}$. To do that, first we divide Eq.(6.6) in two terms, H_{ph}, which is the phase term and H_{hop} the hopping term. Therefore, we write $H_{eff} = H_{ph} + H_{hop}$. Once $[H_{hop}, H_{ph}] = 0$, the evolution of the state will be

$$|\Psi(t)\rangle_I = e^{-itH_{ph}}e^{-itH_{hop}}|\Psi(0)\rangle. \tag{6.7}$$

Eq. (6.7) shows us that the evolution of the hopping part will be independent of the global phase applied. If we set the initial state of the coupler to be $|1\rangle_c$, the hopping term will be

$$H_{hop} = 2g_{12}(\sigma_1^+\sigma_2^- + \sigma_1^-\sigma_2^+). \tag{6.8}$$

Using the basis $\{|0,1\rangle, |1,0\rangle\}$, we can write this term in the matrix form

$$H_{hop} = 2g_{12}\begin{bmatrix} 0 & 1 \\ 1 & 0 \end{bmatrix}, \tag{6.9}$$

that have the eigenenergies $E_{\pm} = \pm 2g_{12}$ and the eigenstates $|\Psi_{\pm}\rangle = (|0,1\rangle \pm |1,0\rangle)/\sqrt{2}$. Now, by solving $|\Psi(t)\rangle_{hop} = e^{-iH_{hop}t}|\Psi(0)\rangle$ we can find the hopping dynamics. As an example, let $|\Psi(0)\rangle = |1,0\rangle_{1,2}|1\rangle_c$, then we find

$$\begin{aligned} |\Psi(t)\rangle_{hop} &= \frac{1}{\sqrt{2}}e^{-2ig_{12}t}|\Psi_+\rangle - \frac{1}{\sqrt{2}}e^{2ig_{12}t}|\Psi_-\rangle \\ &= \frac{e^{-2ig_{12}t} - e^{2ig_{12}t}}{\sqrt{2}}|0,1\rangle + \frac{e^{-2ig_{12}t} + e^{2ig_{12}t}}{\sqrt{2}}|1,0\rangle \\ &= \cos(2g_{12}t)|0,1\rangle - i\sin(2g_{12}t)|1,0\rangle . \end{aligned} \tag{6.10}$$

This shows that during the dynamics, both estates $|1,0\rangle$ and $|0,1\rangle$ will be populated in alternated times. After the time interval $t_{tr} = \pi/g_{12}$ our system will be in the state $|\Psi(t)\rangle_{hop} = |0,1\rangle_{1,2}|1\rangle_c$ with maximal probability, and the information will be transferred from Q_1 to Q_2 conditioned to the state of the coupler. To visualize this dynamics we can use the QuTiP library to define the operators in Eq.(6.6) and numerically solve the effective dynamics. In those simulations, we will assume the parameters as seen in Table 1. These are similar to the parameters used in the experiment that demonstrated the transistor dynamics [75].

Table 1 – Parameters used in the numerical simulations of our system. All values were based on the experimental values used in [75], however, they are not equal.

ω(GHz)			α(MHz)			Coupling (MHz)		
Q_1	Q_c	Q_2	Q_1	Q_c	Q_2	g_1	g_{12}	g_2
4.628	5.741	4.620	-210	-370	-240	122	12	105

As can be seen in Figure 15, when the initial state of the circuit is $|\Psi_0\rangle = |1\rangle_1|0\rangle_C|0\rangle_2$ the system state remains unchanged during the dynamics of the system, which means we have the blockade of the information flow between Q_1 and Q_2. Here, this case is called the "off" state of the transistor. In this figure, the σ_i^j, represent the population of the i-th qubit in the j-th state. On the other hand, if we prepare the system in the initial state $|\Psi_0\rangle = |1\rangle_1|1\rangle_C|0\rangle_2$, we will have the "on" state of the transistor. As we can see in Figure 16, the excitation initially in Q_1 will be transferred to Q_2 after an interaction time of $\approx$ 65ns, while the coupler state remains in $|1\rangle$. These results demonstrate the concept of transference of information conditioned to the initial state of the coupler. It is possible then, to conclude that the coupler works as the base of a quantum transistor and Q_1 and Q_2 being the collector and emitter. Here, however, due to the quantum aspect of our system, the information could be transferred from Q_1 to Q_2 and vice-versa. Therefore, both Q_1 and Q_2 can work as the emitter or the collector.

Figure 15 – Effective dynamics of the system in the "off" state. Using $|0\rangle_c$ as the initial state, our system is unable to perform the change between Q_1 and Q_2. To obtain this transference blocking we used the condition $\Delta = -g^2/g_{12}$. The other parameters of the system remain the same as in Table 1.

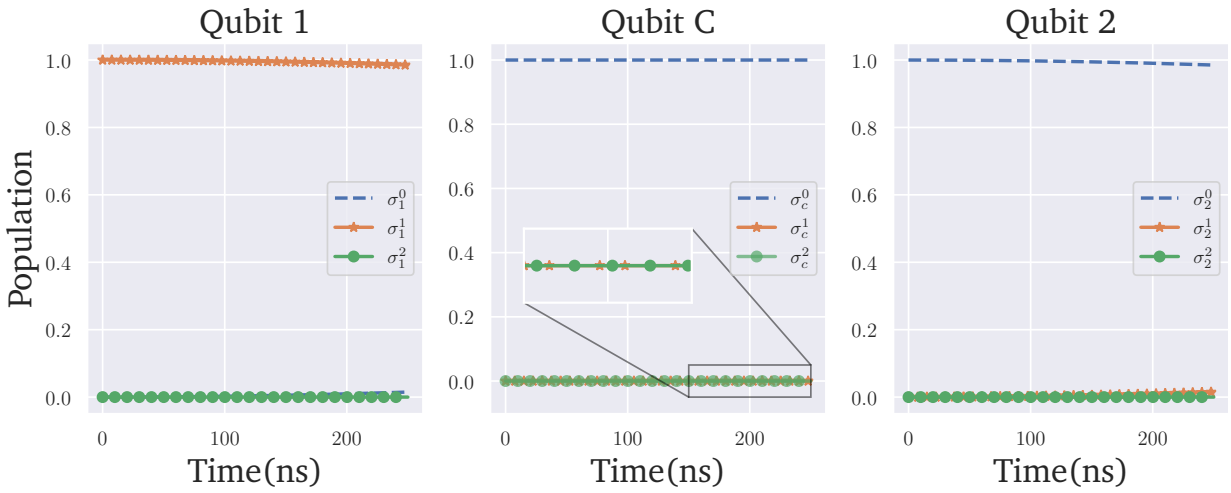

Source: The author.

Figure 16 – Effective dynamics of our system in the 'on' state in the two level approximation. Using $|1\rangle_c$ as the initial state, we obtain a population transference between Q_1 and Q_2 maintaining the coupler state unchanged. The parameters used in this simulation can be seen in Table 1.

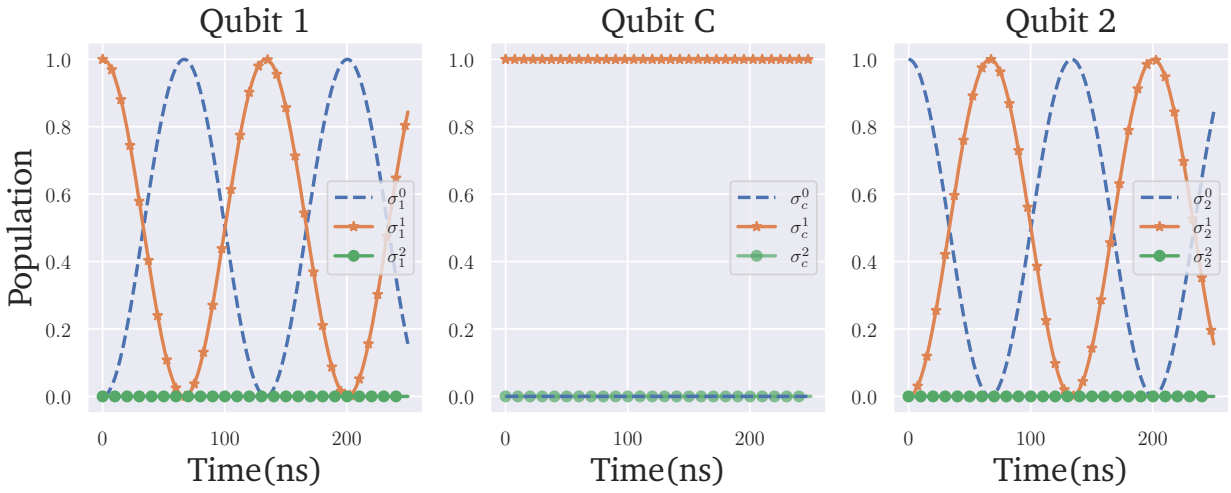

Source: The author.

Once defined the effective dynamics, describing the behavior of the effective coupling as a function of the detuning and other parameters, the next task to be done is its experimental investigation. Such parameter (effective coupling) can be understood as the effective rate of exchange of energy in our circuit and can be obtained from the interaction terms in Eq.(6.5)

and reads

$$g_{eff}^{|n\rangle_c}(\Delta) = g_{12} + (-1)^n \frac{g^2}{\Delta}. \tag{6.11}$$

In this expression, the variable 'n' denotes the coupler state, and it makes clear that we have different effective dynamics depending on the coupler state $|n\rangle_c$, $n = 0, 1$. Such equation was previously deduced in [70], however, as we will see, the assumption made of neglecting the third level will result in an incomplete description of the real system evolution.

6.4 Total dynamics of the transistor

In order to confirm that the effective dynamics derived previously is describing the behaviour of the system, we can proceed to simulate the total Hamiltonian for the circuit to analyze its dynamics. Remembering the total Hamiltonian derived in Section 4.2, we have

$$H = \sum_{i=1,2,c} \left(\omega_i a_i^\dagger a_i + \frac{\alpha_i}{2} a_i^\dagger a_i^\dagger a_i a_i \right) + \sum_{j=1,2} g_j \left(a_j^\dagger a_c + a_j a_c^\dagger \right) + g_{12} \left(a_1^\dagger a_2 + a_1 a_2^\dagger \right). \tag{6.12}$$

Using QuTiP matrices to define this Hamiltonian, we can simulate its dynamics using the appropriate solver, and plot the results, to see the behavior of the quantum transistor. The parameters used are the same as those in Table 1 for the effective dynamics.

First we plot, in Figure 17, the dynamics for the initial "off" state of the transistor, $|\Psi_0\rangle = |0\rangle_1 |0\rangle_C |1\rangle_2$. As expected, there is no transference of the excitation in Q_2 to Q_1. Then, using the "on" state $|\Psi_0\rangle = |0\rangle_1 |1\rangle_C |1\rangle_2$, we see in Figure 18 the transference of information conditioned to the coupler state.

We should remember, that, in this conservative case, our system conserves the total amount of excitation, with one qubit only being excited in exchange for the decaying of the other qubit. In addition, we can see, that neither the qubits nor the coupler, are ever excited to states higher than the first excited. Therefore, we verify that it is sufficient to truncate the numerical space for the simulations in 4 dimensions since no excitation to the $|3\rangle$ state should be expected.

By comparing Figure 16 for the two-level approximation and Figure 18 the total Hamiltonian one realizes that the exchange of excitation is occurring in the effective dynamics much faster than the total Hamiltonian predicts. While in the total Hamiltonian, the inversion occurs for $t \approx 160$ns, in the effective Hamiltonian this transference occurs at $t \approx 65$ns, less than half the expected time. Such difference is one of the aspects pointing out that the two-level effective Hamiltonian description is not completely valid. The solution to this discrepancy will be detailed in next chapter.

Figure 17 – Simulation of the dynamics for the complete Hamiltonian, using the experimental parameters defined in Table 1 and the initial state $|1,0\rangle_{1,2}|0\rangle_c$. In this state, the excitation in Q_1 remains in this state through all the dynamics. For this reason this is called the off state of the transistor. The parameters used in this simulation can be seen in Table 1.

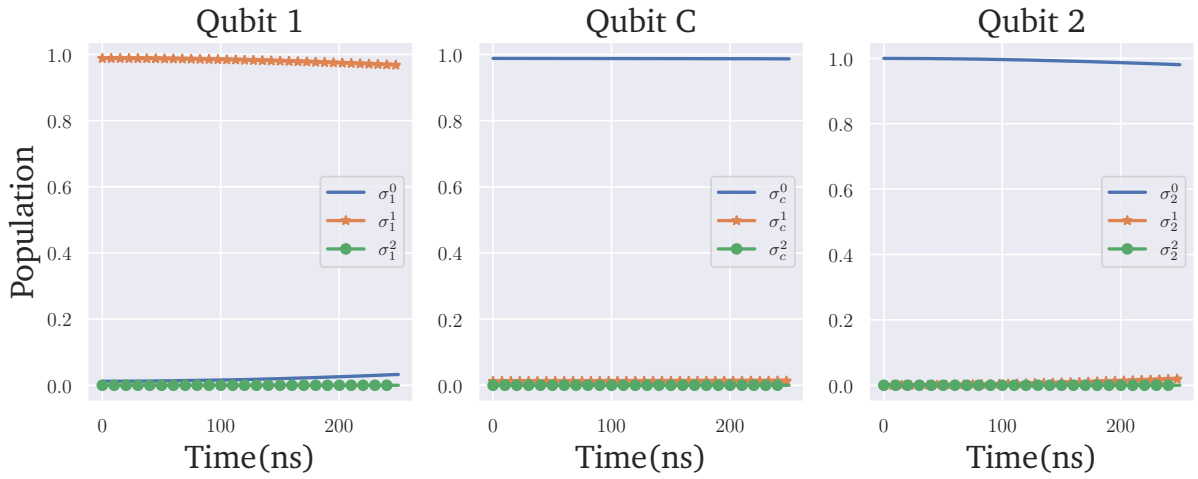

Source: The author.

Figure 18 – Dynamics of the populations of the qubits and coupler, considering $|\psi(0)\rangle = |1,0\rangle_{1,2}|1\rangle_c$ as the initial state to solve Equation (5.3), we can verify the transference of states between the logical qubits. Differently form the effective Hamiltonian, here we have a non-zero probability of populating the higher excited states or our system. The parameters used in the simulation are in Table 1.

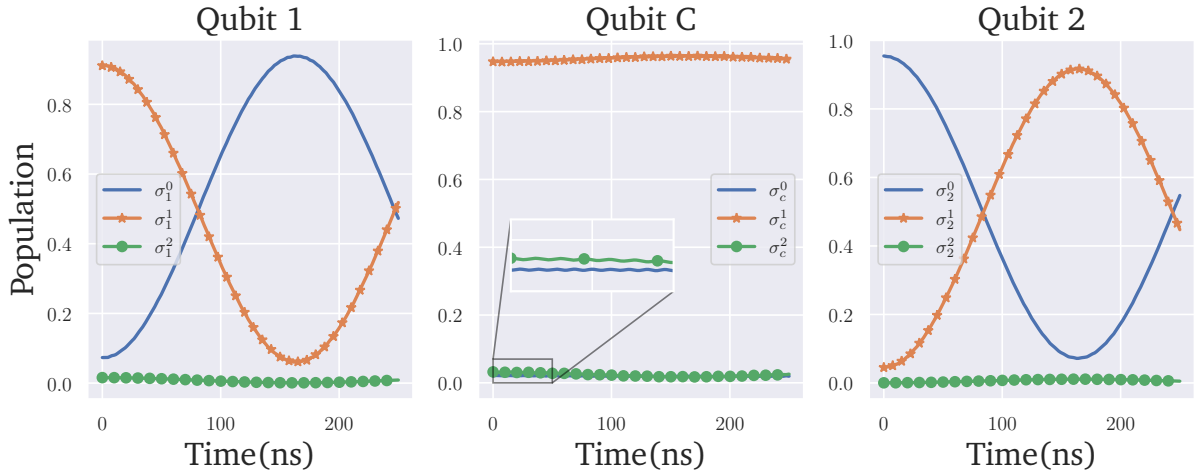

Source: The author.

Chapter 7

The effective dynamics of a qutrit system

This chapter is focused on explaining the new approach for describing the effective dynamics of our system of three artificial atoms in the configuration shown in Figure 12. This will be done using the same tools of effective dynamics, but now in a system of qutrits. The considerable gain in the number of terms will be balanced out with a more precise description that will allow us for a deeper understanding of the circuit.

7.1 Effective Hamiltonian of the qutrit

If a qubit is a quantum system that can store information in two states, it is also valid to define the qutrit as the system that stores information in three levels. We could also generalize this concept for a d-dimensional qudit [76]. As mentioned in the previous chapters, the anharmonic oscillators used in superconducting circuits are usually treated as two-level systems, due to the role that the anharmonicity has on preventing population of the higher levels of energy. However, despite not being populated, such higher levels still exist in the system and this presence will affect the dynamics.

To verify how this change occurs, we will again calculate the effective dynamics of the system. The complete algebraic passages in this process can be seen in Appendix D. To distinguish the three and two level approaches, entities that considers the system as a qutrit will be denoted with a tilde (˜). Similarly as in Section 6.3, we start with the total Hamiltonian Eq.(5.3), and define $\tilde{H}_0 = \sum_{i=1,2,c}\left(\omega_i\, a_i^\dagger a_i + \frac{\alpha_i}{2}\, a_i^\dagger a_i^\dagger a_i a_i\right)$ as the unperturbed Hamiltonian and use the unitary operator $U(t) = e^{-\mathrm{i}\tilde{H}_0 t}$ to write the complete Hamiltonian in the interaction picture. The key difference will be the definition of the population operators Σ_i to describe the populations in our qutrits as

$$a_i \to \Sigma_i^- = \sum_{k=1}^{2} \sqrt{k}\,|k-1\rangle\langle k|\,, \qquad a_i^\dagger \to \Sigma_i^+ = \sum_{k=1}^{2} \sqrt{k}\,|k\rangle\langle k-1|\,. \tag{7.1}$$

With this operators, we can show that the transformation $H_I = UHU^\dagger - H_0$ will lead to the Hamiltonian in the interaction picture

$$\begin{aligned}\tilde{H}_I = &\sum_{i=1,2} g_i\left(U^\dagger(t)\Sigma_i^+ U(t) U^\dagger(t)\Sigma_c^- U(t) + h.c.\right)\\ &+ g_{12}\left(U^\dagger(t)\Sigma_1^+ U(t) U^\dagger(t)\Sigma_2^- U(t) + h.c.\right).\end{aligned} \tag{7.2}$$

Working out this expression, we can define the operators $P_{nm}^{(i)} = |n\rangle_i\langle m|$, to write the Hamiltonian as

$$\tilde{H}_I = H_{1,c}(t) + H_{2,c}(t) + H_2(t), \tag{7.3}$$

where

$$\begin{aligned}H_{k,c}(t) = g_k\big[&e^{\mathrm{i}(\omega_k-\omega_c)t} P_{10}^{(k)} P_{01}^{(c)} + e^{\mathrm{i}(\omega_k-\tilde{\omega}_c)t}\sqrt{2} P_{10}^{(k)} P_{12}^{(c)}\\ &+ e^{\mathrm{i}(\tilde{\omega}_k-\omega_c)t}\sqrt{2} P_{21}^{(k)} P_{01}^{(c)} + 2e^{\mathrm{i}(\tilde{\omega}_k-\tilde{\omega}_c)t} P_{21}^{(k)} P_{12}^{(c)} + h.c.\big]\end{aligned} \tag{7.4}$$

and

$$\begin{aligned}H_2(t) = g_{12}\big[&e^{\mathrm{i}(\omega_1-\omega_2)t} P_{10}^{(1)} P_{01}^{(2)} + e^{\mathrm{i}(\omega_1-\tilde{\omega}_2)t}\sqrt{2} P_{10}^{(1)} P_{12}^{(2)}\\ &+ e^{\mathrm{i}(\tilde{\omega}_1-\omega_2)t}\sqrt{2} P_{21}^{(1)} P_{01}^{(2)} + 2e^{\mathrm{i}(\tilde{\omega}_1-\tilde{\omega}_2)t} P_{21}^{(1)} P_{12}^{(2)} + h.c.\big],\end{aligned} \tag{7.5}$$

with $k = 1, 2$ and $\tilde{\omega}_i = \omega_i + \alpha_i$.

To simplify our calculations we assume the resonance of Q_1 and Q_2, $\omega_1 = \omega_2 = \omega$. We also consider $\alpha_1 = \alpha_2 = \alpha$. This is a valid approximation, once the difference between α_1 and α_2 in our experimental setup is much smaller than α_1 and α_2. Then, we find the final expression for the Hamiltonian in the interaction picture

$$\begin{aligned}\tilde{H}_I = H_0 + \sqrt{2}g_{12}\left[e^{it\alpha}\left(P_{21}^{(1)}P_{01}^{(2)} + P_{01}^{(1)}P_{21}^{(2)}\right) + e^{-it\alpha}\left(P_{12}^{(1)}P_{10}^{(2)} + P_{10}^{(1)}P_{12}^{(2)}\right)\right] \\ + \sum_{k=1,2} g_k\left[e^{i\Delta t}P_{10}^{(k)}P_{01}^{(c)} + e^{i\tilde{\Delta}t}\sqrt{2}P_{10}^{(k)}P_{12}^{(c)} + e^{i\tilde{\Delta}'t}\sqrt{2}P_{21}^{(k)}P_{01}^{(c)} + 2e^{i\tilde{\tilde{\Delta}}t}P_{21}^{(k)}P_{12}^{(c)} + h.c.\right], \quad (7.6)\end{aligned}$$

with $H_0 = g_{12}\left(P_{10}^{(1)}P_{01}^{(2)} + 2P_{21}^{(1)}P_{12}^{(2)} + h.c.\right)$ the time independent part of the Hamiltonian, and $\tilde{\Delta} = \omega - \tilde{\omega}_c$, $\tilde{\Delta}' = \tilde{\omega} - \omega_c$ and $\tilde{\tilde{\Delta}} = \tilde{\omega} - \tilde{\omega}_c$ the detunings.

Once in the interaction picture, we use Eq. (3.23) to find the effective Hamiltonian as we did in the two level case. The rotating wave approximation can be done assuming again $\Delta \gg g_1, g_2$, in addition, we also assume $\alpha, \alpha_c \gg g_{12}$ to obtain as result

$$\begin{aligned}H_{eff} = \sum_{k,m=1,2} g_k g_m\left[\frac{1}{\omega - \omega_c}(P_{10}^{(k)}P_{01}^{(m)}P_{00}^{(c)} - P_{01}^{(k)}P_{10}^{(m)}P_{11}^{(c)}) + \frac{2}{\omega - \tilde{\omega}_c}(P_{10}^{(k)}P_{01}^{(m)}P_{11}^{(c)} - P_{01}^{(k)}P_{10}^{(m)}P_{22}^{(c)})\right. \\ \left. + \frac{2}{\tilde{\omega} - \omega_c}(P_{21}^{(k)}P_{12}^{(m)}P_{00}^{(c)} - P_{12}^{(k)}P_{21}^{(m)}P_{11}^{(c)}) + \frac{4}{\tilde{\omega} - \tilde{\omega}_c}(P_{21}^{(k)}P_{12}^{(m)}P_{11}^{(c)} - P_{12}^{(k)}P_{21}^{(m)}P_{22}^{(c)})\right] \\ + \frac{2g_{12}^2}{\alpha}\left(-P_{11}^{(1)}P_{11}^{(2)} + P_{22}^{(1)}P_{00}^{(2)} + P_{20}^{(1)}P_{02}^{(2)} + h.c.\right) + g_{12}\left(P_{10}^{(1)}P_{01}^{(2)} + 2P_{21}^{(1)}P_{12}^{(2)} + h.c.\right). \quad (7.7)\end{aligned}$$

Comparing Eq. (7.7) with Eq. (6.5) it is simple to notice that the qutrit model leads to a dramatic increase in the complexity of effective dynamics. With an explicit dependency both on the anharmonicities and on the second excited state.

To verify how this new expression affects the dynamics, again we use QuTiP to simulate the effective Hamiltonian. As expected, using the initial state $|\Psi(0)\rangle = |1,0\rangle\,|0\rangle_c$ in Figure 19 we obtain the blockage of the information. Then, using $|\Psi(0)\rangle = |1,0\rangle\,|1\rangle_c$ we see in Figure 20, the transference of excitation, but now occurring after an interaction time of 140ns. In both cases the parameters used are the same seen in Table 1, the only exception being the definitions $\alpha = \alpha_1$ and $\omega = \omega_1$.

It is interesting to notice that now, the probability of the population exchange occurring is $\approx 93\%$ while in the two-level approximation such probability was closer to 100%. Plotting all the three dynamics in the same graph using the same parameters and the initial state $|\Psi(0)\rangle = |1,1,0\rangle$, we can verify in Figure 21 that the effective dynamics in the third level approximation ($\tilde{H}_{eff}$) is a better approximation to the total Hamiltonian (H_{tot}) than the two-level case. However, as we can see, the dynamics of H_{tot} tend to be slightly slower than $\tilde{H}_{eff}$. To understand the differences between the qutrit approximation and the total Hamiltonian, it is useful to consider the anharmonicities 10 times larger than the real ones. Under this regime, we see in Figure 22, a good agreement between H_{tot} and $\tilde{H}_{eff}$. The

Figure 19 – Effective dynamics in the three level approximation. In the initial state $|\Psi(0)\rangle = |1,0\rangle\,|0\rangle_c$, the blocking of information is achieved as in the previous cases. Here we consider both qubits Q_1 and Q_2 in perfect resonance, assuming $\alpha = \alpha_1 = \alpha_2 = -210$MHz and $\omega = \omega_1 = \omega_2 = 4.628$GHz. The other parameters are the same as in Table 1.

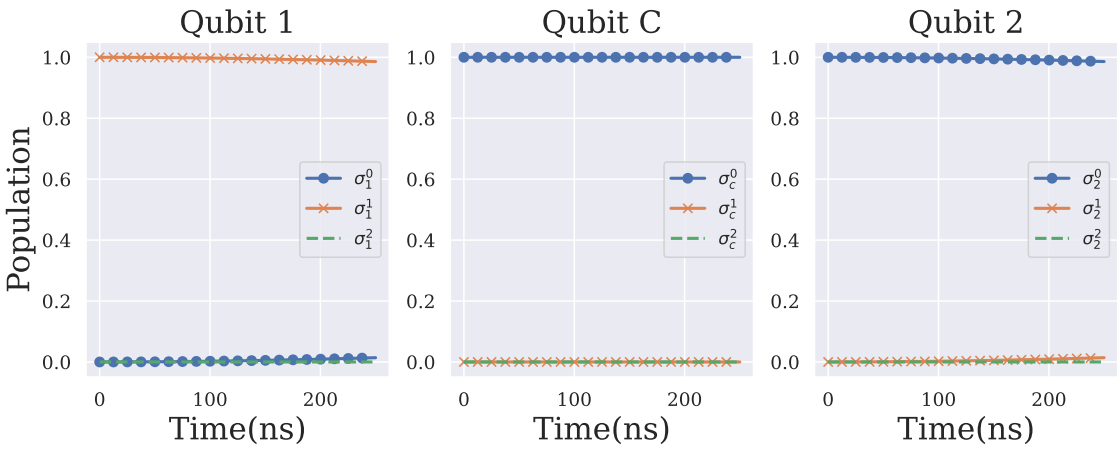

Source: The author.

Figure 20 – Effective dynamics considering three levels for the "on" state of the coupler. As expected, the conditional state transference is maintained. In this simulation we assumed $\alpha = \alpha_1 = \alpha_2 = -210$MHz and $\omega = \omega_1 = \omega_2 = 4.628$GHz, and used the parameters from Table 1.

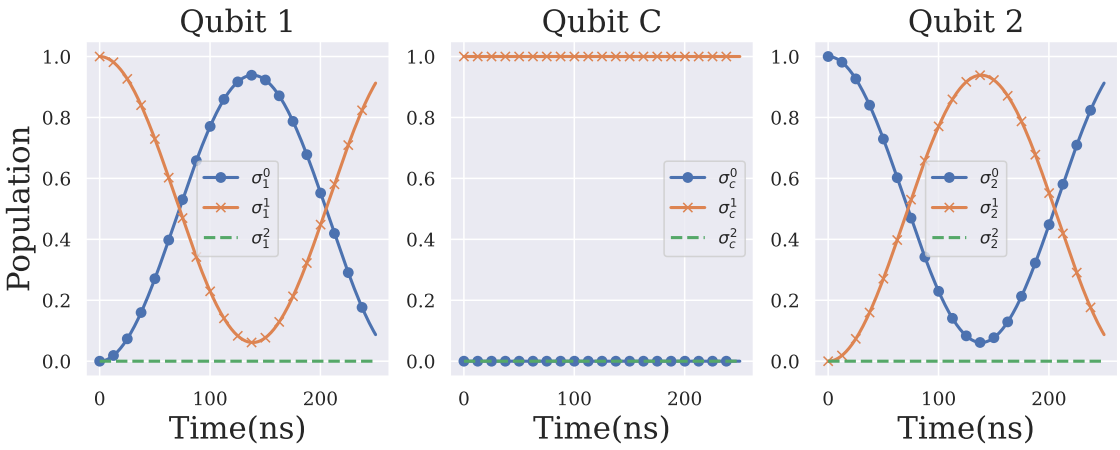

Source: The author.

two-level approximation, however, remains not a good approximation. This result has a significant implication when concerning systems of transmons qubits coupled via a coupler, that is, the impossibility to treat such a system as a real qubit when the coupler is excited. The accordance between the three Hamiltonians is only achieved when we assume an anharmonicity 100 times higher.

In principle, it could be only an experimental problem of obtaining greater anharmonicities. However such a regime would not be simple, once the anharmonicities are defined

Figure 21 – Comparison between the dynamics of the system according to all three Hamiltonians deduced in this work, the Hamiltonian without approximations (H_{tot}), the effective Hamiltonians in the two (H_{eff}) and three ($\tilde{H}_{eff}$) level approximations. All using the same parameters from Table 1 and simulated with the initial state $|\Psi(0)\rangle = |1,1,0\rangle$

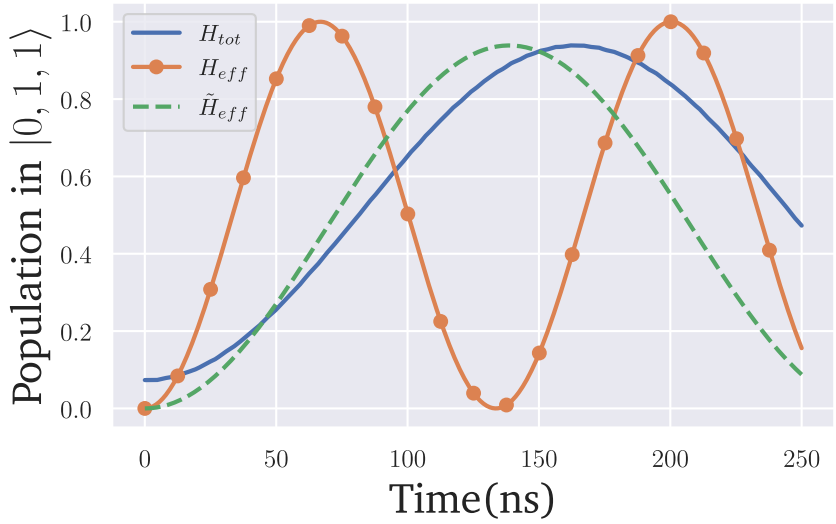

Source: The author.

in terms of the capacitive energy as $\alpha = -E_C$. The transmon regime, on the other hand, requires $E_J \gg E_C$, therefore, augmenting the anharmonicity would require the increasing of the Josephson energy. However, augmenting both E_C and E_J will also increase the transition frequency $\omega = \sqrt{8E_C E_J} - E_C$. This will lead to the problem that augmenting the anharmonicity leads to a higher transition frequency, in a balance that is not trivial to obtain.

7.2 The effective coupling in the qutrit approximation

In section 6.3 we obtained the effective coupling in the two-level approximation. However as we demonstrated, such an assumption is not valid. Once again, we can proceed to deduce the effective coupling but now, for the Hamiltonian in Eq.(7.7). It can be shown (see Appendix D) that the effective coupling can be written in the following form

$$\tilde{g}_{eff}^{|n\rangle_c}(\Delta) = g_{12} + g_1 g_2 \left(\frac{2}{\Delta - \delta_{n1}\alpha_c} - \frac{1}{\Delta} \right), \tag{7.8}$$

where δ_{n1} is the Kronecker delta, that is equal to 0 when $n \neq 1$ and is 1 when $n = 1$. As expected two different behaviors of the system are predicted. Comparing Eq. (7.8) with the effective coupling obtained in Eq. (6.11) we can notice that both equations return the same coupling when the coupler is in the ground state. This is precisely the condition that allow us to set $\Delta = -(g_1 g_2)/g_{12}$ to block the passage of information in the circuit when the transistor is off.

Figure 22 – Comparison between the dynamics of the system, under the assumption of an anharmonicity 10 and 100 times higher than the experimental values. This results demonstrate that even for a high anharmonicity, the artificial atoms in our analysis can not be completely described as a two level system. The parameters used are the ones in Table 1.

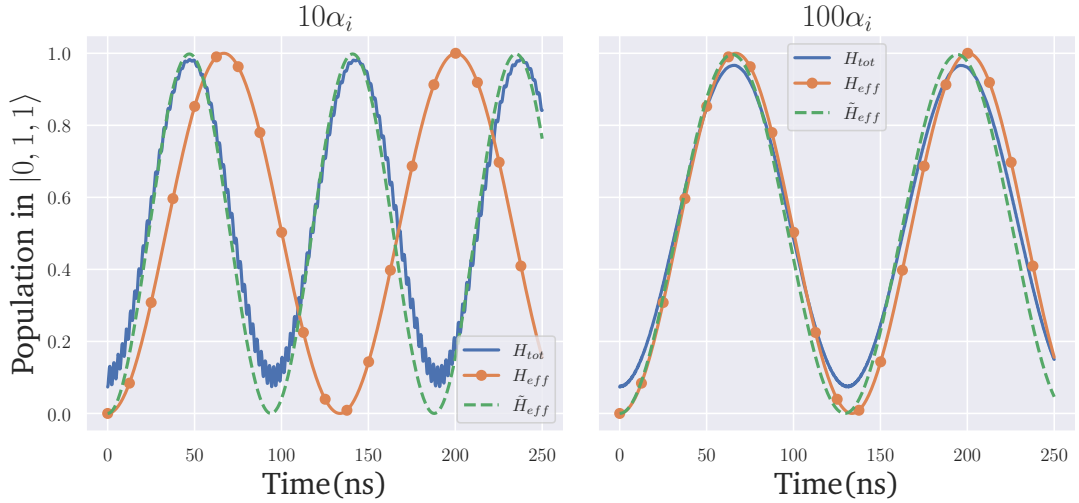

Source: The author.

The difference in our considerations will occur when the transistor is set on. In this situation, the three-level effective coupling will be shifted by a factor of $2/(\Delta-\alpha_c)$ in comparison to the two-level coupling. If we take the limit $\alpha_c \to \infty$ for the on state in Eq.(7.8) we find

$$\lim_{\alpha_c\to\infty} g_{12} + g_1 g_2 \left(\frac{2}{\Delta-\alpha_c} - \frac{1}{\Delta}\right) = g_{12} - \frac{g_1 g_2}{\Delta}, \tag{7.9}$$

and recover the effective coupling for the two level approximation when $g_1 = g_2 = g$, which is in accordance with the behavior presented in Figure 22. Thus, only for very high anharmonicities the qubit approximation is valid. Since $\Delta > \alpha$, and Δ is the tunable parameter of the system, another interesting limiting case to analyze is

$$\lim_{\Delta\to\alpha_c} g_{12} + g_1 g_2 \left(\frac{2}{\Delta-\alpha_c} - \frac{1}{\Delta}\right) = \infty. \tag{7.10}$$

In this scenario, the more close Δ gets to α_c, faster the dynamics will be, tending to an asymptotic behavior. This demonstrates that it is not possible to set the parameters in order to mitigate the effects of the third level.

In Figure 23 we plot $g_{eff}^{|n\rangle_c}(\Delta)$ and $\tilde{g}_{eff}^{|n\rangle_c}(\Delta)$ as a function of the detuning $\Delta = \omega - \omega_c$. In this graphic, we see the great impact the consideration of the third level of energy has in the effective coupling. And also helps to explain the switching pattern. To block the passage of information in the transistor, we set the detuning to ≈ 1.07GHz at the point where the

effective coupling for the ground state will be zero. Then, maintaining the same detuning, we change the coupler state to the first excited state. This will lead to a non-null effective coupling allowing the passage of information between Q_1 and Q_2.

Figure 23 – Effective coupling in the two and three level approximations as a function of the detuning. As we can see, the $|0\rangle_c$ state returns the same effective coupling. However, when the transistor is turned on, the three level approximation is shifted from the two level case. The curves of the two level approximation, where plotted using Eq.(6.11) and the parameters from Table 1. The three level approximation curves where plotted using Eq.(7.8) and the parameters in Table 1.

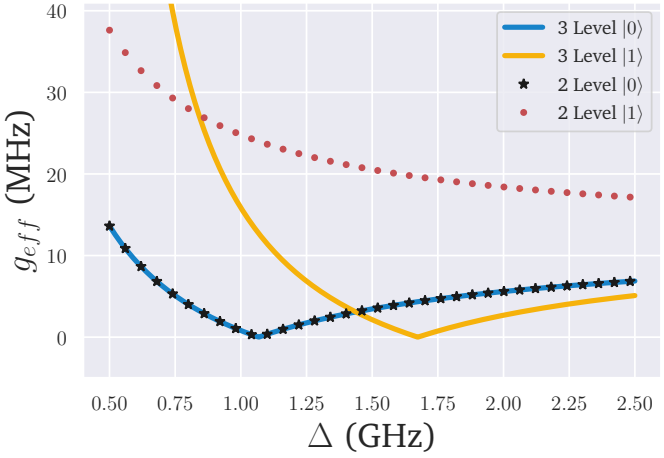

Source: The author.

This behaviour is the same obtained in the article [75] where the experimental results obtained in collaboration with a Chinese experimental team corroborate our theoretical predictions. These results can be seen in Figure 24 that use experimental parameters slightly different from the ones used previously in our work. We can notice that when the detuning is set to ≈ 1.6GHz the predicted coupling in the two-level approximation is ≈ 28MHz, a value higher than the experimentally measured 9MHz that fits the three-level effective dynamics. This fact explains the faster transition predicted by the qubit approximation observed in Figure 21.

As a last example, we can use the total Hamiltonian to map the exchange of population in the system for different coupler frequencies. This map can be seen in Figure 25 where we plot the Chevron pattern for the population transfer between Q_1 and Q_2 using the same parameters from Table 1. In this figure, we can see the region marked with a dashed line close to $\omega_c = 5.6$GHz called the *idling point*. Such a region is where the interaction between the qubits is canceled and where experimentally the measurements of the circuit are implemented. However, as we can see in Figure 26, when the coupler is set in the "on" state, the idling point is shifted to $\omega_c = 6.2$GHz, and the previously non-interacting region of $\omega_c = 5.6$GHz now promotes the exchange of excitation.

Figure 24 – Experimental results (dots) for the effective coupling, along with the two and three level approximations (solid lines). The behavior obtained is similar to the theoretical predictions seen in Figure 23. The parameters used where the same in the original paper, $g_1 = 110\text{MHz}$,$g_2 = 105\text{MHz}$, $g_{12} = 7.6\text{MHz}$, $\alpha_c = -370\text{MHz}$.

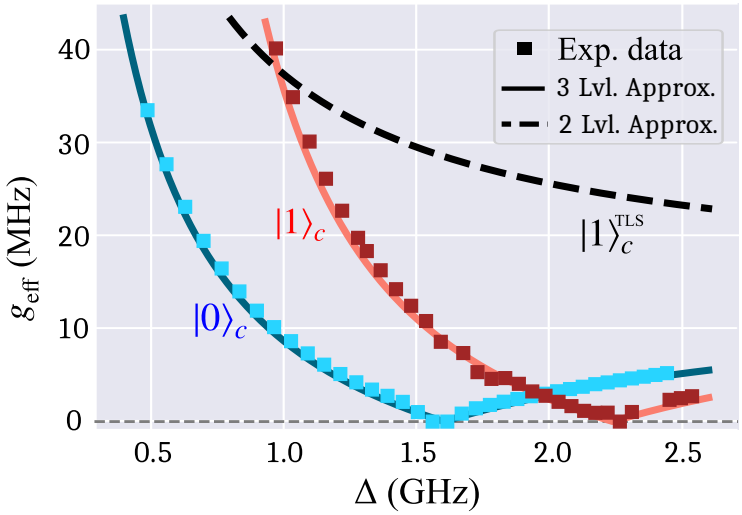

Source: Adapted from [75].

Figure 25 – Simulation of the population exchange for different frequencies of the coupler, using the total Hamiltonian and the initial state $|\Psi(0)\rangle = |0,0,1\rangle$. The white dashed line indicates the idling region, where the exchange of energy between the qubits is blocked. The parameters used can be seen in Table 1.

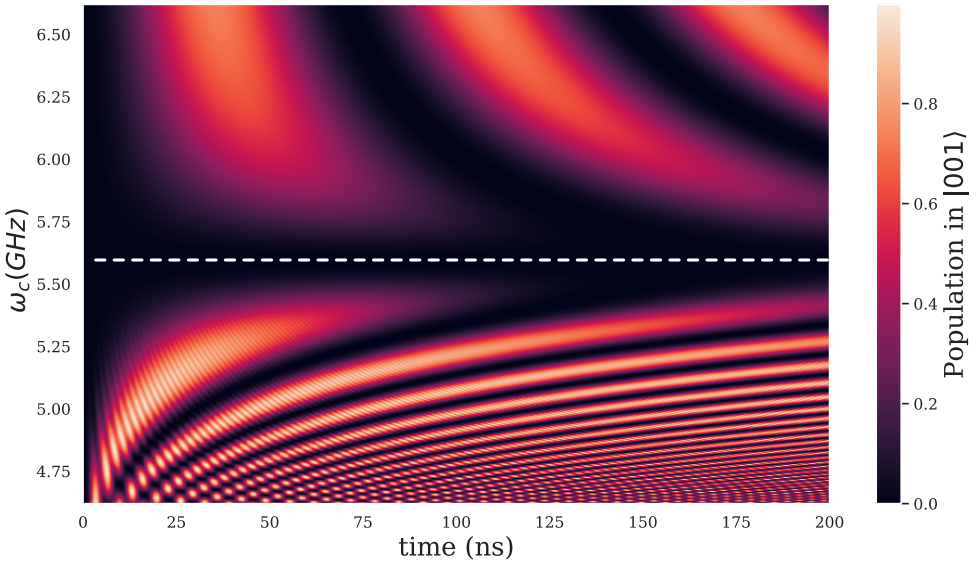

Source: The author.

Figure 26 – Simulation of the population exchange for different frequencies of the coupler, using the total Hamiltonian and the initial state $|\Psi(0)\rangle = |0,1,1\rangle$. Here, the idling point is shifted to a higher frequency. The parameters used can be seen in Table 1.

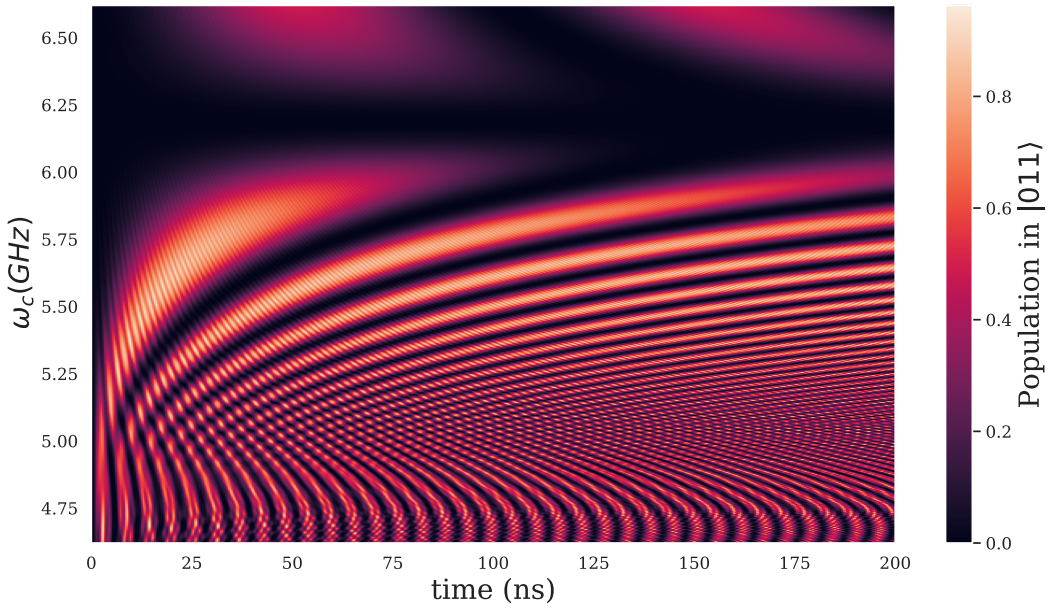

Source: The author.

Chapter 8

Conclusions

In this master thesis, we obtained two main results. First, we described the theoretical tools needed to develop and optimize a quantum transistor using superconducting qubits. In addition to this, we were able to identify and explain an unexplored effect that the third level of energy of superconducting circuits has on the dynamics of those devices. Both results were in good agreement with the experimental results.

We demonstrated that the usual description of artificial atoms as simple two-level systems was unable to accurately describe the dynamics of our quantum transistor when the coupler was excited. To solve this problem, we introduced the consideration of the third energy level in the deduction of the effective Hamiltonian, leading to more complex and accurate effective dynamics. We considered also the interaction of this circuit with its environment to describe the dissipative regime of the circuit, not described in the main text, but discussed in the Appendix C. In this analysis, we demonstrated that, given the experimental parameters, the effects of decoherence are negligible. However, this dissipative description was used to demonstrate the quantum signature of our transistor. Once in the highly dissipative regime of the coupler, the loss of coherence led to a vanishing of the transistor behavior, making clear that this system depends on its quantum characteristics to work properly.

Our results demonstrate that in the current age of artificial atoms with small anharmonicities, approximating such devices as perfect two-level systems is not an adequate description. Therefore, we believe that the consideration of the higher states or energy in superconducting qubits should be a factor of interest in further investigations on the subject, once such effects can have significant effects on the system dynamics. In addition, efforts on increasing the anharmonicities of superconducting qubits, while still maintaining the transmon regime, would be a relevant addition to the field and could lead to significant improvement in the fidelity of those devices.

We hope the results presented here will contribute positively to the development of new applications and devices in quantum computation, and could be useful in fomenting more investigations about the effects here described.

The quartic term in the Hamiltonian of a qubit

In this section we will focus ourselves in expanding the terms in the total Hamiltonian for the qubit in Eq.(4.26)

$$H = \overbrace{\omega_0 a^\dagger a}^{H_0} + \underbrace{\frac{\alpha}{12}(a+a^\dagger)^4}_{V}, \tag{A.1}$$

with $\omega_0 = \sqrt{8E_cE_J}$ and $\alpha = -E_c$. To simplify the notation, in this Appendix, we will omit the hats in the notation of the operators.

To do so, we will first write the Hamiltonian in the interaction picture, using the transformation $H_I = U^\dagger V U$ where $U = e^{-iH_0 t/\hbar}$

$$H_I = e^{iH_0 t/\hbar}\frac{\alpha}{12}(a+a^\dagger)^4 e^{-iH_0 t/\hbar}. \tag{A.2}$$

Expanding each of the terms in the Hamiltonian, we find 16 different combinations of the annihilation and creation operators,

$$\begin{aligned}
\frac{\alpha}{12} &= \left(a+a^\dagger\right)^4 && \text{(A.3)}\\
&= \left(aa + aa^\dagger + a^\dagger a + a^\dagger a^\dagger\right)^2 && \text{(A.4)}\\
&= \big(aaaa + aaaa^\dagger + aaa^\dagger a + aaa^\dagger a^\dagger && \text{(A.5)}\\
&\quad + aa^\dagger aa + aa^\dagger aa^\dagger + aa^\dagger a^\dagger a + aa^\dagger a^\dagger a^\dagger && \text{(A.6)}\\
&\quad + a^\dagger aaa + a^\dagger aaa^\dagger + a^\dagger aa^\dagger a + a^\dagger aa^\dagger a^\dagger && \text{(A.7)}\\
&\quad + a^\dagger a^\dagger aa + a^\dagger a^\dagger aa^\dagger + a^\dagger a^\dagger a^\dagger a + a^\dagger a^\dagger a^\dagger a^\dagger\big). && \text{(A.8)}
\end{aligned}$$

To understand how each term will be transformed in the interaction picture, first we calculate the result of the transformation, $e^{iH_0 t/\hbar} a e^{-iH_0 t/\hbar}$. To do that we apply the Baker-Campbell-Hausdorff formula [77],

$$e^A B e^{-A} = B + [A,B] + \frac{1}{2}[A,[A,B]] + ... \frac{1}{n!}[A,[A,...[A,B]...] + ... \tag{A.9}$$

Calculating the commutator between H_0 and the operator a , we find

$$[H_0, a] = \omega_0 a^\dagger aa - \omega_0 aa^\dagger a = \omega_0(a^\dagger a - aa^\dagger)a = -\omega_0 a. \tag{A.10}$$

Therefore, the final form of the annihilation operator in the interaction picture, will be

$$e^{iH_0 t/\hbar} a e^{-iH_0 t/\hbar} = a e^{-i\omega_0 t/\hbar}, \tag{A.11}$$

a similar approach can be used to find that the creation operator will be

$$e^{iH_0 t/\hbar} a^\dagger e^{-iH_0 t/\hbar} = a^\dagger e^{i\omega_0 t/\hbar}. \tag{A.12}$$

With those two relations, the terms in Eq.(A.3) can be find, simply applying the identity between each operator, e.g. the term

$$\begin{aligned} U^\dagger aa^\dagger aaU &= U^\dagger aUU^\dagger a^\dagger UU^\dagger aUU^\dagger aU \\ &= aa^\dagger aae^{-2i\omega t/\hbar}. \end{aligned} \tag{A.13}$$

Proceeding with this same calculation for the other 15 terms in Eq.(A.3), we will find two different classes of terms. The first ones are those with a different number of creation and annihilation operators. They will have a time dependence, that is proportional to $e^{\pm\lambda i\omega t/\hbar}$. The second class is concerning the terms with the same number of creation and annihilation operators. Those, on the other hand, will be time independent, since the exponential terms will add to remove the time dependence. To simplify this Hamiltonian, we can apply the Rotating wave approximation, to neglect all time dependent terms, since those will oscillate very fast and will not contribute to the dynamics. This approximation results in the approximate Hamiltonian

$$\begin{aligned} H_I \approx\ & aaa^\dagger a^\dagger + aa^\dagger aa^\dagger + aa^\dagger a^\dagger a \\ & + a^\dagger aaa^\dagger + a^\dagger aa^\dagger a + a^\dagger a^\dagger aa. \end{aligned} \tag{A.14}$$

Then, we can use the commutation relation $\left[a, a^\dagger\right] = aa^\dagger - a^\dagger a = \mathbb{1}$ to write these terms in the normal order $\left(a^\dagger\right)^n a^m$,

$$a^\dagger aa^\dagger a = a^\dagger(1 + a^\dagger a)a = a^\dagger a + a^\dagger a^\dagger aa, \tag{A.15}$$

$$a^\dagger aaa^\dagger = a^\dagger a(1 + a^\dagger a) = a^\dagger a + a^\dagger aa^\dagger a = 2a^\dagger a + a^\dagger a^\dagger aa, \tag{A.16}$$

$$aa^\dagger a^\dagger a = (1 + a^\dagger a)a^\dagger a = a^\dagger a + a^\dagger aa^\dagger a = 2a^\dagger a + a^\dagger a^\dagger aa, \tag{A.17}$$

$$aa^\dagger aa^\dagger = (1 + a^\dagger a)aa^\dagger = aa^\dagger + a^\dagger aaa^\dagger = 1 + 3a^\dagger a + a^\dagger a^\dagger aa, \tag{A.18}$$

$$aaa^\dagger a^\dagger = a(1 + a^\dagger a)a^\dagger = aa^\dagger + aa^\dagger aa^\dagger = 2 + 4a^\dagger a + a^\dagger a^\dagger aa, \tag{A.19}$$

Finally, using these relations, we can write the Hamiltonian of the qubit, considering both the frequency and the anharmonic term simplified using the *RWA*,

$$H_I = \frac{\alpha}{12}\left(3 + 12a^\dagger a + 6a^\dagger a^\dagger aa\right), \tag{A.20}$$

The term proportional to the identity will only add a shift of energy, and will not contribute to the dynamics, therefore it can be neglected. The term $a^\dagger a$ will be the same number operator that appears in Eq.(A.1), therefore it can be considered as a simple correction to the qubit frequency which then will be written as $\omega = \omega_0 + \alpha = \sqrt{8E_cE_j} - E_c$. Finally, the third term will describe the anharmonic effect of the Hamiltonian. It will shift the energy of each level $|n\rangle$, by an amount proportional $n\alpha/2$. In the superconducting device considered in our work, this shift will be negative and the energy difference between each level becomes smaller with the higher levels. The final for of the Hamiltonian will then be written as

$$H = \omega a^\dagger a + \frac{\alpha}{2} a^\dagger a^\dagger a a. \tag{A.21}$$

Appendix B

Complete deduction of the Hamiltonian for the superconducting circuit

The approach we will use to deduce this Hamiltonian is mainly based in the method presented in [43]. In this work, a general method is proposed to deduce any Hamiltonian for a superconducting circuit, starting from its classical Lagrangian. The first step is to identify every node in the circuit analyzed, which are the points where one or more components will connect. Then we choose the spanning three of the circuit. This spanning three is the path that will connected every node of the circuit only once. The spanning three and the fluxes ϕ_λ for each node in the circuit can be seen in Figure 27. In this circuit we also considered the two parallel Josephson junctions of each qubit as a single junction, with an energy

$$E_{J,i} = -2E_J \cos\left(\pi \frac{\tilde{\Phi}_i}{\Phi_0}\right) \cos\phi_i. \tag{B.1}$$

that depends on the external flux, as demonstrated in section 4.4.

Figure 27 – Circuit diagram with the spanning three defined to calculate the fluxes ϕ_λ passing trough each element.

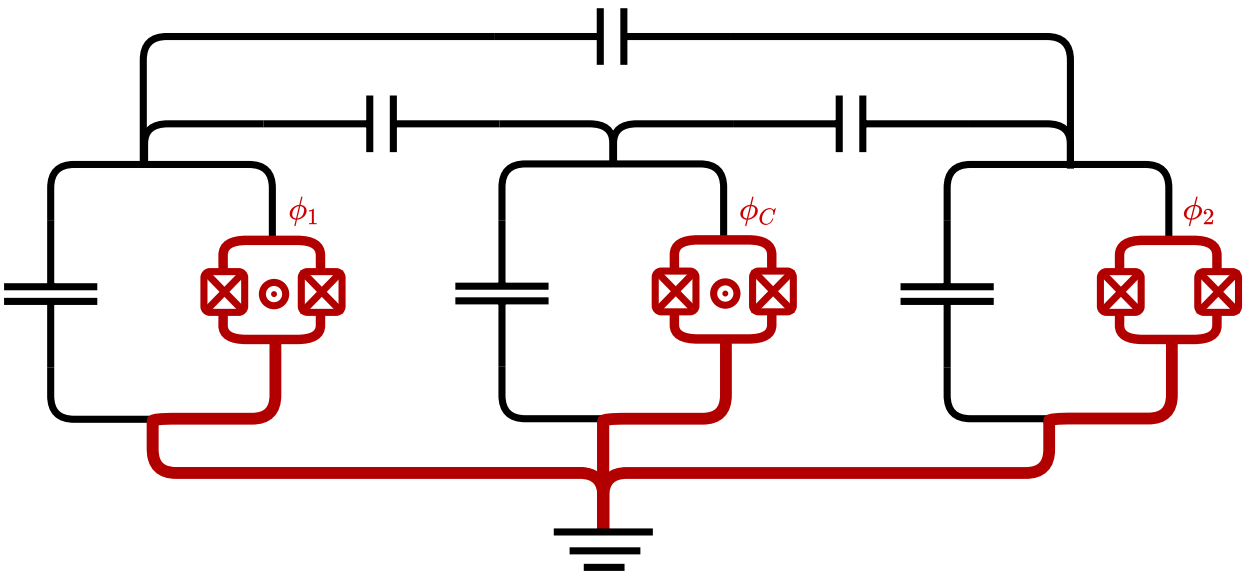

Source: The author.

Once we have defined the spanning three, we can write the flux vector and the capacitance matrix. This approach of writing the circuit elements in a matricial form is a way to simplify the notation and the calculations in circuits with a large number of components. The flux vector,

$$\vec{\phi}^T = \begin{pmatrix} \phi_1 & \phi_c & \phi_2 \end{pmatrix}, \tag{B.2}$$

is the column vector whose elements are the fluxes passing through each node of the circuit. Here, the T stands for the transpose of the vector.

We can also define the capacitance matrix as the square matrix whose nondiagonal terms $C_{m,n}$ corresponds to the capacitance that connects the nodes m and n. The diagonal

terms, consists of the sum of the capacitance that connect the respective node to the ground, in addition to the off diagonal terms of each row or column, multiplied by −1. In our case, the matrix will be written as

$$\boldsymbol{C} = \begin{pmatrix} C_1 + C_{1C} + C_{12} & -C_{1C} & -C_{12} \\ -C_{1C} & C_C + C_{1C} + C_{2C} & C_{2C} \\ -C_{12} & -C_{2C} & C_2 + C_{C2} + C_{12} \end{pmatrix}. \tag{B.3}$$

The lagrangian of the circuit can then be written as

$$\mathscr{L} = T_{cap} - U_J = \frac{1}{2}\dot{\vec{\phi}}^T \mathbf{C} \dot{\vec{\phi}} - \sum_{i=1,C,2} E_{J_i}(1 - \cos\phi_i). \tag{B.4}$$

To find the hailtonian, first we calculate the conjugate momentum

$$\vec{q} = \frac{d\mathscr{L}}{d\dot{\vec{\phi}}} = \boldsymbol{C}\dot{\phi}, \tag{B.5}$$

and then use the expression,

$$H = \dot{\vec{\phi}}^T \vec{q} - \mathscr{L} = \frac{1}{2}\vec{q}^T \mathbf{C}^{-1} \vec{q} + U_J. \tag{B.6}$$

Therefore, if $\boldsymbol{C}$ is an invertible matrix, it is simple to find the Hamiltonian. Inverting Eq.(B.3) we find

$$\mathbf{C}^{-1} = \frac{1}{\beta}\begin{pmatrix} c_{11} & c_{12} & c_{13} \\ c_{21} & c_{22} & c_{23} \\ c_{31} & c_{32} & c_{33} \end{pmatrix}, \tag{B.7}$$

where $\beta = C_1C_CC_2 + C_1C_{1C}C_{12} + C_1C_{12}C_{1C} + C_{1C}C_{12}C_C + C_1C_{1C}C_{2C} + C_1C_{12}C_{2C} + C_1C_CC_{2C} + C_{1C}C_CC_{2C} + C_{12}C_CC_{2C} + C_1C_{1C}C_2 + C_{1C}C_{12}C_2 + C_{1C}C_CC_2 + C_{12}C_CC_2 + C_1C_{2C}C_2 + C_{1C}C_{2C}C_2 + C_{12}C_{2C}C_2$, and, the terms c_{mn} are

$$c_{11} = C_2C_C + C_2(C_{1C} + C_{2C}) + C_C(C_{2C} + C_{12}) + C_{1C}C_{2C} + C_{2C}C_{12} + C_{1C}C_{12}; \tag{B.8}$$

$$c_{22} = C_1C_2 + C_1(C_{12} + C_{2C}) + C_2(C_{12} + C_{1C}) + C_{1C}C_{2C} + C_{2C}C_{12} + C_{12}C_{1C}; \tag{B.9}$$

$$c_{33} = C_1C_C + C_1(C_{1C} + C_{2C}) + C_C(C_{12} + C_{1C}) + C_{1C}C_{2C} + C_{2C}C_{12} + C_{12}C_{1C}; \tag{B.10}$$

$$c_{12} = c_{21} = C_{1C}(C_2 + C_{1C} + C_{2C}) + C_{2C}C_{12}; \tag{B.11}$$

$$c_{23} = c_{32} = C_1C_{2C} + C_{12}C_{1C} + C_{1C}C_{2C} + C_{2C}C_{12}; \tag{B.12}$$

$$c_{13} = c_{31} = C_CC_{12} + C_{1C}C_{2C} + C_{12}C_{1C} + C_{2C}C_{12}. \tag{B.13}$$

This elements can be simplified if we assume the capacitances of each qubit are much greater than the capacitances coupling qubits, which means $C_i \gg C_{jC} \gg C_{12}$. This assumption allow us to discard some terms of small magnitude in each of the elements of the matrix, leading to $\beta \approx C_1C_CC_2$, $c_{11} \approx C_2C_C$, $c_{22} \approx C_1C_2$, $c_{33} \approx C_1C_C$, $c_{12} = c_{21} \approx C_2C_{1C}$,

$c_{23} = c_{32} \approx C_1 C_{2C}$, $c_{13} = c_{31} \approx C_C C_{12} + C_{1C} C_{2C}$, and the simplified approximate inverse matrix,

$$\mathbf{C}^{-1} \approx \begin{pmatrix} \frac{1}{C_1} & \frac{C_{1C}}{C_1 C_C} & \frac{C_{12}}{C_1 C_2}(1+\eta) \\ \frac{C_{1C}}{C_1 C_C} & \frac{1}{C_C} & \frac{C_{2C}}{C_C C_2} \\ \frac{C_{12}}{C_1 C_2}(1+\eta) & \frac{C_{2C}}{C_C C_2} & \frac{1}{C_2} \end{pmatrix}, \tag{B.14}$$

with $\eta = C_{1C} C_{2C} / C_{12} C_C$.

Then we use Eq.(B.6) to find the final Hamiltonian, assuming the vector of the node charges is $q^T = (q_1 \ q_c \ q_2)$,

$$H = \sum_{i=1,C,2} \frac{q_i^2}{2C_i} + q_1 q_C \frac{C_{1C}}{C_1 C_C} + q_C q_2 \frac{C_{2C}}{C_C C_2} + q_1 q_2 \frac{C_{12}}{C_1 C_2}(1+\eta) + U_J. \tag{B.15}$$

Defining $E_{C,i} = e^2/2C_i$, and promoting q and ϕ to quantum operators $q = -2ce$ and ϕ, we can manipulate this Hamiltonian to find

$$\begin{aligned} H = {} & 4E_{C,1} c_1^2 - E_{J,1} \cos\phi_1 + 4E_{C,C} c_C^2 - E_{J,C} \cos\phi_C + 4E_{C,2} c_2^2 - E_{J,2} \cos\phi_2 \\ & + 8\, c_1 c_C \sqrt{E_{C,1} E_{C,C}}\, \frac{C_{1C}}{\sqrt{C_1 C_C}} + 8\, c_C c_2 \sqrt{E_{C,C} E_{C,2}}\, \frac{C_{2C}}{\sqrt{C_C C_2}} \\ & + 8(\eta+1)\, c_1 c_2 \sqrt{E_{C,1} E_{C,2}}\, \frac{C_{12}}{\sqrt{C_1 C_2}}. \end{aligned} \tag{B.16}$$

As done early, we expand in Taylor series the cossine terms, and assume the transmon regime $E_J \gg E_C$, in order to exclude terms of order higher than 4. The final result

$$\begin{aligned} H = {} & 4E_{C,1} c_1^2 - \frac{E_{J,1}}{2}\phi_1^2 + 4E_{C,C} q_C^2 + \frac{E_{J,C}}{2}\phi_C^2 + 4E_{C,2} c_2^2 + \frac{E_{J,2}}{2}\phi_2^2 \\ & + \frac{E_{J,1}}{24}\phi_1^4 + \frac{E_{J,1}}{24}\phi_C^4 + \frac{E_{J,2}}{24}\phi_2^4 \\ & + 8\, c_1 c_C \sqrt{E_{C,1} E_{C,C}}\, \frac{C_{1C}}{\sqrt{C_1 C_C}} + 8\, c_C c_2 \sqrt{E_{C,C} E_{C,2}}\, \frac{C_{C2}}{\sqrt{C_C C_2}} \\ & + 8\, c_1 c_2 \sqrt{E_{C,1} E_{C,2}}\, (\eta+1) \frac{C_{12}}{\sqrt{C_1 C_2}}, \end{aligned} \tag{B.17}$$

can be written in terms of the a and $a^\dagger$ operators as follows,

$$H = \sum_{i=1,C,2} \omega_i a_i^\dagger a_i + \frac{\alpha_i}{2} a_i^\dagger a_i^\dagger a_i a_i + \sum_{j=1,2} g_j \left(a_j^\dagger a_C + a_j a_C^\dagger \right) + g_{12} \left(a_1^\dagger a_2 + a_1 a_2^\dagger \right), \tag{B.18}$$

where we defined,

$$\omega_i = \sqrt{8 E_{J,i} E_{C,i}} - E_{C,i} \tag{B.19}$$

$$\alpha_i = -E_{C,i} \tag{B.20}$$

$$g_j = \frac{1}{2} \frac{C_{jC}}{\sqrt{C_j C_C}} \sqrt{\omega_j \omega_C} \tag{B.21}$$

$$g_{12} = \frac{1}{2}(1+\eta) \frac{C_{12}}{\sqrt{C_1 C_2}} \sqrt{\omega_1 \omega_2}. \tag{B.22}$$

Appendix C

The dissipative case

C.1 Disspative quantum systems

So far, we have considered the superconducting circuit as a closed system. That means, no interaction with the environment was modeled. In general, superconducting circuits are very well insulated in order to minimize any losses, since the quantum characteristics are very sensible and unstable [43]. However, even when well insulated, every real system is in contact with the environment, leading to losses of energy. In quantum computing, such losses lead to noises and alterations in the quantum state of the system, in a process called decoherence [21]. Then, it is necessary to take such interactions in consideration, when analyzing any real system.

Let H_s be the Hamiltonian of the perfectly insulated system, then we define H_e as the environment Hamiltonian and H_{se} as the interaction between the system and its environment. Then, the total Hamiltonian is

$$H_T = H_s + H_e + H_{se}, \tag{C.1}$$

with the Hilbert space of the total system $\mathscr{H}_T = \mathscr{H}_s \otimes \mathscr{H}_e$ being the product of both the system $\mathscr{H}_s$ and environment $\mathscr{H}_e$ spaces. The total state of the system is described by the density matrix ρ that, at the initial time $t = 0$ is

$$\rho = \rho_s \otimes \rho_e, \tag{C.2}$$

with $\rho_s(\rho_e)$ the density matrix of the system (environment).

In the context of superconducting qubits, the two main processes causing decoherence are the longitudinal and transverse relaxation [13].

The longitudial relaxation rate, denoted Γ_1 also called the "energy relaxation" or "energy decay" describes the exchange of energy between the system and the environment. In this process, both excitation and decaying of the qubit occurs at rates Γ_+ and Γ_- respectively and we can write,

$$\Gamma_1 = \Gamma_+ + \Gamma_-. \tag{C.3}$$

However, since superconducting qubits are operated at very low temperatures, the loss of energy from the qubit to the environment, is much greater than the opposite. Therefore, the decaying rate $\Gamma_- \gg \Gamma_+$, and usually the excitation Γ_+ can be neglected [43].

In the Bloch sphere, such relaxation can be interpreted as the movement of the state towards the north pole ($|0\rangle$) as depicted in Figure 28.

Pure dephasing describes the depolarization along the x-y plane at a rate Γ_φ. It causes fluctuations in the qubit frequency such that it is no longer equal to the frequency in the interaction frame. In the Bloch sphere, it will cause the state to precess forward or backward in the x-y plane as denoted in Figure 29.

Figure 28 – Representation of the longitudinal relaxation in the Bloch sphere. The longitudinal noise in the x-y plane leads to $|0\rangle \leftrightarrow |1\rangle$ transitions. The qubit in state $|0\rangle$ gains energy from the environment and is excited to the state $|1\rangle$ at a rate Γ_+ (pink curved arrow). The state $|1\rangle$ on the other hand decays to $|0\rangle$ with a rate Γ_- (yellow curved arrow).

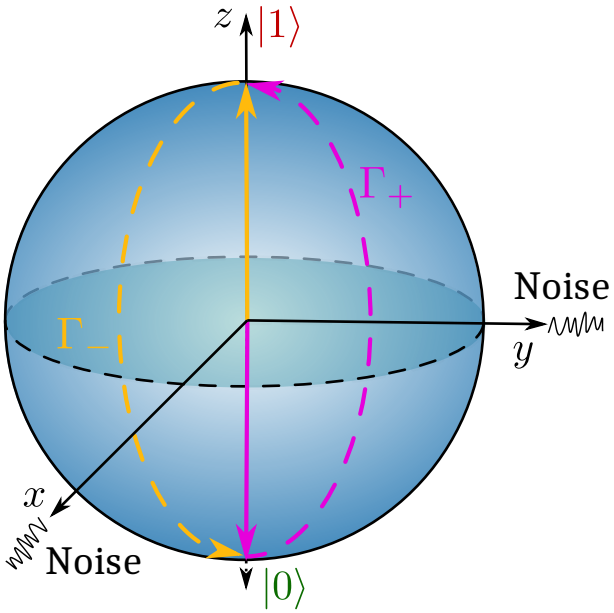

Source: The author.

Figure 29 – Representation of the pure dephasing in the Bloch sphere. The noise along the z-axis will cause the state of a qubit to process in the x-y plane

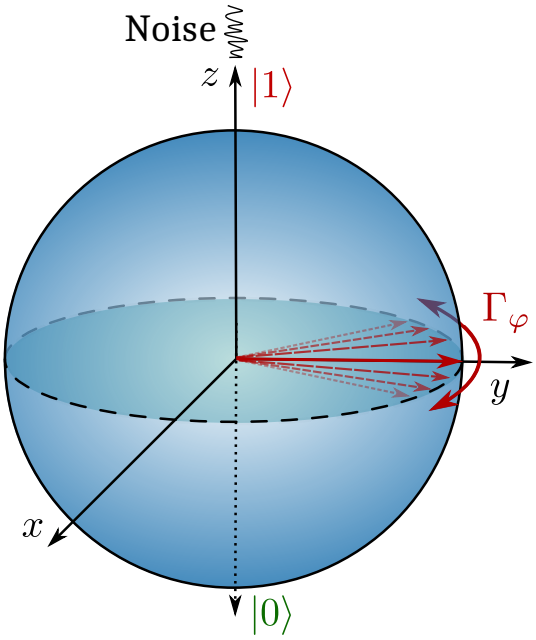

Source: The author.

The combined effects of pure dephasing and longitudinal noise leads to the transverse relaxation, described by the rate

$$\Gamma_2 = \frac{\Gamma_1}{2} + \Gamma_\varphi. \tag{C.4}$$

It describes the loss of coherence in a superposition state, due to noises in all the three axis of the Bloch sphere. While the x-y noises will lead to losses of energy and decaying of the excited state of the qubit. Z noises will shift the qubit frequency, in a process that causes loss of coherence.

C.2 The master equation

The description of a quantum system interacting with the environment is done using the formalism of the master equation. If we assume the system interaction with the environment is weak, it is possible to treat it as a markovian system [22]. It means a system where the dynamics do not depend on the past states of the system, only in its present state [78]. In such markovian systems, the evolution of the complete Hamiltonian considering the interactions with the environment will be described using the Lindblad master equation

$$\frac{d}{dt}\rho(t) = -\mathrm{i}\,[H, \rho(t)] + \sum_i \gamma_i \left(L_i \rho L_i^\dagger - \frac{1}{2}\left\{ L_i^\dagger L_i, \rho \right\} \right), \tag{C.5}$$

with the $\{\ ,\ \}$ the anticommutator of ρ with the operators L_i that describes the i-th dissipative mechanism of the system, and γ_i the rate at which a given mechanism dissipates energy [22].

In our system such operators L_i will be the number operator $a_i^\dagger a_i$ of each mode in the system when modeling the T_2 process. The process T_1 on the other hand, will be described using the annihilation operators a_i. Therefore, we can write the master equation that describes the dynamics of our open system as

$$\begin{aligned} \frac{d}{dt}\rho(t) = -\mathrm{i}\,[H, \rho(t)] &+ \sum_{i=1,C,2} \frac{\Gamma_{1_i}}{2} \left(2a_i \rho(t) a_i^\dagger - \left\{ a_i^\dagger a_i, \rho(t) \right\} \right) \\ &+ \sum_{i=1,C,2} \frac{\Gamma_{2_i}}{2} \left(2a_i^\dagger a_i \rho(t) a_i a_i^\dagger - \left\{ a_i a_i^\dagger a_i^\dagger a_i, \rho(t) \right\} \right), \end{aligned} \tag{C.6}$$

where $\Gamma_{1_i}(\Gamma_{1_i})$ is the longitudinal (transverse) relaxation rate of each qubit.

The numerical solution for Eq.(C.6) can be obtained defining the relevant operators in QuTiP and using the numerical solver `mesolve`. Assuming Eq.(5.3) as the Hamiltonian of the system and the parameters in Table 2 to describe the relaxation, we obtain the graphic seen in Figure 30. As it can be seen, the relaxation rates are small enough to have a negligible effect over the dynamics.

One elucidative way to demonstrate the quantum signature of our quantum transistor, is assuming the coupler as a high dissipative element. For example, making the dissipation

Table 2 – Longitudinal relaxation times $T_1 = 1/\Gamma_1$ and transverse relaxation times $T_2 = 1/\Gamma_2$, for each superconducting element in the experimental circuit. Values obtained from [62].

	Q_1	C	Q_2
T_1	6.51 *us*	4.06 *us*	6.58 *us*
T_2	0.54 *us*	0.27 *us*	7.43 *us*

Figure 30 – Comparison between the dissipative and the conservative dynamics for the transistor system using the total Hamiltonian and the initial state $|\Psi(0) = |0,1,1\rangle\rangle$. The dissipation rates used are the ones in Table 2. The other parameters of the circuit are in Table 1.

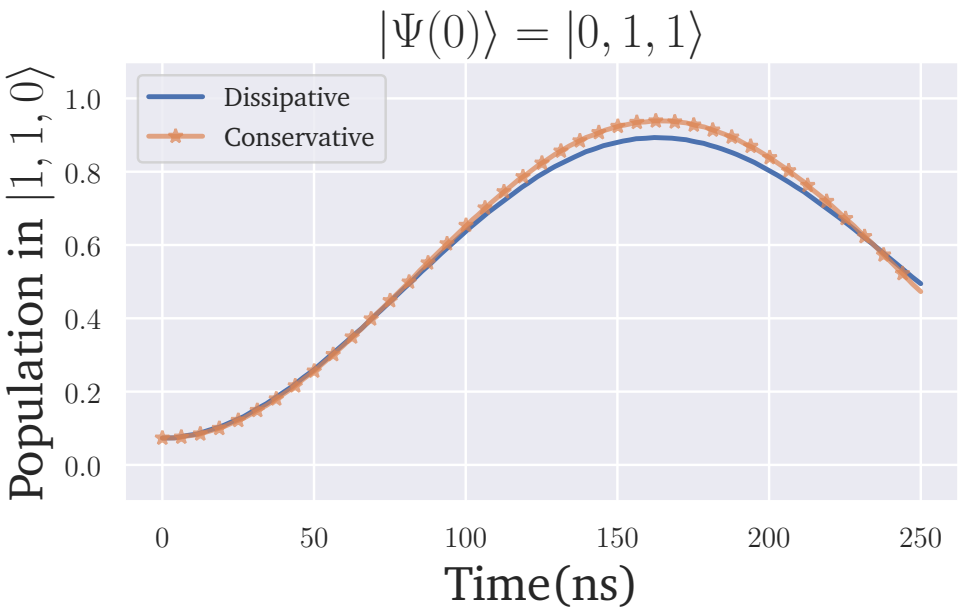

Source: The author.

rate in the coupler equal to the coupling g_1. In such high dissipative case, as we can see in Figure 31, once on, the state of the transistor rapidly decays to the off state and no population exchange occur. Such result demonstrate that only due to the quantum behaviour of the system, the transistor can efficiently switch the information. Once the coherence is lost, the fidelity of the transistor operations is drastically affected and therefore reassuring the quantum aspect of this device.

Figure 31 – Simulation of the system, when the dissipation rate on the coupler is equal to the coupling $\Gamma_{1_c} = g_1$. In this high dissipative regime, the coupler rapidly loses coherence and the population exchange between Q_1 and Q_2 can not occur. The parameters used in the simulation are in Table 1.

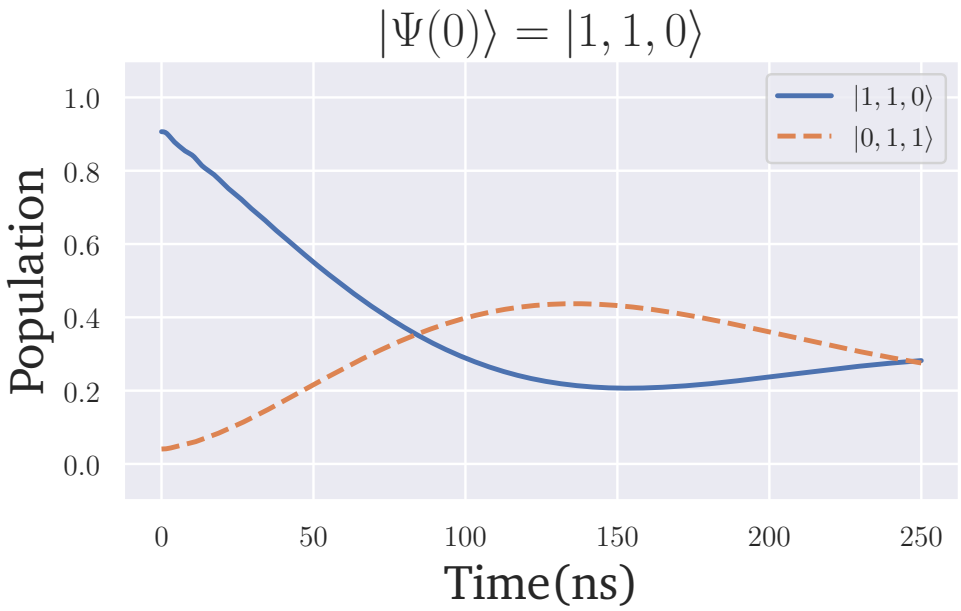

Source: The author.

Appendix D

Effective Hamiltonian for the transistor

D.1 Two level system effective Hamiltonian

If our system is described by the total Hamiltonian in Schrödinger picture

$$H = \omega(\sigma_1^1 + \sigma_2^1) + \omega_c\sigma_c^1 + g_{12}(\sigma_1^+\sigma_2^- + h.c.) + g_1(\sigma_1^+\sigma_c^- + h.c.) + g_2(\sigma_2^+\sigma_c^- + h.c.), \quad \text{(D.1)}$$

we can use an unitary transformation $H_i = UHU^\dagger - H_0$,with $H_0 = \omega(\sigma_1^1 + \sigma_2^1) + \omega_c\sigma_c^1$ and $U = e^{-iH_0t}$ to write it in the interaction picture as

$$\begin{aligned} H_i &= g_1(\sigma_1^+\sigma_c^- e^{i\Delta t} + h.c.) + g_2(\sigma_2^+\sigma_c^- e^{-i\Delta t} + h.c.) + g_{12}(\sigma_1^+\sigma_2^- + h.c.) \\ &= \underbrace{g(\sigma_1^+ + \sigma_2^+)\sigma_c^- e^{i\Delta t} + g(\sigma_1^- + \sigma_2^-)\sigma_c^+ e^{-i\Delta t}}_{H^{(1)}} + \overbrace{g_{12}(\sigma_1^+\sigma_2^- + h.c.)}^{H^{(2)}}, \end{aligned} \quad \text{(D.2)}$$

where, $\Delta = \omega - \omega_c$ and, $g = g_{1c} = g_{2c}$. To calculate the effective dynamics, we then take the time dependent terms in Eq.(D.2) to find the effective Hamiltonian according to Eq. (3.23)

$$\begin{aligned} H_{eff}^{(1)} &\approx \left[-iH_1(t)\int_0^t H_1(t')dt'\right]_{RWA} \\ &\approx -ig[(\sigma_1^+ + \sigma_2^+)\sigma_c^- e^{i\Delta t} + (\sigma_1^- + \sigma_2^-)\sigma_c^+ e^{-i\Delta t}] \\ &\times \int_0^t g[(\sigma_1^+ + \sigma_2^+)\sigma_c^- e^{i\Delta t'} + (\sigma_1^- + \sigma_2^-)\sigma_c^+ e^{-i\Delta t'}]dt'. \end{aligned} \quad \text{(D.3)}$$

Integrating and manipulating we find

$$\begin{aligned} H_{eff}^{(1)} &\approx -ig[(\sigma_1^+ + \sigma_2^+)\sigma_c^- e^{i\Delta t} + (\sigma_1^- + \sigma_2^-)\sigma_c^+ e^{-i\Delta t}] \\ &\times\left[\frac{g}{i\Delta}(e^{i\Delta t} - 1)(\sigma_1^+ + \sigma_2^+)\sigma_c^- + \frac{g}{-i\Delta}(e^{-i\Delta t} - 1)(\sigma_1^- + \sigma_2^-)\sigma_c^+\right] \\ &\approx \frac{g^2}{\Delta}(\sigma_1^+ + \sigma_2^+)\sigma_c^-(\sigma_1^- + \sigma_2^-)\sigma_c^+ - \frac{g^2}{\Delta}(\sigma_1^- + \sigma_2^-)\sigma_c^+(\sigma_1^+ + \sigma_2^+)\sigma_c^- \\ &\approx \frac{g^2}{\Delta}[(\sigma_1^+\sigma_1^- + \sigma_2^+\sigma_2^- + \sigma_1^+\sigma_2^- + \sigma_2^+\sigma_1^-)\sigma_c^0 - (\sigma_1^-\sigma_1^+ + \sigma_2^-\sigma_2^+ + \sigma_1^-\sigma_2^+ + \sigma_2^-\sigma_1^+)\sigma_c^1]. \end{aligned} \quad \text{(D.4)}$$

Then, taking the coupler operators to evidence, we find

$$H_{eff}^{(1)} \approx \frac{g^2}{\Delta}[(\sigma_1^1 + \sigma_2^1)\sigma_c^0 - (\sigma_1^0 + \sigma_2^0)\sigma_c^1 + (\sigma_1^+\sigma_2^- + \sigma_1^-\sigma_2^+)(\sigma_c^0 - \sigma_c^1)].$$

Finally, we add the time independent term $H^{(2)}$ and can write the total Hamiltonian for the two level system in the interaction picture

$$\begin{aligned} H_{eff} \approx& \frac{g^2}{\Delta}\left[(\sigma_1^1 + \sigma_2^1)\sigma_c^0 - (\sigma_1^0 + \sigma_2^0)\sigma_c^1 + (\sigma_1^-\sigma_2^+ + \sigma_1^+\sigma_2^-)(\sigma_c^0 - \sigma_1^0)\right] \\ &+ g_{12}(\sigma_1^-\sigma_2^+ + \sigma_2^-\sigma_1^+)\mathbb{1}_c. \end{aligned} \quad \text{(D.5)}$$

if we assume $\Delta = -g^2/g_{12}$, we find the condition to the system behaving as a quantum transistor

$$H_{eff} \approx g_{12}(\sigma_1^0 + \sigma_2^0)\sigma_c^1 - g_{12}(\sigma_1^1 + \sigma_2^1)\sigma_c^0 + g_{12}(\sigma_1^+\sigma_2^- + \sigma_1^-\sigma_2^+)(\mathbb{1}_c + \sigma_c^1 - \sigma_c^0). \quad \text{(D.6)}$$

D.2 Three level system effective Hamiltonian

Here we proceed with the detailed calculations on the effective Hamiltonian for the qutrit system. To do so the fist step is to write Eq.(5.3) in the interaction picture, to do that again we define $U(t) = e^{-iH_0 t}$ and calculate the transformation $H_i = UHU^\dagger - H_0$, that reads

$$H_I = U^\dagger(t)V_0U(t) = \sum_{i=1,2} g_i\left(U^\dagger(t)a_i^\dagger a_c U(t) + U^\dagger(t)a_i a_c^\dagger U(t)\right) + g_{12}U^\dagger(t)\left(a_1^\dagger a_2 + a_1 a_2^\dagger\right)U(t). \tag{D.7}$$

Now, let us use the commutation relation $[a, a^\dagger]=\mathbb{1}$, to write the commutator

$$\begin{aligned}[a^{\dagger 2}a^2, a^\dagger a] &= [a^\dagger N a, N] \\ &= a^\dagger N \underbrace{[a, N]}_{a} + \underbrace{[a^\dagger, N]}_{-a^\dagger} Na \\ &= a^\dagger Na - a^\dagger Na = 0,\end{aligned} \tag{D.8}$$

then we can write

$$e^{-i\omega a^\dagger a - i\alpha(a^\dagger)^2a^2} = e^{-i\omega a^\dagger a}e^{-i\alpha(a^\dagger)^2a^2}, \tag{D.9}$$

for any α and ω. This allow us to write the operator $U(t)$ as

$$\begin{aligned}U(t) &= e^{\sum_{k=1,2,c} -i\omega_k a_k^\dagger a_k - i\frac{\alpha_k}{2}(a_k^\dagger)^2a_k^2} \\ &= \underbrace{e^{-i\omega a_1^\dagger a_1 - i\frac{\alpha_1}{2}(a_1^\dagger)^2a_1^2}}_{U_1(t)}\underbrace{e^{-i\omega a_c^\dagger a_c - i\frac{\alpha_c}{2}(a_c^\dagger)^2a_c^2}}_{U_c(t)}\underbrace{e^{-i\omega a_2^\dagger a_2 - i\frac{\alpha_2}{2}(a_1^\dagger)^2a_2^2}}_{U_2(t)} \\ &= U_1(t)U_c(t)U_2(t).\end{aligned} \tag{D.10}$$

In addition, by acting $(a^\dagger)^2a^2$ in any Fock state $|n\rangle$ we get

$$\begin{aligned}(a^\dagger)^2a^2|n\rangle &= (a^\dagger)^2a\sqrt{n}\,|n-1\rangle \\ &= (a^\dagger)^2\sqrt{n(n-1)}\,|n-2\rangle = a^\dagger\sqrt{(n-1)}\sqrt{n(n-1)}\,|n-1\rangle \\ &= \left(\sqrt{n(n-1)}\right)^2|n\rangle = n(n-1)\,|n\rangle\,.\end{aligned} \tag{D.11}$$

Therefore, now we can make the consideration that each artificial atom in the circuit is a three-level system, by doing the transformations

$$a_j \to \Sigma_j^- = \sum_{k=1}^{2}\sqrt{k}\,|k-1\rangle\langle k|\ ,\quad a_j^\dagger \to \Sigma_j^+ = \sum_{k=1}^{2}\sqrt{k}\,|k\rangle\langle k-1|\,, \tag{D.12}$$

by doing that Eq. (D.11) reads

$$(\Sigma_j^+)^2(\Sigma_j^-)^2|n\rangle = 2\delta_{2,n}|n\rangle\,. \tag{D.13}$$

Now, it is easy to show that

$$\begin{aligned} U_j^\dagger(t)\left|n\right\rangle &= e^{i\omega_j a_j^\dagger a_j t + i\frac{\alpha_j}{2}(a_j^\dagger)^2 a_j^2 t}\left|n\right\rangle = e^{i\omega_j a_j^\dagger a_j t} e^{i\frac{\alpha_j}{2}(a_j^\dagger)^2 a_j^2 t}\left|n\right\rangle \\ &= e^{i\omega_j a_j^\dagger a_j t} e^{i\alpha_j \delta_{2,n} t}\left|n\right\rangle = e^{i\alpha_j \delta_{2,n} t} e^{i\omega_j a_j^\dagger a_j t}\left|n\right\rangle \\ &= e^{i\alpha_j \delta_{2,n} t} e^{i\omega_j n t}\left|n\right\rangle . \end{aligned} \tag{D.14}$$

Therefore

$$\begin{aligned} U_j^\dagger(t)\Sigma_j^- U_j(t) &= \sum_{n=1}^{2} \sqrt{n} U_j^\dagger(t)\left|n-1\right\rangle \left\langle n\right| U_j(t) \\ &= \sum_{n=1}^{2} \sqrt{n}\Big[U_j^\dagger(t)\left|n-1\right\rangle\Big]\Big[\left\langle n\right| U_j(t)\Big], \end{aligned} \tag{D.15}$$

where we can use that in the range where $n=\{0,1,2\}$ we have $U_j^\dagger(t)\left|n-1\right\rangle = e^{i\omega_j(n-1)t}\left|n-1\right\rangle$, thus we get

$$\begin{aligned} U_j^\dagger(t)\Sigma_j^- U_j(t) &= \sum_{n=1}^{2} \sqrt{n}\Big[e^{i\omega_j(n-1)t}\left|n-1\right\rangle\Big]\Big[\left\langle n\right| e^{-i\alpha_j\delta_{2,n}t} e^{-i\omega_j n t}\Big] \\ &= \sum_{n=1}^{2} \sqrt{n} e^{i\omega_j(n-1)t} e^{-i\alpha_j\delta_{2,n}t} e^{-i\omega_j n t}\left|n-1\right\rangle\left\langle n\right| \\ &= e^{-i\omega_j t}\sum_{n=1}^{2} \sqrt{n} e^{-i\alpha_j\delta_{2,n}t}\left|n-1\right\rangle\left\langle n\right| \\ &= e^{-i\omega_j t}\Big[\left|0\right\rangle\left\langle 1\right|_j + \sqrt{2}e^{-i\alpha_j t}\left|1\right\rangle\left\langle 2\right|_j\Big]. \end{aligned} \tag{D.16}$$

Then, it is convenient to define the operators $P_{nm}^{(j)} = \left|n\right\rangle\left\langle m\right|_j$, to simplify the notation, so that

$$U_j^\dagger(t)\Sigma_j^- U_j(t) = e^{-i\omega_j t} P_{01}^{(j)} + e^{-i\tilde{\omega}_j t}\sqrt{2} P_{12}^{(j)}, \tag{D.17}$$

where $\tilde{\omega} = \omega_j + \alpha_j$. Then, the Hamiltonian in interaction picture reads

$$\begin{aligned} H_I = &\sum_{k=1,2} g_i\left(U^\dagger(t)\Sigma_k^+ U(t) U^\dagger(t)\Sigma_{\mathrm{c}}^- U(t) + h.c.\right) \\ &+ g_{12}\left(U^\dagger(t)\Sigma_1^+ U(t) U^\dagger(t)\Sigma_2^- U(t) + h.c.\right). \end{aligned} \tag{D.18}$$

By working each term, we have

$$\begin{aligned} U^\dagger(t)\Sigma_k^+ U(t) U^\dagger(t)\Sigma_{\mathrm{c}}^- U(t) &= \Big[e^{i\omega_k t} P_{10}^{(k)} + \sqrt{2} e^{i\tilde{\omega}_k t} P_{21}^{(k)}\Big]\Big[e^{-i\omega_{\mathrm{c}} t} P_{01}^{(\mathrm{c})} + \sqrt{2} e^{-i\tilde{\omega}_{\mathrm{c}} t} P_{12}^{(\mathrm{c})}\Big] \\ &= e^{i\omega_k t} P_{10}^{(k)}\Big[e^{-i\omega_{\mathrm{c}} t} P_{01}^{(\mathrm{c})} + \sqrt{2} e^{-i\tilde{\omega}_{\mathrm{c}} t} P_{12}^{(\mathrm{c})}\Big] \\ &+ e^{i\tilde{\omega}_k t} P_{21}^{(k)}\sqrt{2}\Big[e^{-i\omega_{\mathrm{c}} t} P_{01}^{(\mathrm{c})} + \sqrt{2} e^{-i\tilde{\omega}_{\mathrm{c}} t} P_{12}^{(\mathrm{c})}\Big] \\ &= \Big[e^{i(\omega_k - \omega_{\mathrm{c}})t} P_{10}^{(k)} P_{01}^{(\mathrm{c})} + e^{i(\omega_k - \tilde{\omega}_{\mathrm{c}})t}\sqrt{2} P_{10}^{(k)} P_{12}^{(\mathrm{c})}\Big] \\ &+ \Big[e^{i(\tilde{\omega}_k - \omega_{\mathrm{c}})t}\sqrt{2} P_{21}^{(k)} P_{01}^{(\mathrm{c})} + 2 e^{i(\tilde{\omega}_k - \tilde{\omega}_{\mathrm{c}})t} P_{21}^{(k)} P_{12}^{(\mathrm{c})}\Big]. \end{aligned} \tag{D.19}$$

On the other hand, the hermitian conjugate will be

$$\begin{aligned} U^{\dagger}(t)\Sigma_1^{+}U(t)U^{\dagger}(t)\Sigma_2^{-}U(t) &= \left[e^{i\omega_1 t}P_{10}^{(1)} + \sqrt{2}e^{i\tilde{\omega}_1 t}P_{21}^{(1)}\right]\left[e^{-i\omega_2 t}P_{01}^{(2)} + \sqrt{2}e^{-i\tilde{\omega}_2 t}P_{12}^{(2)}\right] \\ &= \left[e^{i(\omega_1-\omega_2)t}P_{10}^{(1)}P_{01}^{(2)} + e^{i(\omega_1-\tilde{\omega}_2)t}\sqrt{2}P_{10}^{(1)}P_{12}^{(2)}\right] \\ &+ \left[e^{i(\tilde{\omega}_1-\omega_2)t}\sqrt{2}P_{21}^{(1)}P_{01}^{(2)} + 2e^{i(\tilde{\omega}_1-\tilde{\omega}_2)t}P_{21}^{(1)}P_{12}^{(2)}\right]. \end{aligned} \tag{D.20}$$

Therefore, the Hamiltonian is written as

$$H_I = H_{1,c}(t) + H_{2,c}(t) + H_2(t). \tag{D.21}$$

where

$$\begin{aligned} H_{k,c}(t) = g_k\big[&e^{i(\omega_k-\omega_c)t}P_{10}^{(k)}P_{01}^{(c)} + e^{i(\omega_k-\tilde{\omega}_c)t}\sqrt{2}P_{10}^{(k)}P_{12}^{(c)} \\ &+ e^{i(\tilde{\omega}_k-\omega_c)t}\sqrt{2}P_{21}^{(k)}P_{01}^{(c)} + 2e^{i(\tilde{\omega}_k-\tilde{\omega}_c)t}P_{21}^{(k)}P_{12}^{(c)} + h.c.\big], \end{aligned} \tag{D.22}$$

and

$$\begin{aligned} H_2(t) = g_{12}\big[&e^{i(\omega_1-\omega_2)t}P_{10}^{(1)}P_{01}^{(2)} + e^{i(\omega_1-\tilde{\omega}_2)t}\sqrt{2}P_{10}^{(1)}P_{12}^{(2)} \\ &+ e^{i(\tilde{\omega}_1-\omega_2)t}\sqrt{2}P_{21}^{(1)}P_{01}^{(2)} + 2e^{i(\tilde{\omega}_1-\tilde{\omega}_2)t}P_{21}^{(1)}P_{12}^{(2)} + h.c.\big]. \end{aligned} \tag{D.23}$$

Calling $\Delta_k = \omega_k - \omega_c$, $\tilde{\Delta}_k = \omega_k - \tilde{\omega}_c$, $\tilde{\Delta}'_k = \tilde{\omega}_k - \omega_c$ and $\tilde{\tilde{\Delta}}_k = \tilde{\omega}_k - \tilde{\omega}_c$

$$\begin{aligned} H_{k,c}(t) = g_k\big[&e^{i\Delta_k t}P_{10}^{(k)}P_{01}^{(c)} + e^{i\tilde{\Delta}_k t}\sqrt{2}P_{10}^{(k)}P_{12}^{(c)} \\ &+ e^{i\tilde{\Delta}'_k t}\sqrt{2}P_{21}^{(k)}P_{01}^{(c)} + 2e^{i\tilde{\tilde{\Delta}}_k t}P_{21}^{(k)}P_{12}^{(c)} + h.c.\big]. \end{aligned} \tag{D.24}$$

Now we assume the condition of perfect resonance between Q_1 and Q_2, in order to do $\Delta_{12} = \omega_1 - \omega_2 = 0$. In the same way, we assume $\alpha_1 = \alpha_2$. With that, also $\tilde{\tilde{\Delta}}_{12} = 0$, notice however, that the terms $\tilde{\Delta}_{12}$ and $\tilde{\Delta}_{12}$ can not be supposed null. This lead the Hamiltonian $H_2(t)$ to be divided in two parts,

$$\begin{aligned} H_2(t) = g_{12}\big[&\left(e^{i\tilde{\Delta}_{12}t}\sqrt{2}P_{10}^{(1)}P_{12}^{(2)} + e^{i\tilde{\Delta}'_{12}t}\sqrt{2}P_{21}^{(1)}P_{01}^{(2)} + h.c.\right) \\ &+ \left(P_{10}^{(1)}P_{01}^{(2)} + 2P_{21}^{(1)}P_{12}^{(2)} + h.c.\right)\big], \end{aligned} \tag{D.25}$$

where $\tilde{\Delta}_{12} = \omega_1 - \tilde{\omega}_2 = -\alpha$, and $\tilde{\Delta}'_{12} = \tilde{\omega}_1 - \omega_2 = \alpha$.

After those considerations, our Hamiltonian assumes the form

$$H_I = \overbrace{\sum_{k=1,2} g_k \left[e^{i\Delta_k t} P_{10}^{(k)} P_{01}^{(c)} + e^{i\tilde{\Delta}_k t} \sqrt{2} P_{10}^{(k)} P_{12}^{(c)} + e^{i\tilde{\Delta}'_k t} \sqrt{2} P_{21}^{(k)} P_{01}^{(c)} + 2e^{i\tilde{\tilde{\Delta}}_k t} P_{21}^{(k)} P_{12}^{(c)} + h.c. \right]}^{H_{k,c}(t)}$$
$$+ g_{12} \underbrace{\left(e^{i\tilde{\Delta}_{12} t} \sqrt{2} P_{10}^{(1)} P_{12}^{(2)} + e^{i\tilde{\Delta}'_{12} t} \sqrt{2} P_{21}^{(1)} P_{01}^{(2)} + h.c. \right)}_{H_{1,2}(t)} + \underbrace{g_{12} \left(P_{10}^{(1)} P_{01}^{(2)} + 2P_{21}^{(1)} P_{12}^{(2)} + h.c. \right)}_{H_0}, \tag{D.26}$$

and we can write the effective Hamiltonian as follows:

$$H_{eff} \approx -i \left(H_{k,c} \int_0^t H_{k,c}(t')\, dt' + H_{k,c} \int_0^t H_{1,2}(t')\, dt' + H_{1,2} \int_0^t H_{k,c}(t')\, dt' + H_{1,2} \int_0^t H_2(t')\, dt' \right) + H_0. \tag{D.27}$$

Calculating the integrals we find for $H_{k,c}$

$$\begin{aligned} \int_0^t H_{k,c}(t')\, dt' &= \sum_{k=1,2} \int_0^t dt' g_k \left[e^{i\Delta_k t'} P_{10}^{(k)} P_{01}^{(c)} + \sqrt{2} \left(e^{i\tilde{\Delta}_k t'} P_{10}^{(k)} P_{12}^{(c)} + e^{i\tilde{\Delta}'_k t'} P_{21}^{(k)} P_{01}^{(c)} \right) \right. \\ &\quad \left. + 2e^{i\tilde{\tilde{\Delta}}_k t'} P_{21}^{(k)} P_{12}^{(c)} + h.c. \right] \\ &= \sum_{k=1,2} g_k \left[\frac{\left(e^{it\Delta_k} - 1 \right)}{i\Delta_k} P_{10}^{(k)} P_{01}^{(c)} - \frac{\left(e^{-it\Delta_k} - 1 \right)}{i\Delta_k} P_{01}^{(k)} P_{10}^{(c)} \right. \\ &\quad + \sqrt{2} \frac{\left(e^{it\tilde{\Delta}_k} - 1 \right)}{i\tilde{\Delta}_k} P_{10}^{(k)} P_{12}^{(c)} - \sqrt{2} \frac{\left(e^{-it\tilde{\Delta}_k} - 1 \right)}{i\tilde{\Delta}_k} P_{01}^{(k)} P_{21}^{(c)} \\ &\quad + \sqrt{2} \frac{\left(e^{it\tilde{\Delta}'_k} - 1 \right)}{i\tilde{\Delta}'_k} P_{21}^{(k)} P_{01}^{(c)} - \sqrt{2} \frac{\left(e^{-it\tilde{\Delta}'_k} - 1 \right)}{i\tilde{\Delta}'_k} P_{12}^{(k)} P_{10}^{(c)} \\ &\quad \left. + 2 \frac{\left(e^{it\tilde{\tilde{\Delta}}_k} - 1 \right)}{i\tilde{\tilde{\Delta}}_k} P_{21}^{(k)} P_{12}^{(c)} - 2 \frac{\left(e^{-it\tilde{\tilde{\Delta}}_k} - 1 \right)}{i\tilde{\tilde{\Delta}}_k} P_{12}^{(k)} P_{21}^{(c)} \right], \end{aligned} \tag{D.28}$$

and for $H_{1,2}$

$$\begin{aligned} \int_0^t H_{1,2}(t')\, dt' &= \int_0^t g_{12} \left[e^{i\tilde{\Delta}_{12} t'} \sqrt{2} P_{10}^{(1)} P_{12}^{(2)} + e^{i\tilde{\Delta}'_{12} t'} \sqrt{2} P_{21}^{(1)} P_{01}^{(2)} + h.c \right] dt' \\ &= \frac{g_{12}}{i} \left[\frac{\left(e^{it\tilde{\Delta}_{12}} - 1 \right)}{\tilde{\Delta}_{12}} \left(\sqrt{2} P_{10}^{(1)} P_{12}^{(2)} \right) - \frac{\left(e^{-it\tilde{\Delta}_{12}} - 1 \right)}{\tilde{\Delta}_{12}} \left(\sqrt{2} P_{01}^{(1)} P_{21}^{(2)} \right) \right. \\ &\quad \left. + \frac{\left(e^{it\tilde{\Delta}'_{12}} - 1 \right)}{\tilde{\Delta}'_{12}} \left(\sqrt{2} P_{21}^{(1)} P_{01}^{(2)} \right) - \frac{\left(e^{-it\tilde{\Delta}'_{12}} - 1 \right)}{\tilde{\Delta}'_{12}} \left(\sqrt{2} P_{12}^{(1)} P_{10}^{(2)} \right) \right]. \end{aligned} \tag{D.29}$$

Then, we can calculate each term from the effective Hamiltonian and use the Rotating wave approximation to neglect those fast oscillatory. The results are

$$\begin{aligned}
H_{1,2}\int_0^t H_{1,2}\left(t'\right)dt' =& g_{12}\left[e^{i\tilde{\Delta}_{12}t}\sqrt{2}P_{10}^{(1)}P_{12}^{(2)} + e^{i\tilde{\Delta}'_{12}t}\sqrt{2}P_{21}^{(1)}P_{01}^{(2)}\right.\\
&\left. + e^{-i\tilde{\Delta}_{12}t}\sqrt{2}P_{01}^{(1)}P_{21}^{(2)} + e^{-i\tilde{\Delta}'_{12}t}\sqrt{2}P_{12}^{(1)}P_{10}^{(2)}\right]\\
&\times\frac{g_{12}}{i}\left[\frac{\left(e^{it\tilde{\Delta}_{12}}-1\right)}{\tilde{\Delta}_{12}}\left(\sqrt{2}P_{10}^{(1)}P_{12}^{(2)}\right) - \frac{\left(e^{-it\tilde{\Delta}_{12}}-1\right)}{\tilde{\Delta}_{12}}\left(\sqrt{2}P_{01}^{(1)}P_{21}^{(2)}\right)\right.\\
&\left. + \frac{\left(e^{it\tilde{\Delta}'_{12}}-1\right)}{\tilde{\Delta}'_{12}}\left(\sqrt{2}P_{21}^{(1)}P_{01}^{(2)}\right) - \frac{\left(e^{-it\tilde{\Delta}'_{12}}-1\right)}{\tilde{\Delta}'_{12}}\left(\sqrt{2}P_{12}^{(1)}P_{10}^{(2)}\right)\right]\\
=&\frac{g_{12}^2}{i}\left[\frac{2}{\tilde{\Delta}_{12}}\left(P_{00}^{(1)}P_{22}^{(2)} - P_{11}^{(1)}P_{11}^{(2)}\right) + \frac{2}{\tilde{\Delta}'_{12}}\left(P_{11}^{(1)}P_{11}^{(2)} - P_{22}^{(1)}P_{00}^{(2)}\right)\right],
\end{aligned}$$

$$\begin{aligned}
H_{1,2}\int_0^t H_{k,c}\left(t'\right)dt' =& g_{12}\left(e^{i\tilde{\Delta}_{12}t}\sqrt{2}P_{10}^{(1)}P_{12}^{(2)} + e^{i\tilde{\Delta}'_{12}t}\sqrt{2}P_{21}^{(1)}P_{01}^{(2)}\right.\\
&\left. + e^{-i\tilde{\Delta}_{12}t}\sqrt{2}P_{01}^{(1)}P_{21}^{(2)} + e^{-i\tilde{\Delta}'_{12}t}\sqrt{2}P_{12}^{(1)}P_{10}^{(2)}\right)\\
&\times\sum_{k=1,2} g_k\left[\frac{\left(e^{it\Delta_k}-1\right)}{i\Delta_k}P_{10}^{(k)}P_{01}^{(c)} - \frac{\left(e^{-it\Delta_k}-1\right)}{i\Delta_k}P_{01}^{(k)}P_{10}^{(c)}\right.\\
&+\sqrt{2}\frac{\left(e^{it\tilde{\Delta}_k}-1\right)}{i\tilde{\Delta}_k}P_{10}^{(k)}P_{12}^{(c)} - \sqrt{2}\frac{\left(e^{-it\tilde{\Delta}_k}-1\right)}{i\tilde{\Delta}_k}P_{01}^{(k)}P_{21}^{(c)}\\
&+\sqrt{2}\frac{\left(e^{it\tilde{\Delta}'_k}-1\right)}{i\tilde{\Delta}'_k}P_{21}^{(k)}P_{01}^{(c)} - \sqrt{2}\frac{\left(e^{-it\tilde{\Delta}'_k}-1\right)}{i\tilde{\Delta}'_k}P_{12}^{(k)}P_{10}^{(c)}\\
&\left. + 2\frac{\left(e^{it\tilde{\tilde{\Delta}}_k}-1\right)}{i\tilde{\tilde{\Delta}}_k}P_{21}^{(k)}P_{12}^{(c)} - 2\frac{\left(e^{-it\tilde{\tilde{\Delta}}_k}-1\right)}{i\tilde{\tilde{\Delta}}_k}P_{12}^{(k)}P_{21}^{(c)}\right] \overset{RWA}{\approx} 0,
\end{aligned}$$

$$\begin{aligned}
H_{k,c}\int_0^t H_{1,2}\left(t'\right)dt' =& \sum_{k=1,2} g_k\left(e^{i\Delta t}P_{10}^{(k)}P_{01}^{(c)} + e^{i\tilde{\Delta}t}\sqrt{2}P_{10}^{(k)}P_{12}^{(c)}\right.\\
&\left. + e^{i\tilde{\Delta}'t}\sqrt{2}P_{21}^{(k)}P_{01}^{(c)} + 2e^{i\tilde{\tilde{\Delta}}t}P_{21}^{(k)}P_{12}^{(c)} + h.c.\right)\\
&\times\frac{2g_{12}^2}{i\alpha}\left(\sqrt{2}P_{11}^{(1)}P_{11}^{(2)} - P_{22}^{(1)}P_{00}^{(2)} - P_{20}^{(1)}P_{02}^{(2)} + h.c.\right)\overset{RWA}{\approx} 0, \qquad \text{(D.30)}
\end{aligned}$$

$$
\begin{aligned}
H_{k,c}\int_0^t H_{k,c}\left(t'\right)dt' = \sum_{k=1,2} g_k \Big(& e^{i\Delta t}P_{10}^{(k)}P_{01}^{(c)} + e^{i\tilde{\Delta}t}\sqrt{2}P_{10}^{(k)}P_{12}^{(c)} + e^{i\tilde{\Delta}'t}\sqrt{2}P_{21}^{(k)}P_{01}^{(c)} + 2e^{i\tilde{\tilde{\Delta}}t}P_{21}^{(k)}P_{12}^{(c)} \\
& + e^{-i\Delta t}P_{01}^{(k)}P_{10}^{(c)} + e^{-i\tilde{\Delta}t}\sqrt{2}P_{01}^{(k)}P_{21}^{(c)} + e^{-i\tilde{\Delta}'t}\sqrt{2}P_{12}^{(k)}P_{10}^{(c)} + 2e^{-i\tilde{\tilde{\Delta}}t}P_{12}^{(k)}P_{21}^{(c)}\Big) \\
& \times \sum_{m=1,2} g_m \left[\frac{\left(e^{it\Delta}-1\right)}{i\Delta}P_{10}^{(m)}P_{01}^{(c)} + \sqrt{2}\frac{\left(e^{it\tilde{\Delta}}-1\right)}{i\tilde{\Delta}}P_{10}^{(m)}P_{12}^{(c)} + \sqrt{2}\frac{\left(e^{it\tilde{\Delta}'}-1\right)}{i\tilde{\Delta}'}P_{21}^{(m)}P_{01}^{(c)} \right. \\
& + 2\frac{\left(e^{it\tilde{\tilde{\Delta}}}-1\right)}{i\tilde{\tilde{\Delta}}}P_{21}^{(m)}P_{12}^{(c)} - \frac{\left(e^{-it\Delta}-1\right)}{i\Delta}P_{01}^{(m)}P_{10}^{(c)} - \sqrt{2}\frac{\left(e^{-it\tilde{\Delta}}-1\right)}{i\tilde{\Delta}}P_{01}^{(m)}P_{21}^{(c)} \\
& \left. - \sqrt{2}\frac{\left(e^{-it\tilde{\Delta}'}-1\right)}{i\tilde{\Delta}'}P_{12}^{(m)}P_{10}^{(c)} - 2\frac{\left(e^{-it\tilde{\tilde{\Delta}}}-1\right)}{i\tilde{\tilde{\Delta}}}P_{12}^{(m)}P_{21}^{(c)} \right]
\end{aligned}
\tag{D.31}
$$

$$
\begin{aligned}
H_{k,c}\int_0^t H_{k,c}\left(t'\right)dt' = \sum_{k,m=1,2} g_k g_m \Bigg[& \frac{1}{i\Delta}(P_{01}^{(k)}P_{10}^{(c)}P_{10}^{(m)}P_{01}^{(c)} - P_{10}^{(k)}P_{01}^{(c)}P_{01}^{(m)}P_{10}^{(c)}) \\
& + \frac{2}{i\tilde{\Delta}}(P_{01}^{(k)}P_{21}^{(c)}P_{10}^{(m)}P_{12}^{(c)} - P_{10}^{(k)}P_{12}^{(c)}P_{01}^{(m)}P_{21}^{(c)}) \\
& + \frac{2}{i\tilde{\Delta}'}(P_{12}^{(k)}P_{10}^{(c)}P_{21}^{(m)}P_{01}^{(c)} - P_{21}^{(k)}P_{01}^{(c)}P_{12}^{(m)}P_{10}^{(c)}) \\
& + \frac{4}{i\tilde{\tilde{\Delta}}}(P_{12}^{(k)}P_{21}^{(c)}P_{21}^{(m)}P_{12}^{(c)} - P_{21}^{(k)}P_{12}^{(c)}P_{12}^{(m)}P_{21}^{(c)}) \Bigg],
\end{aligned}
$$

$$
\begin{aligned}
H_{k,c}\int_0^t H_{k,c}\left(t'\right)dt' = \sum_{k,m=1,2} g_k g_m \Bigg[& \frac{1}{i\Delta}(P_{01}^{(k)}P_{10}^{(m)}P_{11}^{(c)} - P_{10}^{(k)}P_{01}^{(m)}P_{00}^{(c)}) \\
& + \frac{2}{i\tilde{\Delta}}(P_{01}^{(k)}P_{10}^{(m)}P_{22}^{(c)} - P_{10}^{(k)}P_{01}^{(m)}P_{11}^{(c)}) \\
& + \frac{2}{i\tilde{\Delta}'}(P_{12}^{(k)}P_{21}^{(m)}P_{11}^{(c)} - P_{21}^{(k)}P_{12}^{(m)}P_{00}^{(c)}) \\
& + \frac{4}{i\tilde{\tilde{\Delta}}}(P_{12}^{(k)}P_{21}^{(m)}P_{22}^{(c)} - P_{21}^{(k)}P_{12}^{(m)}P_{11}^{(c)}) \Bigg].
\end{aligned}
\tag{D.32}
$$

Finally we can sum those terms to obtain the final effective Hamiltonian for the qutrit system

$$
\begin{aligned}
H_{eff} \approx \sum_{k,m=1,2} g_k g_m \Bigg[& \frac{1}{\omega-\omega_c}(P_{10}^{(k)}P_{01}^{(m)}P_{00}^{(c)} - P_{01}^{(k)}P_{10}^{(m)}P_{11}^{(c)}) + \frac{2}{\omega-\tilde{\omega}_c}(P_{10}^{(k)}P_{01}^{(m)}P_{11}^{(c)} - P_{01}^{(k)}P_{10}^{(m)}P_{22}^{(c)}) \\
& + \frac{2}{\tilde{\omega}-\omega_c}(P_{21}^{(k)}P_{12}^{(m)}P_{00}^{(c)} - P_{12}^{(k)}P_{21}^{(m)}P_{11}^{(c)}) + \frac{4}{\tilde{\omega}-\tilde{\omega}_c}(P_{21}^{(k)}P_{12}^{(m)}P_{11}^{(c)} - P_{12}^{(k)}P_{21}^{(m)}P_{22}^{(c)}) \Bigg] \\
& + \frac{2g_{12}^2}{\alpha}\left(-P_{11}^{(1)}P_{11}^{(2)} + P_{22}^{(1)}P_{00}^{(2)} + P_{20}^{(1)}P_{02}^{(2)} + h.c.\right) \\
& + g_{12}\left(P_{10}^{(1)}P_{01}^{(2)} + 2P_{21}^{(1)}P_{12}^{(2)} + h.c.\right)
\end{aligned}
\tag{D.33}
$$

D.2.1 Effective coupling

To obtain the effective coupling of the Hamiltonian, we need to apply H_{eff} to both possible states of the coupler, to verify how the interaction terms will behave.

- **Coupler in the $|0\rangle_c$ state**

First assuming $|0\rangle_c$ we have,

$$\begin{aligned} H_{eff}|0\rangle_c = &\sum_{k,m=1,2} g_k g_m \left[\frac{1}{\omega-\omega_c}(P_{10}^{(k)}P_{01}^{(m)}) + \frac{2}{\tilde{\omega}-\omega_c}(P_{21}^{(k)}P_{12}^{(m)})\right] \\ &+\frac{2g_{12}^2}{\alpha}\left(-P_{11}^{(1)}P_{11}^{(2)} + P_{22}^{(1)}P_{00}^{(2)} + P_{20}^{(1)}P_{02}^{(2)} + h.c.\right) \\ &+g_{12}\left(P_{10}^{(1)}P_{01}^{(2)} + 2P_{21}^{(1)}P_{12}^{(2)} + h.c.\right) \end{aligned} \tag{D.34}$$

then, we take only the hopping terms in Eq.(D.34) since they will be the relevant for the effective coupling.

$$\begin{aligned} H_{eff}|0\rangle_c = &g_1 g_2\left[\frac{1}{\Delta}(P_{10}^{(1)}P_{01}^{(2)} + h.c.) + \frac{2}{\Delta-\alpha}(P_{21}^{(1)}P_{12}^{(2)} + h.c.)\right] \\ &+g_{12}\left[(P_{10}^{(1)}P_{01}^{(2)} + h.c.) + 2(P_{21}^{(1)}P_{12}^{(2)} + h.c.)\right], \end{aligned} \tag{D.35}$$

rearranging the terms we find,

$$H_{eff}|0\rangle_c = (P_{10}^{(1)}P_{01}^{(2)} + h.c.)\left(\frac{g_1 g_2}{\Delta} + g_{12}\right) + 2(P_{21}^{(1)}P_{12}^{(2)} + h.c.)\left(g_{12} + \frac{g_1 g_2}{\Delta+\alpha}\right). \tag{D.36}$$

Since our Hamiltonian conserves the total amount of excitations, neither Q_1 nor Q_2 will ever populate the second excited state, if we only add one excitation to the system. Then, it is possible to remove the second term in Eq.(D.36) to find the effective coupling

$$\tilde{g}_{eff}^{|0\rangle_c} = \left(\frac{g_1 g_2}{\Delta} + g_{12}\right)\left(P_{10}^{(1)}P_{01}^{(2)} + h.c.\right). \tag{D.37}$$

- **Coupler in the $|1\rangle_c$ state**

By the other hand, when we apply the "on" state of the coupler $|1\rangle_c$ in our Hamiltonian, we find

$$\begin{aligned} H_{eff}|1\rangle_c = &\sum_{k,m=1,2} g_k g_m \left[-\frac{P_{01}^{(k)}P_{10}^{(m)}}{\Delta} + \frac{2P_{10}^{(k)}P_{01}^{(m)}}{\Delta-\alpha_c} - \frac{2P_{12}^{(k)}P_{21}^{(m)}}{\Delta+\alpha} + \frac{4P_{21}^{(k)}P_{12}^{(m)}}{\alpha-\alpha_c}\right] \\ &+g_{12}\left(P_{10}^{(1)}P_{01}^{(2)} + 2P_{21}^{(1)}P_{12}^{(2)} + h.c.\right), \end{aligned} \tag{D.38}$$

which give us an effective coupling

$$
\begin{aligned}
H_{eff}|1\rangle_c =& g_{12}\left[(P_{01}^{(1)}P_{10}^{(2)}+h.c.)+2(P_{12}^{(1)}P_{21}^{(2)}+h.c.)\right] \\
&-g_1g_2\left[\frac{(P_{01}^{(1)}P_{10}^{(2)}+h.c.)}{\Delta}-\frac{2(P_{01}^{(1)}P_{10}^{(2)}+h.c.)}{\Delta-\alpha_c}\right. \\
&\left.+\frac{2(P_{12}^{(1)}P_{21}^{(2)}+h.c.)}{\Delta+\alpha}-\frac{4(P_{21}^{(1)}P_{12}^{(2)}+h.c.)}{\alpha-\alpha_c}\right],
\end{aligned}
\tag{D.39}
$$

that assumes the form

$$
\begin{aligned}
H_{eff}|1\rangle_c =&(P_{01}^{(1)}P_{10}^{(2)}+h.c.)\left[g_{12}-g_1g_2\left(\frac{1}{\Delta}-\frac{2}{\Delta-\alpha_c}\right)\right] \\
&+(P_{12}^{(1)}P_{21}^{(2)}+h.c.)\left[2g_{12}-2g_1g_2\left(\frac{1}{\Delta+\alpha}-\frac{2}{\alpha-\alpha_c}\right)\right].
\end{aligned}
\tag{D.40}
$$

Here, again we find two terms describing the transitions $|0\rangle \mapsto |1\rangle$ and $|1\rangle \mapsto |2\rangle$. And again, we apply the same considerations, to define the new effective coupling

$$
\tilde{g}_{eff}^{|1\rangle_c} = g_{12}-g_1g_2\left(\frac{1}{\Delta}-\frac{2}{\Delta-\alpha_c}\right) \tag{D.41}
$$

Finally, we can write Eq.(D.37) and Eq.(D.41) in a single equation that describes the effective coupling for our transistor system

$$
\tilde{g}_{eff}^{|n\rangle_c}(\Delta) = g_{12}+g_1g_2\left(\frac{2}{\Delta-\delta_{n1}\alpha_c}-\frac{1}{\Delta}\right), \tag{D.42}
$$

where δ_{n1} is the Kronecker delta.

References

1 TURING, A. M. et al. On computable numbers, with an application to the entscheidungsproblem. **J. of Math**, v. 58, n. 345-363, p. 5, 1936. Cited at page 23.

2 J. E. Lilienfeld. **Method and apparatus for controlling electric currents**. 1930. US1745175A. Available at: <https://worldwide.espacenet.com/patent/search/family/035202468/publication/CA272437A?q=pn%3DCA272437A>. Cited at page 23.

3 MOORE, G. E. Cramming more components onto integrated circuits. **Proceedings of the IEEE**, IEEE, v. 38, n. 8, 1965. Cited at page 23.

4 PLANCK, M. Ueber das gesetz der energieverteilung im normalspectrum. **Annalen der Physik**, Wiley, v. 309, n. 3, p. 553–563, 1901. Available at: <https://doi.org/10.1002/andp.19013090310>. Cited at page 23.

5 SCHRöDINGER, E. An undulatory theory of the mechanics of atoms and molecules. **Physical Review**, American Physical Society (APS), v. 28, n. 6, p. 1049–1070, dez. 1926. Available at: <https://doi.org/10.1103/physrev.28.1049>. Cited at page 23.

6 FEYNMAN, R. P. Simulating physics with computers. **International Journal of Theoretical Physics**, Springer Science and Business Media LLC, v. 21, n. 6-7, p. 467–488, jun. 1982. Available at: <https://doi.org/10.1007/bf02650179>. Cited at page 23.

7 MONTANARO, A. Quantum algorithms: an overview. **npj Quantum Information**, Springer Science and Business Media LLC, v. 2, n. 1, jan. 2016. Available at: <https://doi.org/10.1038/npjqi.2015.23>. Cited at page 24.

8 ARUTE, F. et al. Quantum supremacy using a programmable superconducting processor. **Nature**, Springer Science and Business Media LLC, v. 574, n. 7779, p. 505–510, Oct 2019. Available at: <https://doi.org/10.1038/s41586-019-1666-5>. Cited 2 times at pages 24 e 46.

9 ZHONG, H.-S. et al. Quantum computational advantage using photons. **Science**, American Association for the Advancement of Science, v. 370, n. 6523, p. 1460–1463, 2020. Cited at page 24.

10 ZHU, Q. et al. **Quantum Computational Advantage via 60-Qubit 24-Cycle Random Circuit Sampling**. 2021. Cited at page 24.

11 NIELSEN, M. A.; CHUANG, I. L. **Quantum Computation and Quantum Information: 10th Anniversary Edition**. [S.l.]: Cambridge University Press, 2010. Cited 4 times at pages 24, 33, 35 e 36.

12 KJAERGAARD, M. et al. Superconducting Qubits: Current State of Play. **Annual Review of Condensed Matter Physics**, v. 11, p. 369–395, 2020. ISSN 19475462. Cited at page 24.

13 KRANTZ, P. et al. A quantum engineer's guide to superconducting qubits. **Applied Physics Reviews**, v. 6, n. 2, p. 1–66, 2019. ISSN 19319401. Cited 3 times at pages 24, 46 e 94.

14 ELDER, S. S. et al. High-fidelity measurement of qubits encoded in multilevel superconducting circuits. **Physical Review X**, American Physical Society (APS), v. 10, n. 1, jan. 2020. Available at: <https://doi.org/10.1103/physrevx.10.011001>. Cited at page 24.

15 PRESKILL, J. Quantum computing in the NISQ era and beyond. **Quantum**, Verein zur Forderung des Open Access Publizierens in den Quantenwissenschaften, v. 2, p. 79, ago. 2018. Available at: <https://doi.org/10.22331/q-2018-08-06-79>. Accessed on: 23 de Mai. de 2019. Cited at page 24.

16 PIZA, A. F. **Mecânica Quântica**. 1. ed. São Paulo: EdUSP, 2003. 605 p. ISBN 85-314-0748-6. Cited 3 times at pages 28, 41 e 43.

17 GRIFFITHS, D. J. **Mecânica Quântica**. Tradução de Lara Freitas. 2. ed. São Paulo: Pearson, 2011. 347 p. Título original: Introduction to Quantum Mechanics. ISBN 8576059274. Cited at page 28.

18 COHEN-TANNOUDJI, C.; DIU, B.; LALOË, F. **Quantum Mechanics - Vol 1**. 1. ed. [S.l.]: John Wiley & Sons, 1977. 887 p. ISBN 0471164321. Cited 3 times at pages 28, 40 e 42.

19 ZETTI, N. **Quantum Mechanics: Concepts and Applications**. 2. ed. Chippenham, UK: Wiley, 2009. v. 1. 691 p. ISBN 978-0-470-02678-6. Cited 2 times at pages 28 e 40.

20 MOISEYEV, N. **Non-Hermitian Quantum Mechanics**. [S.l.]: Cambridge University Press, 2011. Cited at page 30.

21 NAKAHARA, M.; OHMI, T. **Quantum Computing: From Linear Algebra to Physical Realizations**. 1. ed. Boca Raton, FL: CRC Press, 2008. 438 p. ISSN 00249114. ISBN 9780429146510. Available at: <https://www.taylorfrancis.com/books/9781420012293>. Cited 3 times at pages 31, 35 e 94.

22 BREUER, H.; PETRUCCIONE, F. Quantum master equations. In: _____. **The Theory of Open Quantum Systems**. 1. ed. Oxford: Oxford University Press, 2002. chap. 3, p. 109–216. ISBN 9780198520634. Cited 2 times at pages 32 e 96.

23 STOLZE, J.; SUTER, D. **Quantum computing**: A short course from theory to experiment. 1. ed. Mörlenbach: Wiley, 2004. 246 p. ISBN 9783527404704. Cited 2 times at pages 34 e 35.

24 FREDKIN, E.; TOFFOLI, T. Conservative logic. **International Journal of Theoretical Physics**, Springer Science and Business Media LLC, v. 21, n. 3-4, p. 219–253, abr. 1982. Available at: <https://doi.org/10.1007/bf01857727>. Cited 2 times at pages 36 e 37.

25 LANYON, B. P. et al. Experimental demonstration of a compiled version of shor's algorithm with quantum entanglement. **Physical Review Letters**, American Physical Society (APS), v. 99, n. 25, dez. 2007. Available at: <https://doi.org/10.1103/physrevlett.99.250505>. Cited at page 36.

26 CHUANG, I. L.; YAMAMOTO, Y. Quantum bit regeneration. **Physical Review Letters**, American Physical Society (APS), v. 76, n. 22, p. 4281–4284, maio 1996. Available at: <https://doi.org/10.1103/physrevlett.76.4281>. Cited at page 36.

27 BUHRMAN, H. et al. Quantum fingerprinting. **Physical Review Letters**, American Physical Society (APS), v. 87, n. 16, set. 2001. Available at: <https://doi.org/10.1103/physrevlett.87.167902>. Cited at page 36.

28 CARVALHO, C. M. Estudo das técnicas de obtenção de hamiltonianos efetivos em óptica quântica. Universidade Federal de São Carlos, 2009. Cited at page 43.

29 TAKAYANAGI, K. Unified theory of effective interaction. Elsevier BV, v. 372, p. 12–56, set. 2016. Available at: <https://doi.org/10.1016/j.aop.2016.04.011>. Cited at page 43.

30 JAMES, D. Quantum computation with hot and cold ions: An assessment of proposed schemes. **Fortschritte der Physik**, v. 48, n. 9-11, p. 823–837, 2000. Available at: <https://onlinelibrary.wiley.com/doi/abs/10.1002/1521-3978%28200009%2948%3A9/11%3C823%3A%3AAID-PROP823%3E3.0.CO%3B2-M>. Cited at page 43.

31 JOSEPHSON, B. Possible new effects in superconductive tunnelling. Elsevier BV, v. 1, n. 7, p. 251–253, jul. 1962. Available at: <https://doi.org/10.1016/0031-9163(62)91369-0>. Cited 2 times at pages 45 e 50.

32 JOSEPHSON, B. D. The discovery of tunnelling supercurrents. American Physical Society (APS), v. 46, n. 2, p. 251–254, abr. 1974. Available at: <https://doi.org/10.1103/revmodphys.46.251>. Cited 2 times at pages 45 e 50.

33 SCHREIER, J. A. et al. Suppressing charge noise decoherence in superconducting charge qubits. **Physical Review B**, American Physical Society (APS), v. 77, n. 18, maio 2008. Available at: <https://doi.org/10.1103/physrevb.77.180502>. Cited at page 45.

34 KOCH, J. et al. Charge-insensitive qubit design derived from the cooper pair box. **Physical Review A**, American Physical Society (APS), v. 76, n. 4, out. 2007. Available at: <https://doi.org/10.1103/physreva.76.042319>. Cited 4 times at pages 45, 52, 53 e 55.

35 LOSS, D.; DIVINCENZO, D. P. Quantum computation with quantum dots. **Phys. Rev. A**, American Physical Society, v. 57, p. 120–126, Jan 1998. Available at: <https://link.aps.org/doi/10.1103/PhysRevA.57.120>. Cited at page 46.

36 KANE, B. E. A silicon-based nuclear spin quantum computer. Springer Science and Business Media LLC, v. 393, n. 6681, p. 133–137, maio 1998. Available at: <https://doi.org/10.1038/30156>. Cited at page 46.

37 CIRAC, J. I.; ZOLLER, P. Quantum computations with cold trapped ions. **Phys. Rev. Lett.**, American Physical Society, v. 74, p. 4091–4094, May 1995. Available at: <https://link.aps.org/doi/10.1103/PhysRevLett.74.4091>. Cited at page 46.

38 HAFFNER, H.; ROOS, C.; BLATT, R. Quantum computing with trapped ions. Elsevier BV, v. 469, n. 4, p. 155–203, dez. 2008. Available at: <https://doi.org/10.1016/j.physrep.2008.09.003>. Cited at page 46.

39 RAIMOND, J. M.; BRUNE, M.; HAROCHE, S. Manipulating quantum entanglement with atoms and photons in a cavity. **Rev. Mod. Phys.**, American Physical Society, v. 73, p. 565–582, Aug 2001. Available at: <https://link.aps.org/doi/10.1103/RevModPhys.73.565>. Cited at page 46.

40 VANDERSYPEN, L. M. K.; CHUANG, I. L. Nmr techniques for quantum control and computation. **Rev. Mod. Phys.**, American Physical Society, v. 76, p. 1037–1069, Jan 2005. Available at: <https://link.aps.org/doi/10.1103/RevModPhys.76.1037>. Cited at page 46.

41 MADSEN, L. S. et al. Quantum computational advantage with a programmable photonic processor. **Nature**, v. 606, n. 7912, p. 75–81, jun 2022. ISSN 0028-0836. Available at: <https://www.nature.com/articles/s41586-022-04725-x>. Cited at page 46.

42 KNILL, E.; LAFLAMME, R.; MILBURN, G. J. A scheme for efficient quantum computation with linear optics. **Nature**, v. 409, n. 6816, p. 46–52, jan 2001. ISSN 0028-0836. Available at: <http://www.nature.com/articles/35051009>. Cited at page 46.

43 RASMUSSEN, S. et al. Superconducting Circuit Companion—an Introduction with Worked Examples. **PRX Quantum**, v. 2, n. 4, p. 1–56, 2021. Cited 5 times at pages 46, 57, 58, 90 e 94.

44 CHOW, J.; DIAL, O.; GAMBETTA, J. **IBM Quantum breaks the 100-qubit processor barrier**. 2021. Available at: <https://research.ibm.com/blog/127-qubit-quantum-processor-eagle>. Cited at page 46.

45 WU, Y. et al. Strong quantum computational advantage using a superconducting quantum processor. **Phys. Rev. Lett.**, American Physical Society, v. 127, p. 180501, Oct 2021. Available at: <https://link.aps.org/doi/10.1103/PhysRevLett.127.180501>. Cited at page 46.

46 CHU, J. et al. **Scalable algorithm simplification using quantum AND logic**. arXiv, 2021. Available at: <https://arxiv.org/abs/2112.14922>. Cited at page 46.

47 ZHENG, Y. et al. Solving systems of linear equations with a superconducting quantum processor. **Phys. Rev. Lett.**, American Physical Society, v. 118, p. 210504, May 2017. Available at: <https://link.aps.org/doi/10.1103/PhysRevLett.118.210504>. Cited at page 46.

48 NUSSENZVEIG, H. **Curso de física básica: Eletromagnetismo (vol. 3)**. [S.l.]: Blucher, 2015. ISBN 9788521208020. Cited at page 46.

49 GOLDSTEIN, H. **Classical Mechanics**. 3. ed. San Francisco: Addison Wesley, 1950. 647 p. Cited at page 48.

50 COOPER, L. N. Bound electron pairs in a degenerate fermi gas. **Physical Review**, American Physical Society (APS), v. 104, n. 4, p. 1189–1190, nov. 1956. Available at: <https://doi.org/10.1103/physrev.104.1189>. Cited at page 48.

51 SCHRIEFFER, J. R. **Theory of superconductivity**. 2. ed. Reading, PA: Benjamin-Cummings Publishing Co., Subs. of Addison Wesley Longman, 1983. Cited 2 times at pages 48 e 49.

52 FEYNMAN, R.; LEIGHTON, R.; SANDS, M. **The Feynman Lectures on Physics, Vol. III: The New Millennium Edition: Quantum Mechanics**. Basic Books, 2015. ISBN 9780465040834. Available at: <https://books.google.com.br/books?id=Lb6DBQAAQBAJ>. Cited at page 49.

53 MALOZOVSKY, Y.; FAN, J. Magnetic flux quantization in superconductors and the aharonov–bohm effect. **Physics Letters A**, Elsevier BV, v. 257, n. 5-6, p. 332–337, jul. 1999. Available at: <https://doi.org/10.1016/s0375-9601(99)00250-9>. Cited at page 49.

54 WALLS, D. F.; MILBURN, G. J. **Quantum Optics**. 2. ed. Berlin: Springer, 2008. v. 1. 424 p. ISBN 978-3-540-28573-1. Cited at page 49.

55 DEVORET, M. Quantum Fluctuations in electrical Circuits. In: REYNAUD, S.; GIACOBINO, E.; ZINN-JUSTIN, J. (Ed.). **Fluctuations quantiques: Les Houches, Session LXIII**. Les Houches, France: Elsevier, 1997. p. 351–386. Cited at page 50.

56 ROTH, T. E.; MA, R.; CHEW, W. C. **An Introduction to the Transmon Qubit for Electromagnetic Engineers**. arXiv, 2021. Available at: <https://arxiv.org/abs/2106.11352>. Cited 2 times at pages 50 e 52.

57 BARONE, A.; PATERNò, G. Weak superconductivity - phenomenological aspects. In: _____. **Physics and Applications of the Josephson Effect**. [S.l.]: John Wiley & Sons, Ltd, 1982. chap. 1, p. 1–24. ISBN 9783527602780. Cited at page 51.

58 JAKLEVIC, R. C. et al. Quantum interference effects in josephson tunneling. **Physical Review Letters**, American Physical Society (APS), v. 12, n. 7, p. 159–160, fev. 1964. Available at: <https://doi.org/10.1103/physrevlett.12.159>. Cited at page 54.

59 BARONE, A.; PATERNò, G. Josephson junctions in superconducting loops. In: _____. **Physics and Applications of the Josephson Effect**. [S.l.]: John Wiley & Sons, Ltd, 1982. chap. 12, p. 354–359. ISBN 9783527602780. Cited at page 54.

60 XU, Y. et al. High-fidelity, high-scalability two-qubit gate scheme for superconducting qubits. **Phys. Rev. Lett.**, American Physical Society, v. 125, p. 240503, Dec 2020. Available at: <https://link.aps.org/doi/10.1103/PhysRevLett.125.240503>. Cited at page 58.

61 BARENDS, R. et al. Coherent josephson qubit suitable for scalable quantum integrated circuits. American Physical Society (APS), v. 111, n. 8, ago. 2013. Available at: <https://doi.org/10.1103/physrevlett.111.080502>. Cited at page 58.

62 QIU, J. et al. Suppressing coherent two-qubit errors via dynamical decoupling. **Physical Review Applied**, American Physical Society (APS), v. 16, n. 5, nov. 2021. Available at: <https://doi.org/10.1103/physrevapplied.16.054047>. Cited 4 times at pages 59, 60, 66 e 97.

63 JOHANSSON, J.; NATION, P.; NORI, F. QuTiP: An open-source python framework for the dynamics of open quantum systems. Elsevier BV, v. 183, n. 8, p. 1760–1772, ago. 2012. Available at: <https://doi.org/10.1016/j.cpc.2012.02.021>. Cited at page 64.

64 JOHANSSON, J.; NATION, P.; NORI, F. QuTiP 2: A python framework for the dynamics of open quantum systems. Elsevier BV, v. 184, n. 4, p. 1234–1240, abr. 2013. Available at: <https://doi.org/10.1016/j.cpc.2012.11.019>. Cited at page 64.

65 KAPLAN, D. M.; WHITE, C. G. **Hands-On Electronics**: A practical introduction to analog and digital circuits. Cambridge University Press, 2003. Available at: <https://doi.org/10.1017/cbo9780511754579>. Cited at page 65.

66 PULFREY, D. L. **Understanding Modern Transistors and Diodes**. Cambridge University Press, 2009. Available at: <https://doi.org/10.1017/cbo9780511840685>. Cited at page 65.

67 YAN, F. et al. Tunable coupling scheme for implementing high-fidelity two-qubit gates. **Physical Review Applied**, American Physical Society (APS), v. 10, n. 5, nov 2018. Available at: <https://doi.org/10.1103/physrevapplied.10.054062>. Cited at page 66.

68 LI, X. et al. Tunable coupler for realizing a controlled-phase gate with dynamically decoupled regime in a superconducting circuit. **Physical Review Applied**, American Physical Society (APS), v. 14, n. 2, ago. 2020. Available at: <https://doi.org/10.1103/physrevapplied.14.024070>. Cited at page 66.

69 HAN, X. Y. et al. Error analysis in suppression of unwanted qubit interactions for a parametric gate in a tunable superconducting circuit. **Physical Review A**, American Physical Society (APS), v. 102, n. 2, ago. 2020. Available at: <https://doi.org/10.1103/physreva.102.022619>. Cited at page 66.

70 FENG, W.; WANG, D. wei. Quantum fredkin gate based on synthetic three-body interactions in superconducting circuits. **Physical Review A**, American Physical Society (APS), v. 101, n. 6, jun. 2020. Available at: <https://doi.org/10.1103/physreva.101.062312>. Cited 2 times at pages 66 e 70.

71 COLLODO, M. C. et al. Implementation of conditional phase gates based on tunable zz interactions. **Phys. Rev. Lett.**, American Physical Society, v. 125, p. 240502, Dec 2020. Available at: <https://link.aps.org/doi/10.1103/PhysRevLett.125.240502>. Cited at page 66.

72 JIN, L. **Implementing High-fidelity Two-Qubit Gates in Superconducting Coupler Architecture with Novel Parameter Regions**. arXiv, 2021. Available at: <https://arxiv.org/abs/2105.13306>. Cited at page 66.

73 STEHLIK, J. et al. Tunable coupling architecture for fixed-frequency transmon superconducting qubits. **Phys. Rev. Lett.**, American Physical Society, v. 127, p. 080505, Aug 2021. Available at: <https://link.aps.org/doi/10.1103/PhysRevLett.127.080505>. Cited at page 66.

74 SUNG, Y. et al. Realization of high-fidelity cz and zz-free iswap gates with a tunable coupler. **Phys. Rev. X**, American Physical Society, v. 11, p. 021058, Jun 2021. Available at: <https://link.aps.org/doi/10.1103/PhysRevX.11.021058>. Cited at page 66.

75 HU, C.-K. et al. Conditional coherent control with superconducting artificial atoms. arXiv, 2022. Available at: <https://arxiv.org/abs/2203.09791>. Cited 3 times at pages 68, 79 e 80.

76 NISBET-JONES, P. B. R. et al. Photonic qubits, qutrits and ququads accurately prepared and delivered on demand. **New Journal of Physics**, IOP Publishing, v. 15, n. 5, p. 053007, maio 2013. Available at: <https://doi.org/10.1088/1367-2630/15/5/053007>. Cited at page 74.

77 SAKURAI, J. J.; NAPOLITANO, J. **Modern Quantum Mechanics**. 2. ed. San Francisco: Addison Wesley, 1994. 550 p. ISBN 0805382917. Available at: <http://www.amazon.com/gp/product/0805382917/ref=pd_lpo_sbs_dp_ss_1?pf_rd_p=1535523722&pf_rd_s=lpo-top-stripe-1&pf_rd_t=201&pf_rd_i=0201539292&pf_rd_m=ATVPDKIKX0DER&pf_rd_r=0F9ZVFXMSJ1718HT9VN2>. Cited at page 86.

78 CARMICHAEL, H. Master equations and sources i. In: _____. **An Open Systems Approach to Quantum Optics: Lectures Presented at the Université Libre de Bruxelles October 28 to November 4, 1991**. Berlin, Heidelberg: Springer Berlin Heidelberg, 1993. p. 5–21. ISBN 978-3-540-47620-7. Available at: <https://doi.org/10.1007/978-3-540-47620-7_2>. Cited at page 96.